Discrete Particle Simulation Techniques for the Analysis of Colliding and Flowing Particulate Media

By

Debanjan Mukherjee

A dissertation submitted in partial satisfaction
of the requirements for the degree of

Doctor of Philosophy

in

Mechanical Engineering

in the

GRADUATE DIVISION

of the

UNIVERSITY OF CALIFORNIA, BERKELEY

Committee in charge:

Professor Tarek I. Zohdi, Chair
Professor Philip Marcus
Professor Per Olof Persson

Fall 2013

Discrete Particle Simulation Techniques for the Analysis of Colliding and Flowing Particulate Media

by

Debanjan Mukherjee

Abstract

Discrete Particle Simulation Techniques for the Analysis of Colliding and Flowing Particulate Media

by

Debanjan Mukherjee

Doctor of Philosophy in Mechanical Engineering

University of California, Berkeley

Professor Tarek I. Zohdi, Chair

Flowing particulate media are ubiquitous in a wide spectrum of applications that include transport systems, fluidized beds, manufacturing and materials processing technologies, energy conversion and propulsion technologies, sprays, jets, slurry flows, and biological flows. The discrete nature of the media, along with their underlying coupled multi-physical interactions can lead to a variety of interesting phenomena, many of which are unique to such media - for example, turbulent diffusion and preferential concentration in particle laden flows, and soliton like excitation patterns in a vibrated pile of granular material. This dissertation explores the utility of numerical simulations based on the discrete element method and collision driven particle dynamics methods for analyzing flowing particulate media. Such methods are well-suited to handle phenomena involving particulate, granular, and discontinuous materials, and often provide abilities to tackle complicated physical phenomena, for which pursuing continuum based approaches might be difficult or sometimes insufficient. A detailed discussion on hierarchically representing coupled, multi-physical phenomena through simple models for underlying physical interactions is presented. Appropriate physical models for mechanical contact, conductive and convective heat exchange, fluid-particle interactions, adhesive and near-field effects, and interaction with applied electromagnetic fields are presented. Algorithmic details on assembling the interaction models into a large-scale simulation framework have been elaborated with illustrations. The assembled frameworks were used to develop a computer simulation library (named 'Software Library for Discrete Element Simulations' (SLIDES) for the sake of reference and continued future development efforts) and aspects of the architecture and development of this library have also been addressed. This is an object-oriented discrete particle simulation library developed in Fortran capable of performing fully 3D simulations of particulate systems. The utility and effectiveness of the developed simulation frameworks have been demonstrated using two case studies. The first study is on the analysis of the high velocity impact of stream of particles on a porous layer of material, which

is a problem of interest in the analysis of erosive wear of manufactured surface coatings. The second case-study is based on the deposition of flowing particulate spray on a target surface, which is a problem of interest in the analysis of particulate deposition-based manufacturing processes. In both cases, the aspect of extracting important information on system behavior from the collective dynamics of the particulate media has been outlined. For the first case, this involved a characterization of material damage due to impact generated stresses, and for the second case, this involved analysis of adhesion and deposited coating properties.

Acknowledgements

It was five years ago when I began my journey as a graduate student seeking a doctoral degree. That young, inexperienced, and yet enthusiastic self of mine stands today at the verge of completing his journey. It was, as many had already told me, a journey of perseverance. It was about learning that when the going gets tough, only the tough can indeed get going. I faced tough times, and then the not so tough ones. No matter what the times were, I would not have been where I am today without the god-gifted presence of a few people in my life. These few pages of my dissertation are for them. I can only attempt to capture my earnest gratitude towards them in the words that follow.

Let me begin, as they say, from the very beginning. In the fall semester of 2008, I got into Berkeley after a rather long wait for my paperwork to get ironed out, and Professor Ronald W. Yeung, who was my major field advisor then, patiently provided all the support required for me to successfully get started here at Berkeley. His role was pivotal in getting me here, and till date I am grateful for that. Towards the end of my first semester at Berkeley, I got to decide on a more long-term research project with Professor Alaa Mansour, and this went on to become my master's thesis a couple of years later. Working under Professor Mansour's mentorship taught me a lot about the value of research in day to day engineering design, and in many ways boosted my enthusiasm to continue further research for my doctoral program. A year after finishing my master's thesis with him, he graciously accepted to be on my qualifying examination committee and guided me through the examination. Unfortunately, our combined project could not be sustained a lot further, and we were unable to continue to work together. It was around this time that I started working under the mentorship and tutelage of Professor Tarek Zohdi. Working with Tarek has been a tremendous learning experience for me. Having switched research areas midway into my program, and yet trying to meet all the program deadlines would have been a much more difficult task to handle had it not been for Tarek's constant presence as a mentor and a guide. Oftentimes I would hit roadblocks in my research, or be going through a tough situation that affected my work. On such occasions, Tarek's patience and perseverance was a big support for me. He has always managed to provide me with more than just a helping hand no matter what the situation was. I am ever so grateful to him for his research advise, his support throughout the three years of my doctoral dissertation research, and the rather interesting discussions we ended up having on topics as esoteric as the music of Glenn Gould and the science behind table tennis along with relatively 'lighter' discussions on particle contact interactions and finite element homogenization. I am thankful to have had a mentor like him guide me through my dissertation.

Midway into my dissertation research, I got the chance to interact with Professor Philip Marcus, Professor Per Persson,and Professor Sanjay Govindjee. I got the opportunity to learn fluid mechanics under the tutelage of Professor Marcus, and, he also served as the

chair of my qualifying examination committee. I will remember how even as he recovered from a rather severe back pain, he patiently helped me through the examination. I got the chance to interact with Professor Persson also through his course on numerical solutions of ordinary differential equations. What I learnt from him has formed a very integral part of the work I presented here in my dissertation. Even outside of the classroom, we have had very pleasant interactions, and he also served as my qualifying examination committee member. Both Professor Marcus and Professor Persson are also members of my dissertation committee, and I deeply cherish my continued interaction with them. Professor Govindjee introduced me to the field of continuum mechanics through his course in my third semester, and about a year later I had the chance to learn about statistical mechanics from him as well. I have learned a lot from him during my interactions with him on both occasions. He also graciously accepted to be on my qualifying examination committee. While I was in the process of completing my master's and finalizing my doctoral research options, Professor Govindjee patiently sat and discussed with me many options that could potentially help me resolve the doubts I had regarding the next step. His time and invaluable suggestions during that phase of my graduate student tenure still means a lot to me. With my qualifying examination committee and dissertation committee, I had the chance to discuss my research and received critical comments and suggestions on my proposed work from all of my committee members. A lot of their suggestions and comments helped me resolve many of the questions that I had en route to finishing my dissertation research, and I am deeply thankful to them.

My doctoral research was partly supported by funding from Siemens Energy, and KAUST, and I would like to take this opportunity to sincerely thank them for their generous support.

I truly believe I have been very fortunate to have had a group of really amazing and wonderful people around me in these five years whom I could call 'friends'. They supported me when I needed support, laughed with me when I was happy, embraced me when I was sad, lent me about ten to fifteen patient ears when I needed just one, and came together to form a support system that would always break the fall when I fell. I had the good fortune to have had very amazing roommates in Aditya Medury, Prateek Bhansali, and Anuj Tewari. Aditya and I have been roommates all throughout my graduate studies - starting from the very first day when he smiled and dragged my heavy suitcase up the stairs of our apartment, which used to be a duplex then. We have had a lot of good times, chatting and discussing about a lot of things that we have in common. In Anuj Tewari I found a very special friend with whom I could share a laugh just as well as my anxieties and worries. In many ways, Anuj was more than just a friend or a roommate - he was nearly equal to a sibling of mine who would be my partner in crime in everything I do. I would also like to mention here about Yasaswini and Brinda. I gained a lot of perspective from Yasaswini's plain matter of fact analysis of many situations I would find myself in, and till date I am a big fan of her prowess as a singer. With Brinda I got to have countless friendly moments and *'chaa and adda'* as we would say in Bengali, where her calm and yet cheerful presence would be a sheer joy. Both Yasaswini and Brinda may have had to locate to geographically distant

locations midway through my doctoral studies, but we have managed to stay in touch, and I pray we can continue to do so. I am also very thankful to have met Avinash. A fantastic artist, athlete and cook, Avinash's ginger-chai after a hard-day's work has made an indelible mark amidst my Berkeley memories.

Frankly speaking, I cannot imagine Berkeley and my five years as a student without the presence of Kranthi. Kranthi has been like a big brother, a friend, philosopher, and guide to me. There is no other person with whom I could have heated arguments about politics, and continuum mechanics at the same time, and then bond over a plate of *'Hyderabadi Dum Biriyani'* minutes later. On countless occasions I would find myself in a really worrisome situation, or would get stuck on a research question, and would almost naturally end up seeking Kranthi's advice. There would often be a mild rebuke, maybe a joke, and always a calm word of advice, no matter what the situation is. A great scientist that he is, I wish him and his wife Deepthi only the best in this world - and I hope he always continues to be the big brother to me like he is today. I am also very fortunate to have met Sushrut on the very second day of my stay here at Berkeley, and to have had a trusted friend and guide in him. Every time when I needed some advice on dealing with a situation, Sushrut has always been there with a broad smile on his face, a calm head on his shoulders, and a pair of helping hands. There have been so many hurdles that we literally managed to jump across together, and looking back, I can imagine how helpless I would have been had I not had Sushrut by my side. I would also like to mention here about another friend and mentor of mine, Adarsh. I can safely say that I have not met anyone who can laugh away all worries that come his/her way better than Adarsh. I had the good fortune of having his advise and guidance during many difficult times during the last five years. He would also be the one to give me company for countless science-fiction and action movies that would hit the theaters and that many of my other friends would just refuse to watch. Towards the end of my tenure as a graduate student, I had the chance to meet Padmini. She is definitely one of the most amazing people I have met, and she's got to be the coolest mother that I personally have had the chance to interact with. On many occasions she helped me gain perspectives that I myself would never have gained, and I am thankful for that. Courtesy me being friends with her, I also got to meet two very special people in Tejas and Medha, and I hope I can continue to be very good friends with them as they grow up.

As an avid music enthusiast, I got the chance to meet up and perform with a set of amazing fellow students here at Berkeley who were also equally enthusiastic about music. We formed a group named Bandish, and there have been many occasions when after a tiring and mentally exhausting day in the lab, I would eagerly go back to our jam sessions and have immense fun and joy while playing music. I would like to take this opportunity to thank all members and associates of Bandish - Hrishikesh, Chandrayee, Sudeep, Aakash, Zahra, Aparna, Vijay, and Aarushi.

During Spring 2012, I got a sudden onset of myofascial pain down my shoulder and arms. This turned out to be a very difficult thing for me to understand and manage - since it

ended up affecting my work hours a lot. Had it not been for my physiotherapist Dr. Susan Sonoda, at the University Health Services, I would not have been able to manage the pain, and then gradually and systematically get rid of it. She patiently worked me through the therapy routines and helped me attain a balanced fitness regimen - which gradually reduced the pain, and literally allowed me to finish my dissertation on time (even after missing out on research for one semester and a summer). I am very grateful towards her for her help and co-operation. I am also very thankful to have met a wonderful bunch of people in the Run For India group with the Berkeley chapter of the Association for India's Development, with whom I could continue my newfound enthusiasm in maintaining a fitness schedule, and with whom I also ended up running my first ever half-marathon.

A special mention now for a special friend that I found in Sharanya - with whom I got the chance to meet very early during my stay in Berkeley, and with whom I got the chance to explore a lot of my interests and spend a lot of time, thereby establishing a unique bond. It seems like we can never get tired of laughing with each other, fighting with each other, and caring for each other. I am fortunate to have had her in my life so far, and her relentless efforts in looking out for me and ensuring my well-being. She simultaneously takes on the part of one of my biggest critics, and one of my strongest supports - and leaves me amazed every time, wondering how she manages to do that. I hope as time flies by, we both have each other by our sides, and continue to laugh, fight, and care as we get to take the next steps of our lives together.

Last but not the least, pursuing doctoral studies involves remarkable levels of support and patience from one's family. I am forever indebted to my father, mother, and my brother for being there for me and for supporting me all through. It was really hard at times, and I went back to my family and just expressed all of my frustrations and concerns. They always had kind words and loving embraces for me. My father and mother have always valued education as the highest priority in an individual's life. They fought against all hardships and made immense sacrifices to make me what I am today. Being a teacher herself, my mother would fight against all odds to find time to sit with her kids everyday to help them with their studies, while my father continued to provide us with top-class resources even with a modest family income. I am thankful that I had such a background to inspire me during the course of my doctoral studies. The true extent of their heroic feat I perhaps will be able to fathom one day. Till then, I will continue to be amazed and astonished with a teardrop in my eye at the tremendous support and unconditional love they have showered me with. Trying to grow up would not have been half as much fun had it not been for my little brother being around me and being my partner in crime. He has a determined self-belief, and an infectious energy that has often taught me a thing or two. It gives me immense joy today as he prepares himself for higher studies as well. I am thankful to him for having made such invaluable contributions in constructing a support system for me as I began my doctoral studies thousands of miles away from home. I thank them from the very bottom of my heart, and hope to continue to make them proud in the times to come.

Dedicated to my father, Durgesh Kumar Mukherjee, my mother, Bani Mukherjee, and my brother, Nilanjan Mukherjee

"Where the mind is without fear and the head is held high;"

"Where knowledge is free;"

"Where the world has not been broken up into fragments"

"By narrow domestic walls;"

"Where words come out from the depth of truth;"

"Where tireless striving stretches its arms towards perfection;"

"Where the clear stream of reason has not lost its way"

"Into the dreary desert sand of dead habit;"

"Where the mind is led forward by thee into ever-widening thought and action;"

"Into that heaven of freedom, my Father, let my country awake."

– Rabindranath Tagore (1861-1941)

Poet, Nobel laureate, and a constant source of inspiration.

I wish I can see freedom and knowledge awaken all Nations one day.

Contents

List of Figures

List of Tables

List of Algorithms

Chapter 1

Introduction

"Nothing is built on stone; All is built on sand, but we must build as if the sand were stone"
- Jorge Luis Borges (Argentinian Poet, 1899-1986)

"To see the world in a grain of sand, and to see heaven in a wild-flower"
"Hold infinity in the palm of your hands, and eternity in an hour"
-William Blake (English poet, 1757-1827)

Evidently, the grains of sand have been a part of the creative corners of the minds of poets for many years and in many different contexts. It doesn't seem to be unexpected, since upon expanding to a broader vision of the materials that surround us - sand, grains, powders, particles - these seem to be ubiquitous in their presence. As we make a transition from the realm of verses to our daily existence, this fact remains unchanged. In fact granular and particulate media comprise the second most widely used material after water, and some sources place the worldwide production of grains and aggregates to an approximate ten billion metric tonnes per annum, and estimate about 10 percent of the world's energy production to be utilized in processing such materials. Despite all of this, the understanding of the physics of such materials is still being developed - and in many areas, the insights available are incomprehensive at best. In this dissertation, we make an attempt to look deeper into the underlying physics of such materials - and we do so from the perspective of computer modeling and simulations. A discourse of any semblance on a category of material so diverse in their physical interactions requires an example which is representative and which can be explored in sufficient detail without losing focus of the brevity of the discourse. Correspondingly, we chose the field of particulate spray based manufacturing processes to generate representative examples to demonstrate the utility of our computational models. It must however be noted that the objective of this dissertation is not only to discuss the phenomena related to such material, but also to illustrate the use of computer simulations as a tool for aiding development of understanding of these phenomena. It is, we believe, a subtle aspect that necessitates us to present here a measured balance of theory and models, and simulation frameworks and algorithms - without making any one of the two the primary

focus. In order for us to present our discourse any further, some foundational details on these two aspects is critical to set the context for the discussion. This is our aim in the subsequent sections, so as to be able to provide the reader with an idea of what kind of materials are being discussed, where they are found, and what kinds of models and algorithms can be used to construct numerical probes for understanding the behavior of such materials.

1.1 Granular and flowing particulate media

We begin by exploring what the terms 'granular media' and 'flowing particulate media' refer to. In a simplistic manner, we can use the terms as a placeholder for any material that is composed of small particles. More precisely, Jaeger & Nagel[75] define them as *'large conglomerations of discrete macroscopic particles'*, and many scientists discuss such media to be an assemblage of particles dominated by pair-wise nearest neighbor interactions. The fact that the particles are macroscopic (size$> \mathcal{O}(\mu m)$) is central to the physical behavior of such media - since at these length scales their energy content is not due to thermal agitations characteristic of traditional Brownian motion. Therefore, the behavior of such media is determined by the collective displacement of the particles involved with inconsequential Brownian motion. An in-depth review of the physics of such media is beyond the scope of this work and the interested reader is referred to the works of Duran [35] for extensive discussions on the physics of dry granular materials, the work of Crowe et. al. [29] for dispersed particle-laden flows, and the extensive works by Jaeger, Nagel and collaborators (for example, [74], [76], and [75]). The manifestations of the physical behavior of an assemblage of such particles can be surprisingly diverse. A collection of grains can often flow like a fluid, and also, under certain conditions, undergo plastic deformations like a solid. When dispersed in a turbulent fluid medium, the grains show an aggregate diffusion owing to fluid media velocity fluctuations - a behavior very similar to Brownian diffusion. A collection of loosely flowing particles can also resemble physical behaviors of a gas. Often called granular gases, such behavior can be found in clouds of dust in outer space.

There are also a very broad range of applications where such media find utility. Granular and flowing particulate materials are the mainstay of a huge number of industrial manufacturing processes - including spray forming, chemical mechanical polishing, and additive manufacturing applications. They are also of immense utility in agricultural and food processing applications, and the pharmaceutical industry where large quantities of stored and flowing grains are processed everyday. High end combustion and propulsion systems often use sprayed particles in combustion chambers to improve efficiency. Floating pollutants and sediments are another example of dispersed, flowing particulates in a fluid - which form an important aspect of environmental fluid dynamics. Yet another important area of application is that of geophysics where much of the behavior of soils, flowing sands, and even

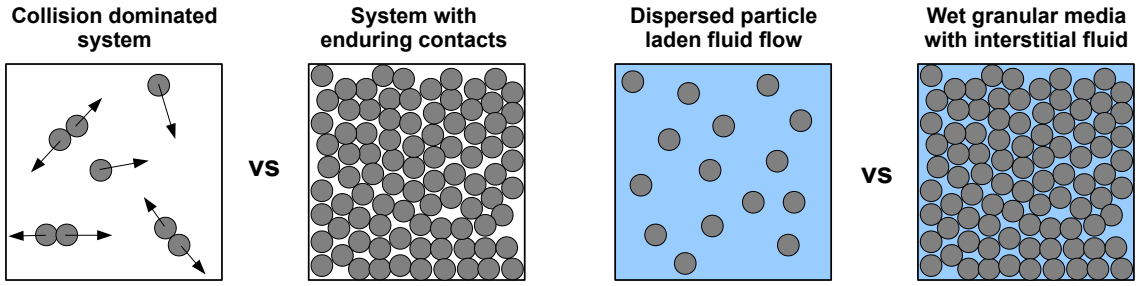

Figure 1.1: *Categorizing granular and particulate media in terms of the inter-particle contacts (left) and in terms of their interaction with a surrounding fluid (right)*

avalanches of snow fall within the realms of this broad class of materials.

In order to understand the different regimes of applications discussed here, we consider the very basic categorizations as presented in Figure 1.1. For the system to be collisionally dominated, the durations of contact of individual particles should be much lesser than characteristic time-scales of the system. For enduring contacts, these two time-scales are of the same order. The presence of interstitial fluids introduce additional interactions between particles, but does not cause much transport phenomena - while the case of dispersed particle-laden flows is a wide area of research of it's own, with much of the focus being on resolving how the particulate and the fluid media interact with each other. It must be noted that while this is by no means an exhaustive categorization - it serves our purpose well to help us broadly define the regimes where we need to focus. *For the most part, this work deals with flowing particulate media which are collisionally dominated and are dispersed in a carrier fluid medium.*

1.2 Computer simulations of colliding particles

The time-honored approach of formulating continuum level global balance laws for mass, momentum and energy has been the focus of many attempts to understand media comprising macroscopic particles. Such methods essentially homogenize the particle-level quantities over certain chosen representative volume elements. For a detailed discussion on homogenization based approaches for particulate media, the reader is referred to Hutter & Rajagopal[70], Goodman & Cowin[56], and the more recent works of Kamrin[80], and Rycroft et.al.[134]. Owing to the complexity of the behavior of such materials, however, a comprehensive continuum theory is difficult to formulate, and reliable theoretical description of the behavior over a wide range of conditions has proven to be a complicated task. Furthermore, for many industrial applications involving particulate media, direct full-scale experimentation is very expensive and time-consuming. With the advent of high-performance computing technolo-

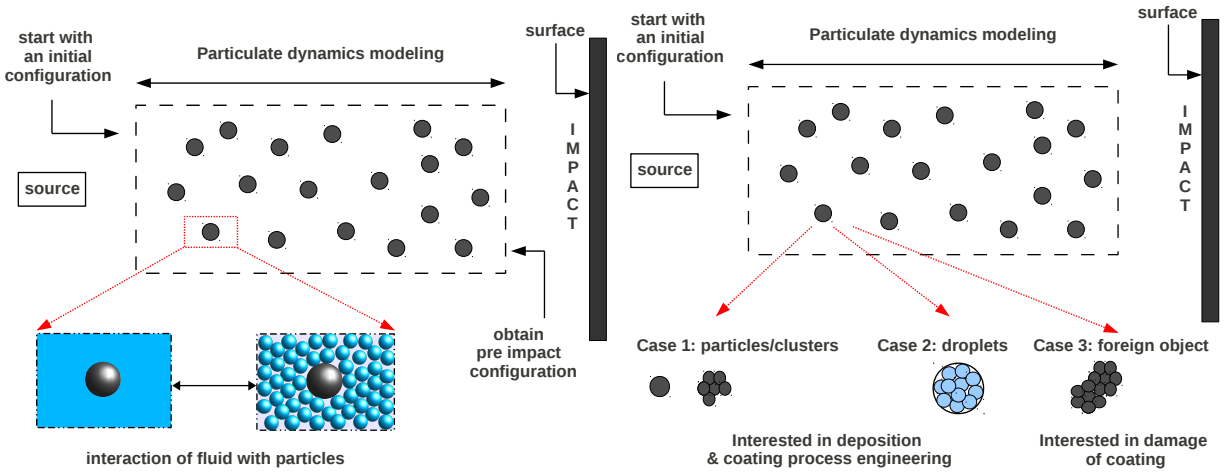

Figure 1.2: *A schematic overview of discrete particle modeling applied to particulate spray coating manufacturing processes. The schematic however is generic enough to include the various different cases that usually need to be modeled - generation of an ensemble of particles from a source, various particle configurations, particle-fluid interactions and interactions with control surfaces.*

gies, computer simulations have found a unique place in the understanding of the behavior of such materials - both in terms of guiding development of new theories and improving existing theories, and in terms of supplementing experimentation efforts to reduce number of trials and thereby reduce costs. The positions and velocities of individual particles can be efficiently tracked and processed using such simulation tools - thereby providing substantial information on the mechanics of the material with even reasonably modest computational efforts. This idea is central to the development of many computer simulation techniques based on discrete particle motions. The interested reader is referred to an excellent review by Poschel & Schwager[122] on discrete computational techniques for granular dynamics, and the classical work of Frenkel & Smit[52] for detailed discussion on molecular dynamics techniques in particular.

The Discrete Element Eethod (henceforth referred to as DEM) comprises a technique very similar to Molecular Dynamics (henceforth referred to as MD) - wherein each particle or grain is considered to be a computational unit, and the equations of motion for each unit are solved systematically. It differs from traditional MD in terms of its ability to deal with collisions between particles, and rotational degrees of freedom of particles. Amongst the first applications of such methods for particulate media was presented in Cundall & Strack[30]. It must be noted, that the computational units (the discrete elements) could also be idealized material elements instead of being actual particles - and henceforth, the words particle and element will be used interchangeably. The aspect of collisions and resolving real mechanical contacts between the particles is perhaps the most critical aspect of these techniques. This

is because resolving collisions by searching every pair of particles in a system of N particles scales as $\mathcal{O}(N^2)$ - making it extremely time-consuming and thereby requiring sophisticated neighbor-list based data structures to make the calculation efficient. Therefore, these types of methods are often also referred to as neighbor-list collision driven particle dynamics. For a system of particles, or an object that can be represented as a collection of discrete particles, we can visualize a computational domain as represented in Figure 1.2 - where the specific area of particulate spray based coatings has been used as an example. The motion equation for each particle can be written, for example, as:

$$m_i \frac{d\mathbf{v}_i}{dt} = \mathbf{F}_i = \mathbf{F}_{i,contact} + \mathbf{F}_{i,fluid} + \mathbf{F}_{i,em} + \mathbf{F}_{i,adh} \tag{1.1}$$

where different kinds of physical interactions are represented in the form of a force that gets added to the right-hand side of the equation - the subscripts 'contact' represents mechanical contact phenomena, 'fluid' represents interactions with surrounding fluid, 'em' represents electromagnetic phenomena, and 'adh' represents adhesive and near-field forces. This offers the flexibility to deal with coupled multi-physics phenomena - and a lot of effort, as shall be seen in the later sections, is focused on obtaining an interaction force model for the phenomena considered. The representation of the particle-interactions as forces lends considerable ease in terms of coupling discrete particle motions to a continuum mesh-based finite element(FEM) type simulation framework as well. A detailed discussion of DEM-FEM coupling is beyond the scope of this work and the interested reader is referred to the extensive discussions in Munjiza [112], and the works of Wellmann & Wriggers[164], and Onate & Rojak[115] for further details.

1.3 Dissertation objectives and outline

Owing to the broad range of coupled physical interactions that are associated with granular and flowing particulate media as described herein, there is a need for hierarchical computational frameworks that can represent a coupled multi-physical phenomena in terms of simple physical interaction models. The discrete element methods, with their inherent flexibility in representing interactions as forces and fluxes at the individual particle level, are well-suited for such materials. With this idea in mind, this dissertation focuses on the use of discrete element based methods to model the dynamics of flowing particulate and granular media. In the context of this broad overall objective, the dissertation was focused on two specific end-goals. The first goal is to particularly implement such modeling and simulation frameworks in industrial manufacturing processes involving particulate media. The second end-goal was to use these frameworks to construct a scientific software library as a general toolkit for performing computer simulations on such materials. This software library is designed using

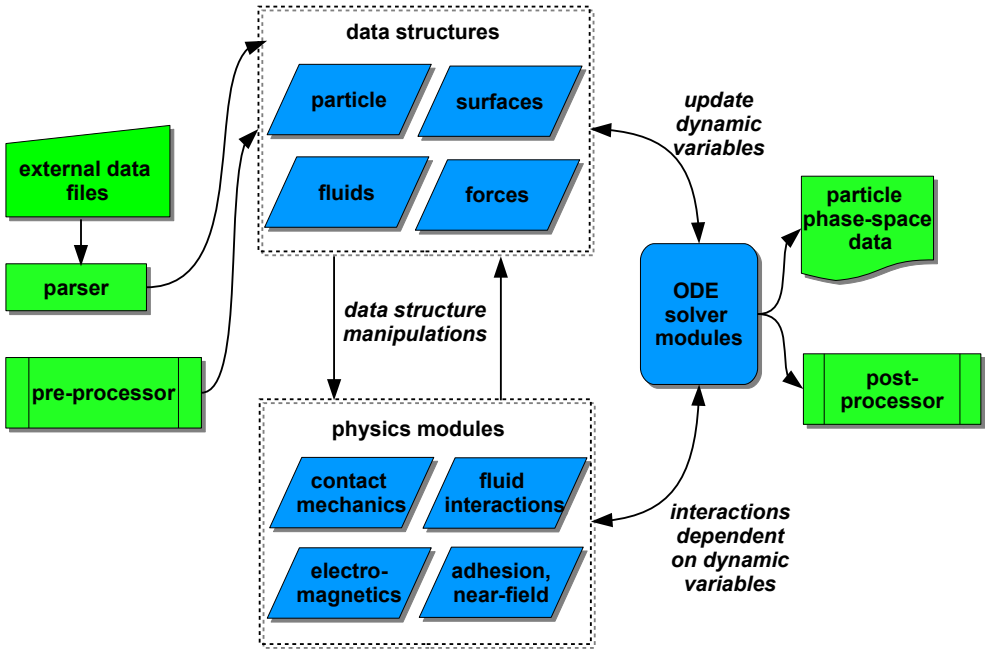

Figure 1.3: *The overall architecture of the simulation libraries. The data obtained for the particle phase-space can either be post-processed, or linked to available finite element codes to enable coupled FEM-DEM type simulation efforts.*

an object-oriented architecture in FORTRAN 95/2003 and is capable of full 3-dimensional simulations of ensembles with rotational degrees of freedom. We present, in Figure 1.3 the basic architecture of the libraries. It is noted herein that there are examples of existing discrete-particle simulation libraries (both open-source and commercial) of varying degrees of specificity - LAMMPS [121] developed and maintained by Sandia National Laboratories is an example of a more popular library based on molecular dynamics. However, the hierarchical computational modeling frameworks discussed here can incorporate a significantly broader range of physical models and phenomena in sufficient detail.

The discussion in the subsequent chapters will be aimed at two main objectives, namely:

- the construction of appropriate physical models for coupled multi-physics phenomena related to the dynamics of particulate media.
- the assembly of these models into algorithmic frameworks and the construction of computer simulation tools

To demonstrate the utility of the simulation codes, two specific problems of importance in manufacturing industry are discussed as examples - namely, particulate spray deposition

process, and the impact dynamics of an erosive jet with a porous surface. One specific focus of this work will be in the area of attempting to capture the synergy between the different physical phenomena through the basic models. The reader will find that this discussion is in accordance with the fundamental assumption presented in Section 1.2, especially from the perspective of translating a particular physical interaction into a force or loading term that can be augmented to the right-hand side of the equations. Another important aspect that will be highlighted, especially through the two case-studies presented, will be to illustrate how resolution of the discrete particle dynamics of each particle provides important information that continuum approaches find hard to provide.

Following this introductory discussion, the force models for particle-particle, particle-surface, and particle-fluid interactions are the subject of discussion in Chapters 2 and 3. Thereafter we shift focus to the topic of developing the overall simulation framework, and the numerical solution of the particle motion and energy equations in Chapter 4. Chapter 5 presents the sample simulations, results and analyses for the two model problems on erosive impact of high velocity particle stream, and deposition of particulate sprays. We conclude in Chapter 6 by linking the present work to broad over-arching future research directions. Details about the simulation libraries, their development and user front-end have been presented as supplementary content in the appendices.

Chapter 2

Particle Interaction Modeling

2.1 Introduction

The first step towards constructing a discrete particle simulation framework is to construct appropriate models for capturing the various particle level multi physics interactions. This will be the focus of this chapter of the dissertation. These interaction models will be the basis of constructing the individual particle level equations - and for this dissertation, we assume the following general forms of the ordinary differential equations for evolution of the particle speed, spin and temperatures (as mentioned briefly in Section 1.2).

$$m_i \frac{d\mathbf{v}_i}{dt} = \mathbf{F}_{i,contact} + \mathbf{F}_{i,fluid} + \mathbf{F}_{i,em} + \mathbf{F}_{i,adh} \tag{2.1}$$

$$I_i \frac{d\omega_i}{dt} = \tau_{i,contact} + \tau_{i,em} + \tau_{i,fluid} \tag{2.2}$$

$$m_i C_i \frac{d\theta_i}{dt} = \mathcal{Q}_i + \mathcal{H}_i + \mathcal{S}_i \tag{2.3}$$

The force terms in Equation 2.1 have been described in Section 1.2. The terms $\tau_{i,contact}$, $\tau_{i,fluid}$, and $\tau_{i,em}$ denote the torques due to contact interactions, fluid-particle interactions, and interactions with an applied external electromagnetic field respectively. It is assumed that adhesive forces are acting along the particle centerlines, and since we work with spherical particle geometries, this force does not have any torque. Furthermore, unless the sphere center of mass and center of charge are unequal - the term $\tau_{i,em}$ will also be 0 - and we retain this case in Equation 2.2. The terms in Equation 2.3 refer to the heat flux due to conduction or convection ($\mathcal{Q}_i$), due to dissipated energy from mechanical or chemical effects ($\mathcal{H}_i$), and due to other sources or sinks ($\mathcal{S}_i$). There exists a broad range of models for the aforementioned particle level interactions for discrete simulations in existing literature. For the discussions presented in this Chapter, in some of the cases, our focus will be to capture

the essence of the existing models and present an overview to the reader. In some other cases, we present to the reader our modifications of the existing models, or slightly different approaches for calculating a particular interaction term. The models presented here, have been incorporated into the various physics modules of the simulation code-library (refer Figure. 1.3) developed as a part of this research.

2.2 Particle contact forces: Force-deformation approach

Consistent evaluation of the impact load is a necessary starting point for such an exercise. There exist a wide range of approaches in characterizing the force between contacting bodies - and the interested reader is referred to the classical work of Johnson [77], and the extensive reviews on contact force models presented by Poschel & Schwager [122], and Shafer et. al. [138]. The most fundamental of these is the Hertzian contact force model for elastic, non-conforming bodies (see the classical work by Hertz [67]). According to Hertz's theory, the contact force for two spherical bodies located at $\mathbf{r}_1$ and $\mathbf{r}_2$ (of radii R_1 and R_2 respectively) is given as:

$$F_c^n = \frac{4}{3}\sqrt{R}E^*\delta_n^{3/2} = K_n\delta_n^{3/2} \tag{2.4}$$

where, as represented schematically in Figure 2.1, $\delta_n = \|\mathbf{r}_1 - \mathbf{r}_2\| - (R_1 + R_2)$ is the relative deformation that they undergo, $1/R = 1/R_1 + 1/R_2$, and the effective elasticity E^* is defined as $\frac{1}{E^*} = \frac{1-\nu_1^2}{E_1} + \frac{1-\nu_2^2}{E_2}$. The terms ν_1, ν_2 denote the material Poisson ratios, and E_1, E_2 denote the material elasticity moduli. Similar to Hertz's approach, Mindlin [106] proposed a model for the tangential compliance during elastic contact, from which the tangential force can be calculated as:

$$F_c^t = \frac{1}{8r_c}\left(\frac{2-\nu_1}{G_1} + \frac{2-\nu_2}{G_2}\right)\delta_t = K_t\delta_t \tag{2.5}$$

where r_c is the radius of the area of contact between the two bodies. Real contacts are however not necessarily elastic, and to take into account the inelastic effects, the aforementioned expressions need to be modified. A common approach in literature to account for this is to write the normal contact force using a simple linear combination of a recovery and a dissipation term as follows:

$$F_c^n = K\delta_n + \gamma_n\frac{d\delta_n}{dt} \tag{2.6}$$

where K, γ_n are model constants. A physical basis of choosing these two constants by linking them constants to the restitution coefficient is provided by Poschel & Schwager [122], which ensures that the model dissipates energy in a physically realistic manner. The relation

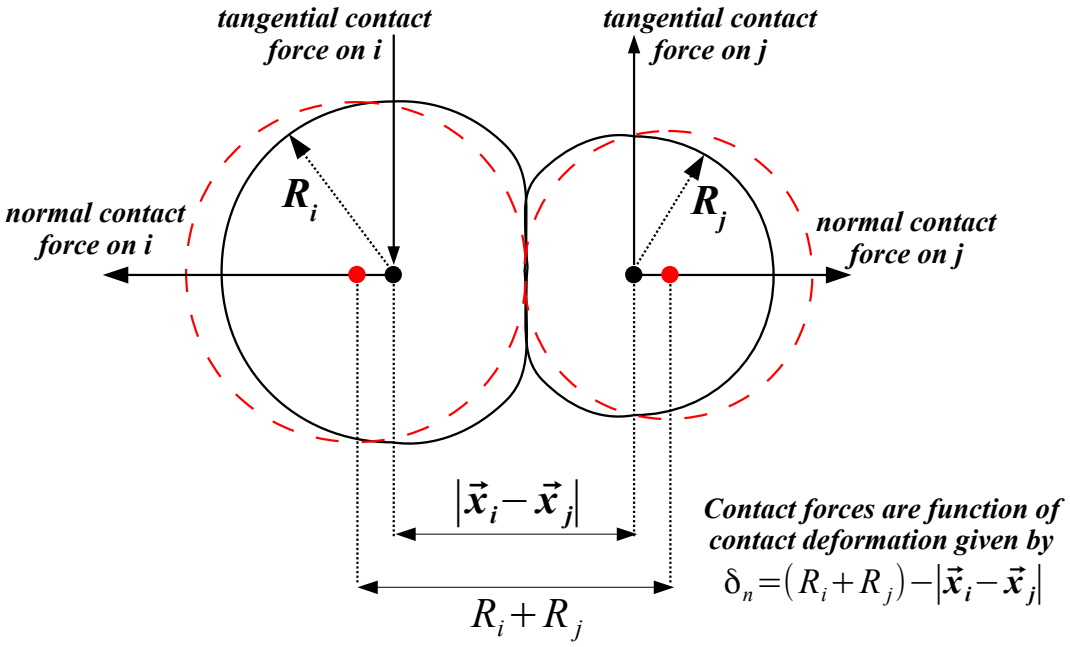

Figure 2.1: *A schematic representation of contact deformation. The original, undeformed configuration is indicated in red, and the final configuration in black. The particles come into contact over a finite contact area.*

they provide is presented as follows:

$$e = \exp\left(-\frac{\pi\gamma_n}{2m_{eff}} \Big/ \sqrt{\frac{Y}{m_{eff}} - \left(\frac{\gamma_n}{2m_{eff}}\right)^2} \right) \tag{2.7}$$

where $m_{eff} = M_i m_j/(m_i + m_j)$ is the effective mass of the binary colliding system. A generalized form of this contact model can be found in Brilliantov et. al.[18] where the force for normal contact between viscoelastic spheres has been expressed in a similar manner by adding a dissipation term to the Hertzian force presented in Equation 2.4 as follows:

$$F_c^n = K_n \delta_n^{3/2} + K_n A(\xi)\sqrt{\delta_n}\frac{d\delta_n}{dt} \tag{2.8}$$

where the term A is a model parameter that depends on the material viscosity(ξ). A more phenomenological approach has been presented by Walton & Braun [163] where the normal interaction is modeled using a partially latched spring, leading to different compliances during the loading (otherwise called the *'compression phase'*) and unloading (otherwise called the *'recovery phase'*) of the contact. This is represented as follows:

$$F_c^n = K_n^L \delta_n \qquad \forall d\delta_n/dt \geq 0 \tag{2.9}$$

$$= K_n^U \left(\delta_n - \delta_0\right) \quad \forall d\delta_n/dt < 0 \tag{2.10}$$

where the superscripts L and U denote loading and unloading phases of the contact respectively. For the tangential contact interactions, friction plays a crucial role in the energy dissipation. Friction forces depend on the magnitude of normal contact forces, and during loading or unloading the normal forces keep changing, which in turn means that Mindlin's results presented in Equation 2.5 only presents the initial compliance as tangential incipient motion occurs. The changing compliances for the unloading and loading phases have been taken into account by Mindlin & Deresiewicz [105], and more recently by Vu Quoc & Zhang [162] that accounts for the loading hysteresis (see [162] for details on the variation in compliances). In general, according to this theory, the tangential forces are expressed as:

$$F_c^t = K_{t,0} \Phi \left(F_c^t, F_c^n, \mu\right) \delta_t \tag{2.11}$$

where $K_{t,0}$ is the compliance expressed in 2.5, and Φ is a function of the tangential and normal loads and the dynamic friction coefficient (μ). A simpler version of this form of a history dependent representation of tangential compliance has also been presented by Walton & Braun [163] where the tangential stiffness is different based on whether there is an increase or decrease in the tangential load due to slip as follows:

$$\Phi \left(F_c^t, F_c^n, \mu\right) = \begin{cases} \left(\dfrac{\mu F_c^n - F_c^t}{\mu F_c^n - F_{sr}}\right)^{\alpha} & \textit{if slip increases } F_c^t \\ -\left(\dfrac{\mu F_c^n + F_c^t}{\mu F_c^n + F_{sr}}\right)^{\alpha} & \textit{if slip decreases } F_c^t \end{cases} \tag{2.12}$$

where the force term F_{sr} is the total tangential force when the last instance of slip reversal occurred, and α is a modeling constant $\approx 1/3$. An alternative simpler implementation based on the Coulomb stick-slip law has been also presented by Haff & Werner[61] where the authors propose an incremental tangential force limited by dynamic Coulomb friction as follows (for an incremental time-stepping calculation with time-step size Δt):

$$F_c^t = -\text{sign}\left(v_{rel}^t\right) \min\left(\left[K_t v_{rel}^t \Delta t + \gamma_t m_{eff} v_{rel}^t + F_c^t(t - \Delta t)\right], \mu \|F_c^n\|\right) \tag{2.13}$$

where K_t is a tangential stiffness measure, and γ_t is a tangential viscosity term that leads to dissipation. A similar form of the tangential force is also found in the canonical work by Cundall & Strack [30], where the force is expressed as:

$$F_c^t = -\text{sign}\left(v_{rel}^t\right) \min\left(\|K_t d_{rel}\|, \mu \|F_c^n\|\right) \tag{2.14}$$

where the relative displacement in contact d_{rel} is given as $d_{rel} = \int_{t_0}^{t} v_{rel}^{t}(t').dt'$. It must be noted that for most of these tangential force-deformation models there are no fundamental microscopic mechanisms that are used to derive the expressions - rather they are more phenomenological. Hence, an accurate estimation of some of these modeling constants become an important issue - one which can be dealt with by careful construction of experiments. Furthermore, the replication of exact stick-slip behavior for friction becomes also a critical issue, especially since the behavior of static collections of granular systems in enduring contact is governed by this behavior. Such systems are handled very well by Equation 2.14, but their behavior is harder to capture using Equation 2.5 or 2.13. Alternatively, a direct balance of the linear and angular momenta of colliding particles can be used to estimate the forces of contact - an approach that does not require an explicit force deformation relation to be evaluated and integrated. This approach has been used for flowing particulate media in the works of Zohdi et. al. (see, for example, the works by Zohdi [178], Arbelaez & Zohdi[4]) - and for problems involving dynamic systems of particles undergoing non-enduring contacts, this provides a theoretically consistent and accurate estimate of contact interactions. Furthermore, such a derivation does not require explicit tracking of the individual contact deformations, thereby relaxing the restrictions on time-step size - which is advantageous in certain kinds of particle dynamics simulations.

2.3 Particle contact forces: Direct impulse-momentum balance

We provide here a derivation of contact forces evaluated from a impulse-momentum balance. The impact of a spherical particle with a surface is considered. Assuming the surface description is known to be in form of a mathematical representation $\mathcal{F}(x, y, z) = 0$, it is possible to define a normal vector to the surface by using the following definition (for the unit outward normal) $\hat{\mathbf{n}} = -\frac{\nabla \mathcal{F}}{\|\nabla \mathcal{F}\|}$. We consider a spherical particle approaching this surface, and denote the point of contact with subscript p, and center of mass with the subscript c. If the surface velocity vector is known to be $\mathbf{v}_{surf}$, then the slip velocity at the point of contact can be obtained as:

$$\mathbf{v}_{slip} = (\mathbf{v}_p - \mathbf{v}_{surf}) - [(\mathbf{v}_p - \mathbf{v}_{surf}) \cdot \hat{\mathbf{n}}]\, \hat{\mathbf{n}} \tag{2.15}$$

following which, the direction of tangential slip can be defined as:

$$\hat{\mathbf{t}} = \frac{\mathbf{v}_{slip}}{\| \mathbf{v}_{slip} \|} \tag{2.16}$$

From Figure 2.2 the generic form of the contact force acting on the particle can be now motivated to be $\mathbf{F}_{contact} = f_N \hat{\mathbf{n}} - f_T \hat{\mathbf{t}}$. The global linear and angular momentum balance for the impacting particle now can be written as follows:

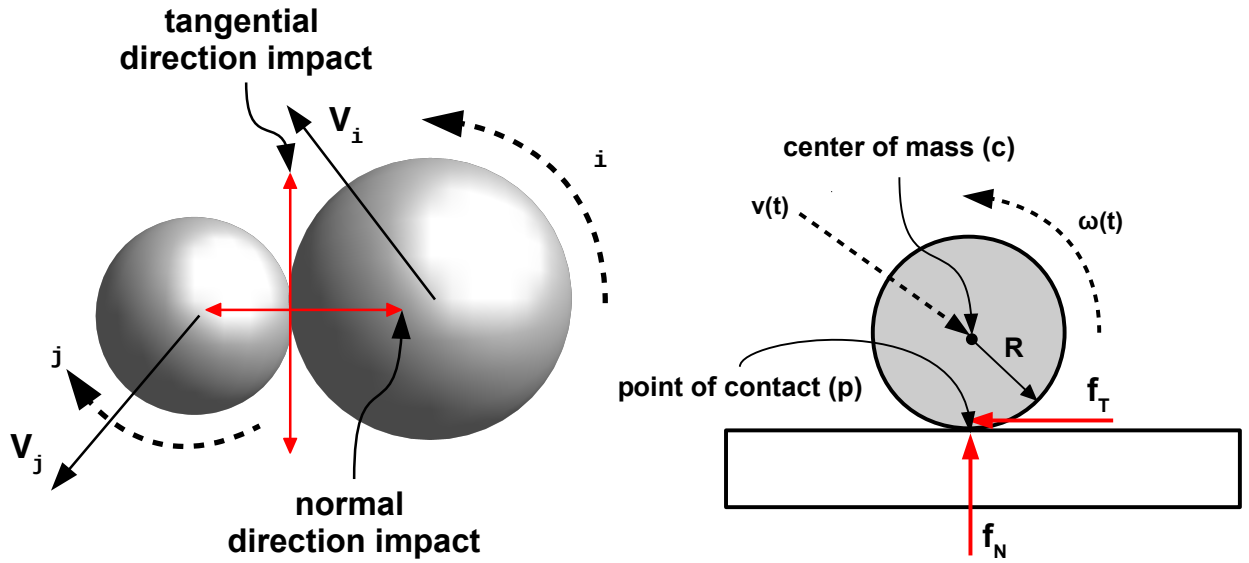

Figure 2.2: *Schematic of particle particle (left) and particle surface (right) contact force calculations using direct impulse-momentum balance.*

$$m\mathbf{v}_c(t+\delta t) - m\mathbf{v}_c(t) = \langle \mathbf{F}^c \rangle \delta t + \langle \mathbf{F}^e \rangle \delta t \tag{2.17}$$

$$I\omega(t+\delta t) - I\omega(t) = \langle \mathbf{r}_{cp} \times \mathbf{F}^c \rangle \delta t + \langle \mathbf{M}^e \rangle \delta t \tag{2.18}$$

wherein, the sum of all external forces and moments other than the contact forces are represented using $\mathbf{F}^e$ and $\mathbf{M}^e$ respectively. Taking the dot product of Eq. 2.17 with the normal vector $\hat{\mathbf{n}}$, we get:

$$mv_{cn}(t+\delta t) - mv_{cn}(t) = \langle f_N \rangle \delta t + \langle F_n^e \rangle \delta t \tag{2.19}$$

where the subscript 'n' denotes the dot product of the corresponding vector quantity with $\hat{\mathbf{n}}$. Note that we assume that the surface is infinitely massive as compared to the impacting particle and hence does not undergo any change in momentum upon impact. The inelastic effects and energy loss during the impact can be characterized by means of the 'Restitution coefficient' e - which for the present discussion, is assumed to be of the following form:

$$e = \frac{recovery\ impulse}{compression\ impulse} = \frac{\int_{t+\delta t_1}^{t+\delta t} f_N dt}{\int_{t}^{t+\delta t_1} f_N dt} \tag{2.20}$$

Correspondingly, decomposing the 'Collide step' into a compression phase and a recovery phase, the following linear momentum balances can be written:

$$m\bar{v} - mv_{cn}(t) = \langle f_N \rangle_C \delta t_1 + \langle F_n^e \rangle \delta t_1 \qquad compression \qquad (2.21)$$

$$mv_{cn}(t+\delta t) - m\bar{v} = \langle f_N \rangle_R (\delta t - \delta t_1) + \langle F_n^e \rangle (\delta t - \delta t_1) \qquad recovery \qquad (2.22)$$

with $\bar{v}$ being the common normal velocity of the particle and the surface at the end of the compression phase, such that normal relative velocity is 0 (which effectively gives $\bar{v} = v_{surf,n}$). Note that the average impulses denoted here by $\langle \cdot \rangle$ are for the corresponding intervals of integration. Simplifying further, by writing the total contact impulse during the collide step for the normal direction impact as follows:

$$\langle f_N \rangle \delta t = \langle f_N \rangle_C \delta t_1 + \langle f_N \rangle_R (\delta t - \delta t_1) = (1+e) \langle f_N \rangle_C \delta t_1 \qquad (2.23)$$

$$= (1+e) \left[mv_{surf,n} - mv_{cn}(t) - \langle F_n^e \rangle \delta t_1 \right] \qquad (2.24)$$

Furthermore, plugging the expression for the total contact impulse into Eq. 2.19, the post impact normal velocity of the particle can be obtained as follows:

$$v_{cn}(t+\delta t) = (1+e) v_{surf,n} - e v_{cn}(t) + \frac{1}{m} \langle F_n^e \rangle_R (\delta t - \delta t_1) - \frac{e}{m} \langle F_n^e \rangle_C \delta t_1 \qquad (2.25)$$

The tangential momentum change can now be approached in a similar way by taking the dot product of Eq. 2.17 with $\hat{\mathbf{t}}$:

$$mv_{ct}(t+\delta t) - mv_{ct}(t) = \langle -f_T \rangle \delta t + \langle F_t^e \rangle \delta t \qquad (2.26)$$

In the implementation of a stick-slip type friction rule, under the assumption that tangential stick occurs, the relative tangential slip velocity will vanish. This leads to the folllowing expressions:

$$\mathbf{v}_{slip} \cdot \hat{\mathbf{t}} = \left[(\mathbf{v}_p - \mathbf{v}_{surf}) - \left[(\mathbf{v}_p - \mathbf{v}_{surf}) \cdot \hat{\mathbf{n}} \right] \hat{\mathbf{n}} \right] \cdot \hat{\mathbf{t}} = 0$$

For the rigid body kinematics, and using the fact that for spherical particles (see Figure 2.2,right) $\mathbf{r}_p - \mathbf{r}_c = -R\hat{\mathbf{n}}$, the tangential-stick condition becomes

$$(\mathbf{v}_c - \mathbf{v}_{surf}) \cdot \hat{\mathbf{t}} - R(\omega \times \hat{\mathbf{n}}) \cdot \hat{\mathbf{t}} = v_{ct} - v_{surf,t} - R\omega_s = 0 \qquad (2.27)$$

where we define a third unit vector $\hat{\mathbf{s}} = \hat{\mathbf{n}} \times \hat{\mathbf{t}}$ to complete a triad, and write components of vectors along this vector with a subsript 's'. Furthermore, taking the dot-product of the angular momentum balance in Eq. 2.18 with $\hat{\mathbf{s}}$, we get:

$$I\omega_s(t+\delta t) - I\omega(t) = \langle \mathbf{r}_{cp} \times \mathbf{F}^c \rangle \cdot \hat{\mathbf{s}} + \langle M_s^e \rangle \delta t = \langle R f_T \rangle \delta t + \langle M_s^e \rangle \delta t \tag{2.28}$$

Using Eq. 2.26, 2.28, 2.27, and performing some simple algebra, the following expression for the total tangential force can be obtained under the condition that tangential stick condition in Eq. 2.27 is satisfied.

$$\begin{aligned} \langle f_T \rangle \delta t &= \frac{1}{\frac{1}{m} + \frac{R^2}{I}} \left[\frac{1}{m} \langle F_t^e \rangle \delta t - \frac{R}{I} \langle M_s^e \rangle \delta t + [v_{ct}(t) - R\omega_s(t)] - v_{surf,t} \right] \\ &= \frac{2}{7} \langle F_t^e \rangle \delta t - \frac{5}{7R} \langle M_s^e \rangle \delta t + \frac{2m}{7} [v_{ct}(t) - R\omega_s(t)] - \frac{2m}{7} v_{surf,t} \qquad \left[with\ I = \frac{2}{5} m R^2 \right] \end{aligned} \tag{2.29}$$

Finally, to complete the implementation of the stick slip model for friction, the tangential force above is compared to the static friction limit, and the following modifications are made:

$$\text{If } \parallel f_T \parallel \leq \mu_s \parallel f_N \parallel \Rightarrow f_T = f_T \qquad \text{stick-condition} \tag{2.30}$$

$$\text{If } \parallel f_T \parallel > \mu_s \parallel f_N \parallel \Rightarrow f_T = \mu_d \parallel f_N \parallel \qquad \text{slip-condition} \tag{2.31}$$

Having obtained the tangential force in Eq. 2.30 and Eq. 2.31, plugging this back into the corresponding linear and angular momentum balance laws in Eq. 2.26 and Eq. 2.28, the respective post-collisional linear and angular velocity component updates can also be obtained as follows:

$$v_{ct}(t+\delta t) = v_{ct}(t) - \frac{1}{m} \langle f_T \rangle \delta t + \frac{1}{m} \langle F_t^e \rangle \delta t \tag{2.32}$$

$$\omega_s(t+\delta t) = \omega_s(t) + \frac{R}{I} \langle f_T \rangle \delta t + \langle M_s^e \rangle \delta t \tag{2.33}$$

Eq. 2.25, 2.32, and 2.33 together provide the corresponding velocity component updates for the particle-surface impact. We remark here that for the case of a particle-surface impact case this provides the exact Coulomb stick-slip friction.

A similar approach is pursued to obtain the collision forces and the post-collisional velocities for the impact of two spherical particles (reference schematic shown in Figure 2.2). As opposed to the collision with a surface, for a pair of particles, we define the normal vector for pairwise collision as:

$$\hat{\mathbf{n}}_{ji} = \frac{\mathbf{r}_j - \mathbf{r}_i}{\parallel \mathbf{r}_j - \mathbf{r}_i \parallel} \qquad \hat{\mathbf{n}}_{ij} = \frac{\mathbf{r}_i - \mathbf{r}_j}{\parallel \mathbf{r}_i - \mathbf{r}_j \parallel} \tag{2.34}$$

The velocities at the point of contact for each spherical particle can thus now be written as:

$$\mathbf{v}_{pi} = \mathbf{v}_{ci} + \omega_i \times (R_i \hat{\mathbf{n}}_{ji}), \qquad \mathbf{v}_{pj} = \mathbf{v}_{cj} + \omega_j \times (R_j \hat{\mathbf{n}}_{ij}) \tag{2.35}$$

The relative velocity at the point of contact can be defined as $\mathbf{v}_{rel} = \mathbf{v}_{pj} - \mathbf{v}_{pi}$. Using the relative velocity at the contact point, the direction of tangential slip can be characterized by a unit vector $\hat{\mathbf{t}}_{ij}$ (similar to the case of particle-surface collision), as follows:

$$\hat{\mathbf{t}}_{ij} = \frac{\mathbf{v}_{rel} - (\mathbf{v}_{rel} \cdot \hat{\mathbf{n}}_{ij})\hat{\mathbf{n}}_{ij}}{\parallel \mathbf{v}_{rel} - (\mathbf{v}_{rel} \cdot \hat{\mathbf{n}}_{ij})\hat{\mathbf{n}}_{ij} \parallel} \tag{2.36}$$

The global linear momentum balance for the pairwise collision of the two particles can now be written as:

$$m_i \mathbf{v}_i(t + \delta t) - m_i \mathbf{v}_i(t) = \langle \mathbf{F}_i^c \rangle \delta t + \langle \mathbf{F}_i^e \rangle \delta t \tag{2.37}$$
$$m_i \mathbf{v}_j(t + \delta t) - m_i \mathbf{v}_j(t) = \langle \mathbf{F}_j^c \rangle \delta t + \langle \mathbf{F}_j^e \rangle \delta t \tag{2.38}$$

Taking the dot product with $\hat{\mathbf{n}}_{ij}$, and writing the contact force as $\mathbf{F}_i^c = f_N \hat{\mathbf{n}}_{ij} + f_T \hat{\mathbf{t}}_{ij}$, we have the following:

$$m_i v_{in}(t + \delta t) - m_i v_{in}(t) = \langle f_N \rangle \delta t + \langle F_{in}^e \rangle \delta t \tag{2.39}$$
$$m_i v_{jn}(t + \delta t) - m_i v_{jn}(t) = \langle -f_N \rangle \delta t + \langle F_{jn}^e \rangle \delta t \tag{2.40}$$

The collision momentum balance can now again be decomposed into a compression and a recovery phase, and the restitution coefficient defined using the ratio of recovery and compression impulses, following which the following relations are obtained:

$$m_i v_{cn} - m_i v_{in}(t) = \langle f_N \rangle_C \delta t_1 + \langle F_{in}^e \rangle_C \delta t_1 \tag{2.41}$$
$$m_i v_{cn} - m_i v_{jn}(t) = \langle -f_N \rangle_C \delta t_1 + \langle F_{jn}^e \rangle_C \delta t_1 \tag{2.42}$$
$$m_i v_{in}(t + \delta t) - m_i v_{cn} = \langle f_N \rangle_R (\delta t - \delta t_1) + \langle F_{in}^e \rangle_R (\delta t - \delta t_1) \tag{2.43}$$
$$m_i v_{jn}(t + \delta t) - m_i v_{cn} = \langle -f_N \rangle_R (\delta t - \delta t_1) + \langle F_{jn}^e \rangle_R (\delta t - \delta t_1) \tag{2.44}$$

where, v_{cn} is the common normal velocity after the compression phase (leading to a zero relative normal velocity). Some algebra simplification using Eq. 2.41 and Eq. 2.42 gives us:

$$\langle f_N \rangle \delta t_1 = \frac{1}{m_i + m_j} \left[m_i \langle F^e_{jn} \rangle_C \delta t_1 - m_j \langle F^e_{in} \rangle_C \delta t_1 \right] - \frac{m_i m_j}{m_i + m_j} \left[v_{in}(t) - v_{jn}(t) \right] \tag{2.45}$$

following which, using the definition of the restitution coefficient, the following expression for the total contact force can be obtained for the collide step:

$$\begin{aligned} \langle f_N \rangle \delta t &= \langle f_N \rangle_C \delta t_1 + \langle f_N \rangle_R (\delta t - \delta t_1) = (1+e) \langle f_N \rangle_C \delta t_1 \\ &= \frac{1+e}{m_i + m_j} \left[m_i \langle F^e_{jn} \rangle_C \delta t_1 - m_j \langle F^e_{in} \rangle_C \delta t_1 \right] - \frac{(1+e) m_i m_j}{m_i + m_j} \left[v_{in}(t) - v_{jn}(t) \right] \end{aligned} \tag{2.46}$$

The contact impulse can now be plugged back in to the linear momentum balance equations to get the respective post collisional velocity updates as follows:

$$\begin{aligned} m_i v_{in}(t+\delta t) &= m_i v_{in}(t) + \langle f_N \rangle \delta t + \langle F^e_{in} \rangle \delta t \\ &= m_i v_{in}(t) + \frac{1+e}{m_i + m_j} \left[m_i \langle F^e_{jn} \rangle_C \delta t_1 - m_j \langle F^e_{in} \rangle_C \delta t_1 \right] \\ &\quad - \frac{(1+e) m_i m_j}{m_i + m_j} \left[v_{in}(t) - v_{jn}(t) \right] + \langle F^e_{in} \rangle \delta t \end{aligned} \tag{2.47}$$

$$\begin{aligned} m_j v_{jn}(t+\delta t) &= m_j v_{jn}(t) + \langle -f_N \rangle \delta t + \langle F^e_{jn} \rangle \delta t \\ &= m_j v_{jn}(t) - \frac{1+e}{m_i + m_j} \left[m_i \langle F^e_{jn} \rangle_C \delta t_1 - m_j \langle F^e_{in} \rangle_C \delta t_1 \right] \\ &\quad + \frac{(1+e) m_i m_j}{m_i + m_j} \left[v_{in}(t) - v_{jn}(t) \right] + \langle F^e_{jn} \rangle \delta t \end{aligned} \tag{2.48}$$

For the tangential component of the contact impulses, the momentum balance in $\hat{\mathbf{t}}_{ij}$ (see Equation.2.36) is used along with a Coulomb stick-slip criteria. Starting with the dot product of the momentum balance in Equation.2.38 with $\hat{\mathbf{t}}_{ij}$, we have:

$$m_i v_{it}(t+\delta t) - m_i v_{it}(t) = \langle f_T \rangle \delta t + \langle F^e_{it} \rangle \delta t \tag{2.49}$$

$$m_j v_{jt}(t+\delta t) - m_j v_{jt}(t) = \langle -f_T \rangle \delta t + \langle F^e_{jt} \rangle \delta t \tag{2.50}$$

Furthermore, defining a third unit vector $\hat{\mathbf{s}}_{ij} = \hat{\mathbf{n}}_{ij} \times \hat{\mathbf{t}}_{ij}$, to complete a triad - and performing a balance of angular momentum along this unit vector, we get the following:

$$I_i\omega_{is}(t+\delta t) - I_i\omega_{is}(t) = \langle \mathbf{r}_{pi} \times \mathbf{F}_i^c \rangle \delta t \cdot \hat{\mathbf{s}}_{ij} + \langle M_{is} \rangle \delta t \tag{2.51}$$

$$I_j\omega_{js}(t+\delta t) - I_j\omega_{js}(t) = \langle \mathbf{r}_{pj} \times \mathbf{F}_j^c \rangle \delta t \cdot \hat{\mathbf{s}}_{ij} + \langle M_{js} \rangle \delta t \tag{2.52}$$

From Figure 2.2 it can be seen that $\mathbf{r}_{pi} = -R\hat{\mathbf{n}}_{ij}$, which leads to $\langle \mathbf{r}_{pi} \times \mathbf{F}_i^c \rangle \delta t \cdot \hat{\mathbf{s}}_{ij} = -Rf_T$. Using this relation also for the j'th particle, we get the following:

$$I_i\omega_{is}(t+\delta t) - I_i\omega_{is}(t) = -R\langle f_T \rangle \delta t + \langle M_{is} \rangle \delta t \tag{2.53}$$

$$I_j\omega_{js}(t+\delta t) - I_j\omega_{js}(t) = -R\langle f_T \rangle \delta t + \langle M_{js} \rangle \delta t \tag{2.54}$$

Assuming now that the particles are tangentially stuck, then tangential components of $\mathbf{v}_{pi}$ and $\mathbf{v}_{pj}$ are going to be equal (no slip velocity). Performing appropriate vector operations, this leads to the following result:

$$v_{it}(t+\delta t) - R_i\omega_{is}(t+\delta t) = v_{jt}(t+\delta t) + R_j\omega_{js}(t+\delta t) \tag{2.55}$$

Substituting $I_i = \frac{2}{5}m_iR_i^2$ for spherical particles, and performing algebra manipulations with the Eq. 2.49, 2.50, 2.53, 2.54, we get the final form of the tangential contact impulse for the 'stick' case:

$$\begin{aligned}\langle f_T \rangle \delta t = \frac{2}{7}\left(\frac{m_i m_j}{m_i + m_j}\right)\Big[\{v_{jt}(t) + R_j\omega_{js}(t)\} - \{v_{it}(t) - R_i\omega_{is}(t)\} \\ + \frac{\delta t}{m_j}\left\{\frac{5}{2}\frac{\langle M_{js} \rangle}{R_j} + \langle F_{jt}^e \rangle\right\} + \frac{\delta t}{m_i}\left\{\frac{5}{2}\frac{\langle M_{is} \rangle}{R_i} - \langle F_{it}^e \rangle\right\}\Big]\end{aligned} \tag{2.56}$$

To implement the complete Coulomb stick-slip condition, we use Equations 2.30 and 2.31, and construct the appropriate velocity and angular velocity updates by plugging in the tangential force from Eq. 2.56 into the linear and angular momentum balance relations in Eq. 2.49, 2.50, 2.53, 2.54. For the i'th particle:

$$v_{it}(t+\delta t) = v_{it}(t) + \frac{1}{m_i}\langle f_T \rangle \delta t + \frac{1}{m_i}\langle F_{it}^e \rangle \delta t \tag{2.57}$$

$$\omega_{is}(t+\delta t) = \omega_{is}(t) - \frac{R_i}{I_i}\langle f_T \rangle \delta t + \frac{1}{I_i}\langle M_{is} \rangle \delta t \tag{2.58}$$

2.4 Velocity-dependent restitution coefficients

The derivation of contact interactions provided here is based on the knowledge of restitution coefficient and the durations of the compression and the recovery phases of collision. A physically consistent model for these parameters is necessary to capture the inelastic effects during a collision, and the dissipation of energy. Experimental data on restitution indicates that the coefficient depends on impact velocity and also material parameters of the impacting bodies (see, for example, the works by Goldsmith [55], and the more recent work of Ramirez et. al. [127]). From a simple integration of motion equation under the action of a Hertzian force (see Johnson [77] for details), it can be shown that the collision times are also dependent on these parameters. The result of this integration, for the contact of two spheres, leads to the following expressions for the maximum contact deformation at the end of the compression phase, and for the total collision duration:

$$\delta_n^{max} = \left(\frac{15mv_n^2}{16\sqrt{R}E^*}\right)^{2/5}, \quad \delta t = 2.94\frac{\delta_n^{max}}{v_n} = 2.87\left(\frac{m^2}{RE^{*2}v_n}\right)^{1/5} \tag{2.59}$$

Since the underlying force considered is purely elastic, the compression and recovery durations should be equal (each being equal to $\delta t/2$ from the expression above). For an inelastic contact this is no longer the case. To include the effects of inelasticity the arguments presented in Johnson [77] for the case of an elastic perfectly plastic contact are re-derived here. From a consideration of rigid fully plastic loading, it can be shown that the required average contact pressure for contact between two spherical bodies is $p_m = 3.0Y$. It can also be shown from a calculation of the initiation of yield that the required average contact pressure for yield onset is $p_m = Y$. In between these two limits of the contact pressure, there exists an elasto-plastic regime, where contact pressure rises from the yield limit and can go up to the point where fully plastic, uncontained flow begins. Using this, we generalize the calculations by Johnson [77], by assuming a maximum contact pressure $p_m = \alpha Y$, and using the following expressions thereafter to get the compliance relation $F_c^n(\delta_n)$:

$$\delta_n = \frac{\pi^2 R}{4E^{*2}}\left(\frac{3}{2}p_m\right)^2 = \frac{9\pi^2\alpha^2}{16}\frac{RY^2}{E^{*2}} \tag{2.60}$$

$$F_c^n = \frac{\pi^3 R^2}{6E^{*2}}\left(\frac{3}{2}p_m^2\right)^3 = \frac{27\pi^3\alpha^3}{48}\frac{R^2Y^3}{E^{*2}} \tag{2.61}$$

For collision durations that are small compared to other dynamic time-scales, the definition of the restitution coefficient used in the previous section reduces to the Newtonian form of $v_{cn}(t+\delta t)/v_{cn}(t)$, and for this case, following the calculation of the compression and recovery work, and using $p_m = \alpha Y$ instead of $3Y$, we can obtain the following for the restitution coefficient:

$$e^2 = \frac{v_{cn}(t+\delta t)^2}{v_{cn}(t)^2} = \frac{3\pi^{5/4}4^{3/4}}{10}\left(\frac{\alpha Y}{E^*}\right)\left(\frac{\frac{1}{2}mv_{cn}(t)^2}{\alpha Y R^3}\right)^{-1/4}$$
$$\Rightarrow e = 1.88\alpha^{5/8}\sqrt{\frac{Y}{E^*}}\left(\frac{\frac{1}{2}mv_{cn}(t)^2}{YR^3}\right)^{-1/8} \tag{2.62}$$

Although a value of $\alpha = 3$ for yielding is realistic for most metals, it has been shown that for other materials this number may differ - for example, Wilsea et. al. [166] shows that for foams and porous ceramics, α is often equal to unity. Therefore, the introduction of this parameter provides more flexibility in terms of material types being modeled. The collision will involve plastic deformations only beyond a threshold level of impacting energy of the particle. Following again the approach in Johnson [77], and generalizing the mean pressure required to initiate yielding to be $p_m = \alpha_Y Y$, we can obtain the following expression for the limiting impact velocity:

$$\frac{1}{2}mv_Y^2 = \left[\left(\frac{2\pi}{3}\right)^5\left(\frac{3}{4}\right)^4\frac{2}{5}\alpha_Y^5\right]\left(\frac{R^3Y^5}{E^{*4}}\right) = 5.1\alpha_Y^5\left(\frac{R^3Y^5}{E^{*4}}\right) \tag{2.63}$$

For impact with energies higher than this threshold, the collision times can be given by the same expressions as presented in the original derivation by Johnson - that is:

$$\delta t_1 = \sqrt{\frac{\pi m}{8R\alpha Y}} \text{ and } \delta t - \delta t_1 = 1.2e\delta t_1 \tag{2.64}$$

This provides a consistent model for incorporating the material properties and the impact severity into the contact forces between the colliding bodies. A comparison of obtained values of restitution coefficients for a few combinations of materials obtained using this model has been presented in Figure 2.3.

2.5 Regularization of stick-slip friction

The classical Coulomb stick-slip friction model in rigid body dynamics has an inherent discontinuity, which, along with often found discontinuities in velocities in rigid body dynamics (for example, in rigid body impact) can lead to paradoxical results in many cases - a classical example being that of Painleve's paradoxes. The interested reader is referred to the work by Klarbring [83] for a discussion on an example of non-uniqueness and non-existence of solutions for quasi static problems with Coulomb friction law, the work by Genot & Brogliato [54] for some recent discussion on Painleve's paradoxes. There have been a variety of different approaches that have been proposed to tackle the inherent discontinuities - and an extensive

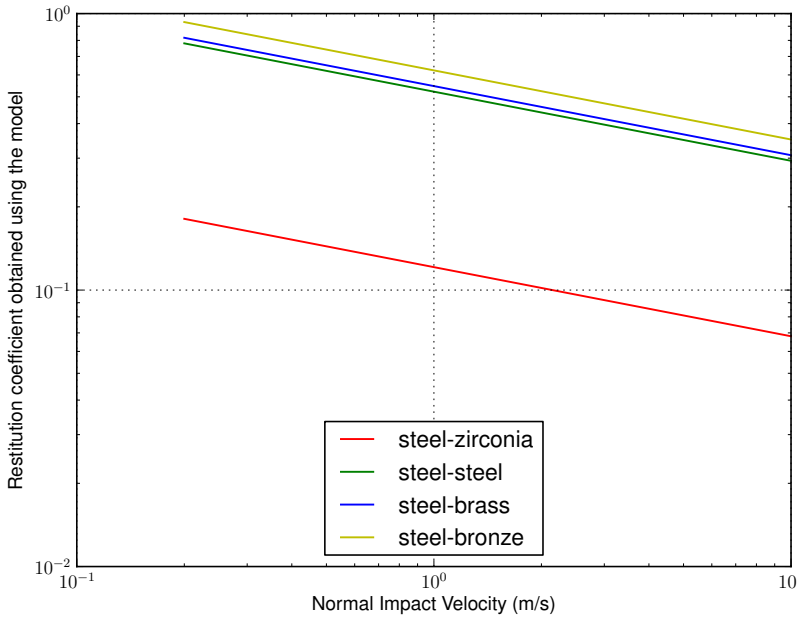

Figure 2.3: *A comparison of restitution coefficients obtained using the model presented in Equation 2.62 for different material combinations, demonstrating the impact velocity dependence*

review of the techniques available can be found in Stewart[145]. The latest developments, as discussed in the review, incorporate the idea of impulsive forces in rigid body dynamics as measures or distributions instead, and the idea of combining the rigid body contact problem with an area of convex analysis called the Linear Complementarity Problem (for mathematical foundations of the method see the text by Murty [113]). The formulation of contact with Coulomb friction as a linear complementarity problem has also been extensively discussed in some of the earlier works on the topic by Moreau [108], and more recently in Raous et. al. [129] where the formulations are extended to adhesive contacts as well. The implementation of such a formulation into the time-discretized motion equations for a system of particles can be a complex task - and has been discussed in the review by Stewart [145]. Further issues may arise with multiple particles undergoing simultaneous contacts - an issue which has been also explored by Chatterjee & Ruina [24], and Chatterjee [25]. For loosely flowing particulate systems, with non-enduring contacts, the exact determination of stick-slip friction in an impulse-momentum balance type contact formulation can be replaced by a simple regularization of the discontinuous Coulomb friction law. Such regularized friction models can lead to robust numerical methods for integrating the motion equations. As was mentioned earlier, for systems of flowing particles with non-enduring contacts, the system behavior is not significantly dependent on the exact stick-slip nature of the contact friction. Thereby, a complete formulation for the complementarity problem for contact friction has not been the focus during the development of the libraries for the dissertation. Discussions

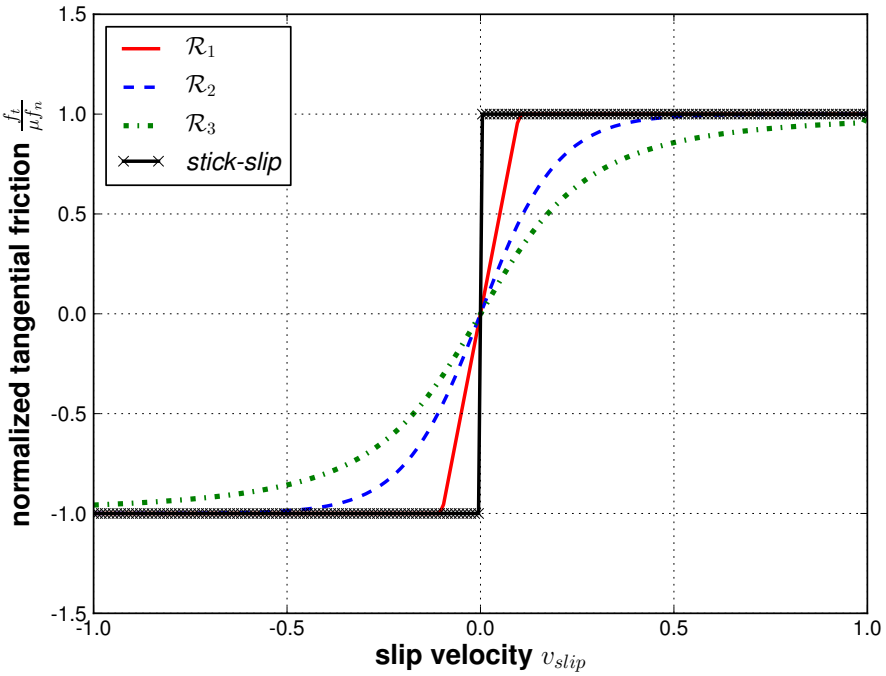

Figure 2.4: *A comparison of various regularization models for Coulomb stick-slip friction that can be used in numerical calculations*

on the models for regularized Coulomb friction can be found in the works by Oden & Pires [116], and by Wriggers [167], and in general, the friction force can be given by:

$$\langle f_T \rangle = \mu \mathcal{R}\left(v_{slip,t}\right) \parallel f_N \parallel \tag{2.65}$$

where $\mathcal{R}\left(v_{slip,t}\right)$ is a regularization function that approximates the discontinuity of the stick-slip criteria. Some possible forms of the regularization function $\mathcal{R}$ can be given as follows:

$$\mathcal{R}_1\left(v_{slip,t}\right) = \begin{cases} -1 & \forall v_{slip,t} < \epsilon \\ \dfrac{v_{slip,t}}{2\epsilon} & \forall -\epsilon \leq v_{slip,t} \leq \epsilon \\ 1 & \forall v_{slip,t} > \epsilon \end{cases} \tag{2.66}$$

$$\mathcal{R}_2\left(v_{slip,t}\right) = \tanh\left(\frac{v_{slip,t}}{\epsilon}\right) \tag{2.67}$$

$$\mathcal{R}_3\left(v_{slip,t}\right) = \frac{v_{slip,t}}{\sqrt{v_{slip,t}^2 + \epsilon^2}} \tag{2.68}$$

The regularization models presented here have been compared in Figure 2.4. It is noted that in all models, smaller values of ϵ will be closer to the stick-slip approximation.

2.6 Adhesive and near-field effects

2.6.1 Adhesive contacts between macroscopic, nearly rigid particles

For many applications involving particle contacts, the near-field and adhesive forces significantly affect inter-particle contact interactions. Important examples include agglomeration and clustering of particles in a flow, and particulate deposition processes, where a quantification of the adhesive forces during contact becomes critical to the understanding of process physics. The interactions between molecules that leads to such phenomena are typically characterized by an appropriately modeled interaction potential $U(\mathbf{r})$ - and the corresponding forces can then be obtained using $\mathbf{F}_{adh} = -\nabla U$. Considering now two macroscopic particles, which are composed of a large number of molecules - the net interaction energy between the particles can then be computed by summing over all possible interactions between the molecules in the individual particles. The general form of this integration can be written as:

$$U_{adh} = \int_{\mathcal{V}_1} d\mathcal{V}_1 \int_{\mathcal{V}_2} d\mathcal{V}_2 \rho_{c1}\rho_{c2} U(\mathbf{r}) \tag{2.69}$$

$$\mathbf{F}_{adh} = \int_{\mathcal{V}_1} d\mathcal{V}_1 \int_{\mathcal{V}_2} d\mathcal{V}_2 \rho_{c1}\rho_{c2} \mathbf{F}(\mathbf{r}) \tag{2.70}$$

where the integrations are done over the volumes $\mathcal{V}_1$ and $\mathcal{V}_2$ of the two bodies with molecule densities ρ_{c1} and ρ_{c2} respectively. The earliest calculations for two rigid spheres using the London Van Der Waals potential form $U(r) = \frac{-C}{r^6}$ was performed by Bradley [17], and later modified slightly by Hamaker [63]. Hamaker's famous calculation for two spheres of radii R_1 and R_2 respectively, separated by a distance D, provides the following expression for the macroscopic interaction energy:

$$U(d) = -\frac{A}{6}\left[\frac{2R_1R_2}{(2R_1+2R_2+d)\,d} + \frac{2R_1R_2}{(2R_1+d)\,(2R_2+d)} + \log\frac{(2R_1+2R_2+d)\,d}{(2R_1+d)\,(2R_2+d)}\right] \tag{2.71}$$

where A is known in the literature as the 'Hamaker constant', and from the derivations it can be shown that $A = \pi^2 C \rho_{c1}\rho_{c2}$. For further mathematical details on the estimation of macroscopic interaction forces for various different cases, the interested reader is referred to the extensive discussions presented in the text by Isarelachvili [73].

In order to find the interaction energy due to any other form of potential, Equation 2.69 has to be numerically integrated. However, particularly for the case of calculating interaction forces and energies between spheres separated by a distance d such that $R_1, R_2 \gg d$, an important result exists due to the work by Derjaguin [32] (see also the discussion in Israelachvili [73] for details). The result, referred to as the *'Derjaguin approximation'*, states that the interaction force between two spheres, for any choice of potential $U(r)$, can be related to the interaction energy between two semi infinite planes as follows:

$$\parallel \mathbf{F}(d)_{spheres} \parallel = 2\pi R U(d)_{planes} \tag{2.72}$$

where R is the effective radius, and for most common potential choices, the integration to obtain $U(d)_{planes}$ is easier to compute than that for spheres. An interesting conclusion that can be drawn from this is the relation between interaction forces and surface energy γ. If we assume that two spheres are in contact, then the actual separation length-scale between the two will be of the order of molecular separation. Representing this separation by ϵ_0, the energy of interaction $U(\epsilon_0) = -2\gamma$, thereby giving:

$$\parallel \mathbf{F}(\epsilon_0) \parallel = -4\pi\gamma R \tag{2.73}$$

The surface energy for creating an interface by bringing two surfaces in contact can be estimated using a simple combination law as follows:

$$\gamma_{12} = \gamma_1 + \gamma_2 - 2\sqrt{\gamma_1\gamma_2} = \left(\sqrt{\gamma_1} - \sqrt{\gamma_2}\right)^2 \tag{2.74}$$

From the aforementioned definition of surface energy in terms of interaction energy at molecular separations, a direct relation between the Hamaker constant a and the surface energy γ can be easily constructed using the interaction energy between two flat surfaces:

$$U_{planes}(\epsilon_0) = -\frac{A}{12\pi\epsilon_0^2} = -2\gamma \Rightarrow \gamma = \frac{A}{24\pi\epsilon_0^2} \tag{2.75}$$

This is a useful relation for us to now embark on some detailed discussion on evaluating the Hamaker constants to account for effect of temperature and non-binary interactions with surrounding particles.

2.6.2 Detailed theoretical discussions on Hamaker constants

The Van Der Waals force between polar molecules is the most important near-field interaction force in a wide range of applications. In reality, this is a combination of three distinct types of interactions (1) the 'induction' force for polar molecules, (2) the 'orientation' force for dipoles induced, and (3) the 'dispersion' force. Consequently, the simple pairwise addition of Van Der Waals forces, will not always provide the correct interaction energies, since

the influence of neighboring molecules on the pairwise addition and influence of the medium in which the pair resides have to be considered. To take into account these aspects, the forces between macroscopic bodies treated as continuum were presented by Lifshitz [87] via the Lifshitz theory of Van Der Waals forces. For detailed reviews on calculating interaction energies using the Lifshitz theory, the interested reader is also referred to Israelachvili [72], Bergstrom [12], Parsegian & Ninham [117], and Visser [160].

The expressions derived in the previous section for the interaction forces and energies will still remain the same when the Lifshitz theory is used - but the Hamaker constants will change, and the effect of temperature, and presence of a medium between particle pair are all incorporated through a detailed calculation of the Hamaker constant A. To present the results for A based on Lifshitz theory, we consider a pair of particles indexed as 1 and 2 respectively, to be interacting across a medium indexed by 3, and the resulting expression is given as follows:

$$A = \pi^2 C \rho_{c1} \rho_{c2} = \frac{3}{2} k_B T \sum_{n=0,1,2,\cdots}^{\infty} \left[\frac{\epsilon_1(i\nu_n) - \epsilon_3(i\nu_n)}{\epsilon_1(i\nu_n) + \epsilon_3(i\nu_n)}\right] \left[\frac{\epsilon_2(i\nu_n) - \epsilon_3(i\nu_n)}{\epsilon_2(i\nu_n) + \epsilon_3(i\nu_n)}\right] \tag{2.76}$$

$$\approx \frac{3}{4} k_B T \left(\frac{\epsilon_1 - \epsilon_3}{\epsilon_1 + \epsilon_3}\right) \left(\frac{\epsilon_2 - \epsilon_3}{\epsilon_2 + \epsilon_3}\right) + \frac{3\hbar}{4\pi} \int_{\nu_1}^{\infty} \left(\frac{\epsilon_1(i\nu) - \epsilon_3(i\nu)}{\epsilon_1(i\nu) + \epsilon_3(i\nu)}\right) \left(\frac{\epsilon_2(i\nu) - \epsilon_3(i\nu)}{\epsilon_2(i\nu) + \epsilon_3(i\nu)}\right) \tag{2.77}$$

where ϵ_j is the static dielectric constant for the j'th entity, and $\epsilon(i\nu)$ is the corresponding dielectric constant values at imaginary frequencies. Following the discussion in Israelachvili [73], we use the fact that the variation of the dielectric constant ϵ_j with frequency is similar to that of the atomic polarizability, and can write the dielectric constant $\epsilon(\nu)$ as:

$$\epsilon(\nu) = 1 + \frac{\text{constant}}{1 - i\nu/\nu_{rot}} + \frac{\text{constant}}{1 - \nu^2/\nu_e^2} \tag{2.78}$$

following which, after some algebra and introducing the definition of the refractive index n_j of the j'th entity, we can write:

$$\epsilon(i\nu) = 1 + \frac{\epsilon - n^2}{1 + \nu/\nu_{rot}} + \frac{n^2 - 1}{1 + \nu^2/\nu_e^2} \tag{2.79}$$

where ν_{rot} is the molecular rotational relaxation frequency, usually in the microwave frequency range or lower ($< 10^{12} Hz$). The term ν_e refers to the main electronic absorption frequency in the ultraviolet range, usually around $3 \times 10^{15} Hz$. It can be shown that $\nu_1 \approx 4 \times 10^{13} Hz \gg \nu_{rot}$ thereby making the third term in Equation 2.79 dominant over the second, and the latter can be neglected. Plugging this expression for $\epsilon_j \approx 1 + \frac{n_j^2 - 1}{1 + \nu^2/\nu_e^2}$ into the integral in Equation. 2.77 we get the final expression for the Hamaker constant to be:

$$A = A_{\nu=0} + A_{\nu>0} \tag{2.80}$$

$$= \frac{3}{4}k_B T \left(\frac{\epsilon_1 - \epsilon_3}{\epsilon_1 + \epsilon_3}\right)\left(\frac{\epsilon_2 - \epsilon_3}{\epsilon_2 + \epsilon_3}\right) + \frac{3\hbar\nu_e}{8\sqrt{2}} \frac{\left(n_1^2 - n_3^2\right)\left(n_2^2 - n_3^2\right)}{\sqrt{\left(n_1^2 + n_3^2\right)\left(n_2^2 + n_3^2\right)}\left[\sqrt{n_1^2 + n_3^2} + \sqrt{n_2^2 + n_3^2}\right]} \tag{2.81}$$

This provides a more general theory for calculating interactions for different temperatures, for different geometries, and for bodies interacting across different media. We remark also that the estimate using Equation 2.76 is more exact, and when required, can be solved numerically as has been presented in the work by Bergstrom [12].

2.6.3 Deformable contacts and Greenwood's mapping

The mechanics of contacting macroscopic particles when the particles undergo significant levels of deformation will involve the combined analysis of the elastic forces and adhesive forces due to Van Der Waals type effects. For contact scenarios where a detailed resolution of the deformations are desired, a rigorous treatment of the adhesive contact mechanics has been provided by Johnson et. al. [79] in terms of their theory referred to as the 'Johnson-Kendall-Roberts (JKR) theory'. According to this theory, the total deformation during contact will increase due to the adhesive forces pulling the surfaces of the two macroscopic particles together in the vicinity of the contact. The net contact area can then be given as:

$$a_c^3 = \frac{3R}{4E^*}\left[F + 3\pi\gamma R + \sqrt{6\pi\gamma RF + (3\pi\gamma R)^2}\right] \tag{2.82}$$

where $F = F_n$ in the context of the discussions presented in Section 2.2. It is evident that for $\gamma = 0$ we get back the Hertzian contact case as discussed in Section 2.2. When the applied external force F is zero, the JKR theory gives a non-zero contact area a_0 given by:

$$a_0 = \left(\frac{9\pi R^2\gamma}{2E^*}\right)^{1/3} \tag{2.83}$$

This indicates that the equilibrium between adhesive forces and elastic forces in the material continua together lead to a deformed configuration even in the absence of any external loading. As the external loading starts separating the particles, a tensile force develops at the contact region and it rises until a cut-off value of the force, when complete detachment of the particles occur (see Figure 2.5 for an illustration). This is called the 'pull-off' or 'adhesive' force, and is given by:

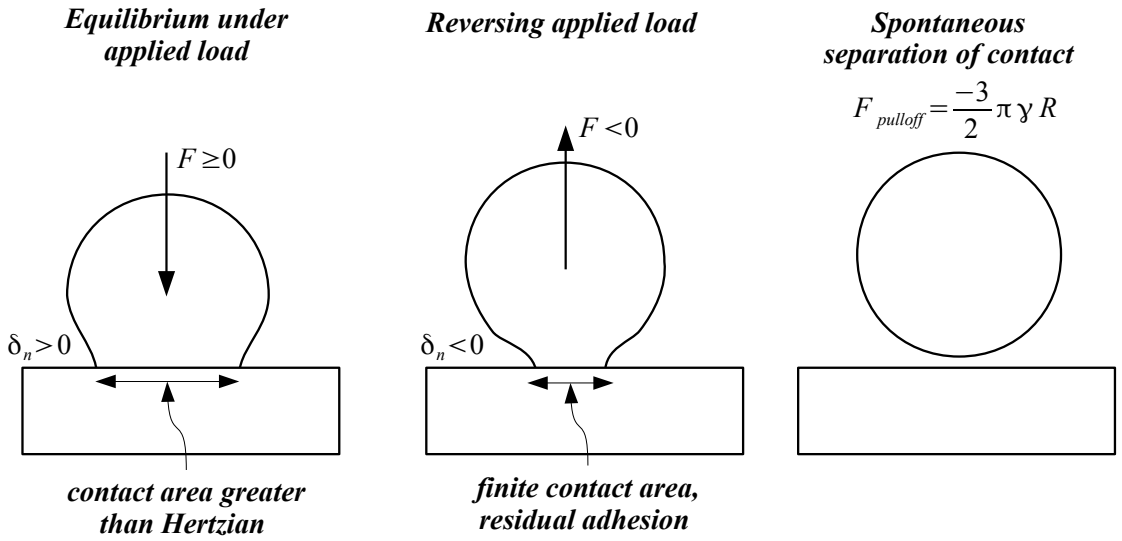

Figure 2.5: *Sequence of schematics illustrating the typical force-deformation behavior seen of adhesive contact predicted by the JKR theory*

$$F_{adh} = -\frac{3}{2}\pi\gamma R \tag{2.84}$$

The corresponding value of the contact area is then given by:

$$a_s = \frac{a_0}{4^{1/3}} \tag{2.85}$$

after which the contact area abruptly becomes zero. During the process of the contact deformations, the net deformation between the centerline δ_n is related to the contact area a_c by the following relation:

$$\delta_n = \frac{a_c^2}{R}\left[1 - \frac{2}{3}\left(\frac{a_0}{a_c}\right)^{3/2}\right] \tag{2.86}$$

An alternative theory to the adhesive contact deformations was presented by Derjaguin et. al. [33] which is commonly refererred to as the 'Derjaguin-Muller-Toporov (DMT) theory'. The basis of this theory is the consideration that the surface forces do not modify the deformed profile obtained from a Hertzian contact solution, and the attractive surface forces all lie outside of the contact area. The original work by Derjaguin et. al. [33] was later modified by Muller et. al. [110] and further discussions in great detail were provided in Muller et. al. [111] - with the primary idea being that of a direct calculation of the force as opposed to an energy based thermodynamic approach presented in the original work. Assuming that the Hertzian deformation remains unchanged during contact, the deformation profile is given

by (see Johnson [77] and Muller et. al. [110] and also the discussions presented in Pashley [118]):

$$H(r, a_c) = \frac{1}{\pi R}\left[a_c\left(r^2 - a_c^2\right)^{1/2} - \left(2a_c^2 - r^2\right)\arctan\left[\frac{r^2}{a_c^2} - 1\right]^{1/2}\right] + \epsilon_0 \tag{2.87}$$

and the force can be calculated directly as:

$$F_{surf} = 2\pi\int_{a_c}^{\infty}\frac{d}{dH}\left[\phi(H(r, a_c)\right] r dr \tag{2.88}$$

$$\frac{d\phi(H)}{dH} = \frac{8\Delta\gamma}{3\epsilon_0}\left[\left(\frac{\epsilon_0}{H}\right)^3 - \left(\frac{\epsilon_0}{H}\right)^9\right] \tag{2.89}$$

where the Equation 2.89 refers to the suitably normalized form of the Lennard Jones potential used in the calculations by Muller at. al. ([110] and [111]). Recalling now from Section 2.2 the expression for Hertzian contact force, the total applied force on the particles can be given now to be:

$$F(a_c) = F_{Hertz}(a_c) - F_{surf}(a_c) \tag{2.90}$$

$$= \frac{4E^* a_c^3}{3R} - 2\pi\int_{a_c}^{\infty}\frac{d}{dH}\left[\phi(H(r, a_c)\right] r dr \tag{2.91}$$

and a_c is related to the deformation δ_n using the Hertzian contact geometry relation $a_c^2 = R\delta_n$. The Equation 2.91 can now be numerically integrated to provide the complete force deformation behavior. Furthermore, as mentioned in Pashley [118] amongst others, for small deformations the total surface force is given to be $2\pi R\gamma$ which is what the original work had predicted. For other cases, the behavior is more realistic and correct. Henceforth, we shall refer to the Equation 2.91 as the DMT theory - instead of any references to the original work. Furthermore, as discussed in many references including Pashley [118], and Greenwood [58] amongst others, the force value predicted by the original work to be $2\pi R\gamma$ is nothing but the result of Equation 2.72 - and hence does not contribute any new result other than representing the results for adhesive forces between nearly rigid macroscopic bodies.

The comparative analysis of these two theories was further extended by Maugis [95] using an analysis based on stresses at a crack tip approximated by the Dugdale model. The details of this theory is not presented here for the sake of brevity, and the reader is referred to the original article cited herein. However, their analysis, along with the discussion presented by Pashley [118], Greenwood [58], and Johnson & Greenwood [78] all refer to the formulation of a common non-dimensional parameter to compare the various approaches and thereby

decide on the regimes where individual approaches are applicable. The existence of such a parameter was originally discussed in the work by Tabor [150], following which Muller et.al.[110] used a modified form of the same parameter to expand upon the calculations for DMT theory. Further validation of the role of such a parameter that combines the material elastic properties, size of the macroscopic bodies in contact, and their surface energies has been presented also by Pashley [118], Maugis [95], Attard & Parker [5], and Greenwood [58] amongst many others. The correct choice of the parameter to be used in any simulation work is complicated by the many different versions that are found in the literature - and the work by Greenwood [58] provides a list of many of these variants as an appendix to their article. For the present discourse, we will be using the slightly modified form of the original variant proposed by Tabor - and call it the Tabor coefficient μ_T given as follows:

$$\mu_T = \left[\frac{R\Delta\gamma^2}{E^{*2}\epsilon_0^3}\right]^{1/3} \tag{2.92}$$

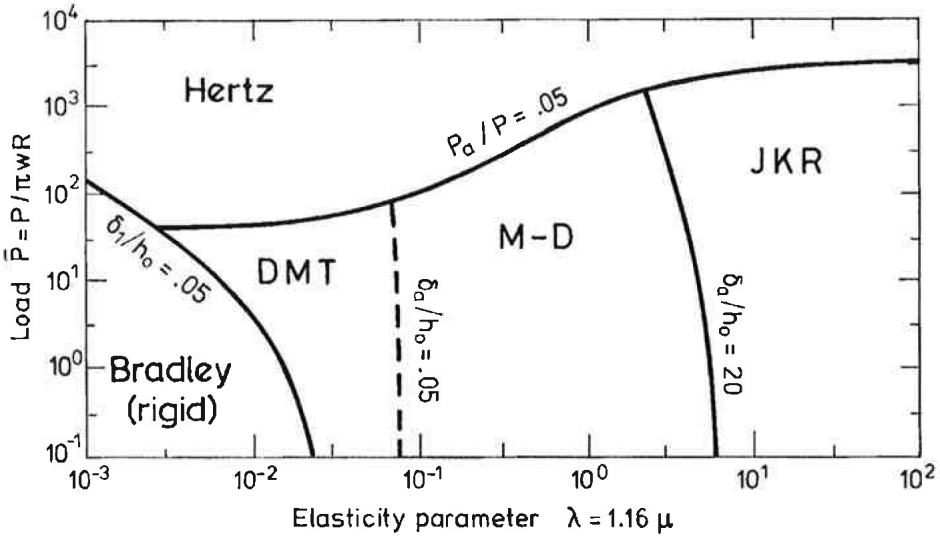

Figure 2.6: *The mapping of adhesion models with varying load intensities and material elasticity parameters as presented by Johnson & Greenwood (figure reproduced from the original article).*

Using this coefficient, Johnson & Greenwood [78] provides a very useful mapping of the different theoretical approaches for contact between two macroscopic bodies, the original form of which has been re-printed here in Figure 2.6. The map provides the regime of application of the Hertzian approach, the rigid-sphere adhesion approach (which is referred to as 'Bradley' in the Figure), and the JKR theory. The DMT theory is considered to be almost equivalent to the rigid-sphere approach - since for small deformation of the macroscopic bodies the theory predicts forces more accurately. Therefore, the regime of application of

DMT theory is presented to be adjacent to the Bradley theory. The intermediate regime, for low impact forces as compared to adhesive forces (low $\bar{P}$ from the map) is best described using the generalized calculations presented by Maugis Dugdale. This classification is not really rigid, and from our survey of the literature, we interpret this as a general qualitative guideline for evaluating the applicability of a theory to a specific problem instead.

2.7 Electromagnetic effects

2.7.1 Force on a charged particle

A description of the forces on a charged particle or computational element is presented here with the assumption that the particle sizes are small compared to the characteristic length-scales of the problem - such that the particles can be treated as lumped charges with their center of mass being the same as the center of charge (that is, there is no variation of charge within the material extent of each particle). With this assumption, the force on a charged particle due to externally applied electric and magnetic fields (of strengths $\mathbf{E}$ and $\mathbf{B}$ respectively) is given by the classical Lorentz force:

$$\mathbf{F}_{em} = q\left(\mathbf{E} + \mathbf{v} \times \mathbf{B}\right) \tag{2.93}$$

The individual charged particles in a collection of particles can interact with each other via Coulomb interactions as well, an efficient treatment of which poses considerable challenges. This particular aspect has been a topic of much discussion - most notably amongst molecular dynamics researchers attempting to study molecular systems and condensed matter. The interaction energy for an N-body system of charged particles is given by:

$$U\left(\mathbf{r}_1, \mathbf{r}_2, \cdots, \mathbf{r}_N\right) = \frac{1}{2}\sum_{i}^{N}\sum_{j\neq i} N\frac{q_i q_j}{|\mathbf{r}_i - \mathbf{r}_j|} \tag{2.94}$$

which amounts to an $\mathcal{O}\left(N^2\right)$ calculation, and is prohibitively expensive for systems with large number of particles. The contributions of the long-range effects of Coulomb interactions are crucial for the behavior of such systems - for a broad review of the various computational techniques available to resolve these interactions see Sagui & Darden [136]. The most prominent of these techniques is that of Ewald summation for periodic systems wherein the interaction potential is decomposed into a short-range and long-range components, and the long-range terms are calculated in the Fourier space (see Frenkel & Smit [52] for a comprehensive discussion on such techniques, and Toukmaji & Board [156] for a survey of Ewald and fast multipole method based techniques). An alternative to the non-trivial algorithmic implementation of such summations that is often used is to truncate the interaction potential by multiplying $U(\mathbf{r}_i, \mathbf{r}_j)$ with a truncation function $\mathcal{T}(\mathbf{r}_i, \mathbf{r}_j)$ that truncates the potential

beyond a chosen truncation distance (characterized here by r_c) so as to calculate the interactions over a more restricted region in space. A discussion of such techniques can be found in Brooks et. al. [71] for example, and three commonly used variants of the functional form of the truncation function are presented as follows:

$$\mathcal{T}\left(|\mathbf{r}_i - \mathbf{r}_j|\right) = \begin{cases} 1 & |\mathbf{r}_i - \mathbf{r}_j| \leq r_c \\ 0 & |\mathbf{r}_i - \mathbf{r}_j| > r_c \end{cases} \tag{2.95}$$

$$\mathcal{T}\left(|\mathbf{r}_i - \mathbf{r}_j|\right) = \begin{cases} \left[1 - \dfrac{|\mathbf{r}_i - \mathbf{r}_j|}{r_c}\right] & |\mathbf{r}_i - \mathbf{r}_j| \leq r_c \\ 0 & |\mathbf{r}_i - \mathbf{r}_j| > r_c \end{cases} \tag{2.96}$$

$$\mathcal{T}\left(|\mathbf{r}_i - \mathbf{r}_j|\right) = \begin{cases} \left[1 - 2\dfrac{\left(|\mathbf{r}_i - \mathbf{r}_j|\right)^2}{r_c}\right] & |\mathbf{r}_i - \mathbf{r}_j| \leq r_c \\ 0 & |\mathbf{r}_i - \mathbf{r}_j| > r_c \end{cases} \tag{2.97}$$

For the function presented in Equation. 2.95 there is a discontinuity in both the potential and its derivative, for Equation. 2.96 the potential is zero at the truncation distance r_c but is continuous, and for Equation 2.97 the derivative is zero at r_c and is continuous. The relative performance of truncation based approaches, and Ewald summation approaches have been presented in the works of Bader & Chandler [7] and York et. al. [169] amongst others - and for atomic or molecular systems the latter has been shown to be more accurate. We remark here that, for the kinds of discrete, macroscopic particle systems being discussed in this work, the thermodynamic nature is essentially different from that of a molecular system. Such systems often are driven by forces that are more dominant than Coulomb interactions - thereby making the use of a truncated potential a viable option. Moreover, the requirement of periodic boundary conditions - as is the case with many Fourier space based summation techniques - might not be satisfied with many such systems (for example, a flowing spray of powder particles).

Particularly we illustrate the aspect of relative dominance of Coulomb interactions through an example where we compare the Lorentz force with Coulombic interactions. Mathematically speaking, the dominance of Lorentz forces entails the observation of a scaling argument between the relative magnitudes of these two forces (assuming the magnetic field contribution for illustration):

$$q|V|B >> \frac{q^2}{4\pi\epsilon r^2} \tag{2.98}$$

where r is a characteristic inter-particle separation for the ensemble of particulates. It can be assumed that $r = \gamma d_p$, where γ is an appropriate scaling measure of the separation between

particles in terms of particle sizes. For most practical applications $d_p \approx \mathcal{O}(20-80\mu m)$, and $q \approx \mathcal{O}(10-100\mu C)$. Plugging these orders of magnitude in, it can be seen that the argument on the relative magnitudes will hold only for very small γ, or very high $|V|$. The factor γ correlates inversely to the volume-fraction of a particulate system - which means that for a low volume-fraction ensemble of particles, the average inter-particle separation is high. This indicates that the Coulomb interactions are weaker for low-volume fraction ensembles traveling at high-velocities - which is precisely the regime that many of the commercial applications of loosely flowing particulates fall under.

2.7.2 Magnetic particles interacting with an applied magnetic field

Many applications of flowing particulate media may involve interactions between magnetic particles and an applied magnetic field. We present here a simple derivation of an expression for this interaction force that can then be easily incorporated into the hierarchical modeling framework. We begin with the Ampere force acting on a current loop carrying current I in an external magnetic field of strength $\mathbf{B}$, which is given by:

$$\mathbf{F}_{loop} = I \oint d\mathbf{l} \times \mathbf{B} \tag{2.99}$$

A plane current loop of sufficiently small size is referred to as an elementary current loop, and its behavior is described using the Magnetic moment μ_m, defined as follows:

$$\mu_m = IS\mathbf{n} \tag{2.100}$$

where I is the current carried by the loop, S is the area bound by the loop, and vector $\mathbf{n}$ is the normal to the surface bounded by the loop. Using the definition of the force in Equation. 2.99, and Equation. 2.100, the total potential energy and force of interaction of an elementary loop with a non-uniform magnetic field can be given by:

$$U_m = -\mu_m \cdot \mathbf{B} \tag{2.101}$$

$$\mathbf{F} = \nabla\left(\mu_m \cdot \mathbf{B}\right) = |\mu_m| \frac{\partial \mathbf{B}}{\partial n} \tag{2.102}$$

For a material, the magnetization vector is defined to be the density of all the vector magnetic moments in a magnetic material at a given point, and mathematically, is represented using the following formulation:

$$\mathbf{M} = \frac{\sum_{\delta V} \mu_m}{\delta V} \tag{2.103}$$

The presence and orientation of these elementary magnetic moments in a material gov-

erns the material bulk behavior in the presence of a magnetic field. For example, diamagnetic materials are such that in the absence of an external magnetic field there are no magnetic moments at the molecular level. When introduced into a magnetic field, expand this formulation further, the integral form of Ampere's law is written for a contour around a material with a collection of such magnetic moments as follows:

$$\oint_C \mathbf{B} \cdot d\mathbf{l} = \underbrace{\mu_0 \int_S \mathbf{J} \cdot d\mathbf{S}}_{\text{conduction current}} + \underbrace{\mu_0 \oint_C \mathbf{M} \cdot d\mathbf{l}}_{\text{magnetization current}} \tag{2.104}$$

$$\oint_C \left(\frac{\mathbf{B}}{\mu_0} - \mathbf{M} \right) \cdot d\mathbf{l} = \mu_0 \int_S \mathbf{J} \cdot d\mathbf{S} \tag{2.105}$$

The magnetic field intensity $\mathbf{H}$ is defined from above as:

$$\mathbf{H} = \frac{\mathbf{B}}{\mu_0} - \mathbf{M} \tag{2.106}$$

For most materials the magnetization vector is a linear function of the local magnetic field vector $\mathbf{B}$, and the relationship is defined in terms of the magnetic susceptibility χ_m as:

$$\mathbf{M} = \chi_m \mathbf{H} \tag{2.107}$$

Furthermore, using the definition of $\mathbf{H}$ as in Equation. 2.106, furthermore we can write:

$$\mathbf{B} = \mu_0 \left(1 + \chi_m\right) \mathbf{H} = \mu_0 \mu_r \mathbf{H} = \mu \mathbf{H} \tag{2.108}$$

where μ_r is the relative magnetic permeability of the material, and μ is the magnetic permeability of the material. For a particle that is small in size (relative to the other dominant length scales of the system) the total magnetic moment can be given as:

$$\sum \mu_m = \mathbf{M} V \tag{2.109}$$

For paramagnetic and ferromagnetic particles, it can be assumed that all of the magnetic dipoles in the material are oriented along th direction of $\mathbf{B}$, following which, using Equation. 2.102, the following expression for the force can be obtained:

$$\mathbf{F}_{mag} = |\mathbf{M} V| \frac{\partial \mathbf{B}}{\partial n} = \left| \frac{\chi_m}{\mu_0 \mu_r} \mathbf{B} V \right| \frac{\partial \mathbf{B}}{\partial n} \tag{2.110}$$

where the definitions of χ_m in Equation. 2.107, and of μ_r in Equation. 2.108 were used to relate the force entirely to the applied external magnetic field $\mathbf{B}$.

2.8 Particles at different temperatures

2.8.1 An energy balance at the particle level

Let us consider the continuum form of the energy balance equation:

$$\rho \frac{De}{Dt} = \mathbf{T} : \nabla \mathbf{v} - \nabla \cdot \mathbf{q} + \rho h \tag{2.111}$$

where, e is the internal energy density of the continuum of the particle, the term $\mathbf{T} : \nabla \mathbf{v}$ is the work done by all the forces in the continuum of the material, $\nabla \cdot \mathbf{q}$ is the total heat flux from the material of the body, and h denotes heat exchange density from a source or a sink. From the discussion on particle level forces as presented here, the total forces acting on the particle can be decomposed into the conservative forces (which include adhesive or surface forces, near-field forces, and electrostatic forces), and dissipative forces (which include frictional forces and viscous drag). In addition, for the rigid body collision model using impulse momentum balance , it is to be noted that the assumption that the particles are rigid is only an idealization - since during the collision, the material continua of colliding particles undergo inelastic deformation, the energy loss due to which is characterized using the restitution coefficient. The sum total of the work done by all these forces can be represented through the mechanical energy balance for the entire particle as below:

$$\Delta KE = \mathcal{W}_{con} + \mathcal{W}_{dis} \tag{2.112}$$

$$\Delta(KE + PE) = \mathcal{W}_{dis} \tag{2.113}$$

where $\mathcal{W}_{con}$ is the work done by all the conservative forces, and $\mathcal{W}_{dis}$ is the work done by all the dissipative forces. The dissipation of this energy can be visualized, at least in parts, to be the generation of heat - and if we make the assumption that the entire dissipated energy is converted into heat, then, writing E as the total internal energy for the particle, and using the mechanical energy balance we can write the following:

$$\Delta E = \Delta \mathcal{H} + \mathcal{Q}\Delta t + \mathcal{S}_{ext}\Delta t \tag{2.114}$$

$$\Delta \mathcal{H} = \Delta \left(KE + PE \right) \tag{2.115}$$

where, $\mathcal{Q}$ is the sum of all heat fluxes from the particle, which may include inter-particle heat exchange between particles of different temperatures, and particle-fluid convective heat transfer, and $\mathcal{S}_{ext}$ is the sum of all external sources and sinks. As a final step towards modeling this energy balance, we represent the internal energy of the particle E in terms of the temperature of the bulk of the particle. This characterization of the entire particle's thermal state with one temperature can be justified on the basis of a non-dimensional parameter

called the Biot number, which captures the ratio of the resistance to heat transfer within the bulk and that to heat transfer across the surface. It is mathematically defined as:

$$Bi = \frac{hL}{K} \tag{2.116}$$

where, h is the convective heat transfer coefficient (which will be explored in more detail in Chapter 3), L is a characteristic length of the body, and K is the thermal conductivity of the body. For small particle length scales, it is evident that the Biot number will also be small, thereby indicating lower resistance to heat transfer across the bulk. Hence, the entire particle can be assumed to conduct heat quickly and the bulk of the body can then be characterized by one temperature. The balance for the energy can then be written as:

$$\Delta(mC\theta) = mC\Delta\theta = \mathcal{Q}\Delta t + \Delta\left(KE + PE\right) + \mathcal{S}_{ext}\Delta t \tag{2.117}$$

We now address the particular aspect of using this energy balance relation in the formulation of a discrete particle simulation framework. This issue needs to be addressed based on considerations of the duration of contact, as was used to categorize various material systems in Figure 1.1 in Chapter 1. For systems with enduring contact (that is $\delta t > \Delta t$), the flux $\mathcal{Q}$ will include the conduction of heat between particles during the entire contact duration, the convection of heat from the particle to the fluid. However, for collisionally dominant systems (that is $\delta t \ll \Delta t$), over the short contact durations, inter-particle thermal conduction will not be a relevant mechanism, and the flux $\mathcal{Q}$ will include contributions due to convection alone. For a single time-step therefore, the forces acting on the particles can be used to update the velocities. Following this, the dissipated energy $\Delta\mathcal{H}$ is calculated from the mechanical energy balance, and used in the overall energy balance in combination with conductive and convective heat flux terms. This therefore motivates a detailed discussion on modeling the flux $\mathcal{Q}$ as a combined sum of contributions from different heat-exchange mechanisms.

2.8.2 Modeling the heat flux

The exchange of heat between particles in a system of particles surrounded by a fluid can be a combination of multiple simultaneous mechanisms - and a simplified modeling of the heat fluxes between particles can therefore become a complicated task. The work by Batchelor & O'Brien[11] address the issue of modeling the heat flux for a collection of static system of particles in enduring, frictionless, elastic contact. Their objective was to obtain the heat fluxes, and thereby, obtain the effective conductivity of the system. The expression they derived, from continuum thermal conduction considerations across the bulk of the contacting particles, for two particles of effective radius R, and conductivity K_p in a fluid (of conductivity K_f) is as follows:

$$\mathcal{Q}_{touch} = \pi K_f \left(T_0 - T_1\right) R \log_e \left(\frac{K_p}{K_f}\right)^2 \tag{2.118}$$

$$\mathcal{Q}_h = \pi K_f \left(T_0 - T_1\right) R \log_e \frac{R}{h} + const. - P(\lambda) \tag{2.119}$$

$$P(\lambda) = \int_0^\infty \frac{f(\sigma)}{\lambda + \sigma^2} 2\sigma d\sigma,\ \sigma = \frac{K_p}{K_f}\frac{r}{R},\ \lambda = \left(\frac{K_p}{K_f}\right)^2 \frac{h}{R} \tag{2.120}$$

where the function $f(\sigma)$ was derived in terms of an integral equation as presented below:

$$f(\sigma) = \int_0^\infty \frac{1 - f(\sigma')}{\lambda + \sigma'^2} I\left(\frac{\sigma'}{\sigma}\right) d\sigma' \tag{2.121}$$

$$I\left(\frac{\sigma'}{\sigma}\right) \approx 2\frac{\sigma'}{\sigma} \text{ as } \frac{\sigma'}{\sigma} \to 0 \tag{2.122}$$

$$I\left(\frac{\sigma'}{\sigma}\right) \approx 2 \text{ as } \frac{\sigma'}{\sigma} \to \infty \tag{2.123}$$

The corresponding expressions for heat exchange over a deformed circular area of contact is also similarly formulated in terms of an integral equation, and the expressions for the total heat flux combines the contributions due to flux across the contact region, and flux across the annular fluid layer immediately around the contact region. For the sake of brevity of the discussion, these expressions are not presented here and the interested reader is referred to the original article. It is evident here that for particles with dissimilar materials would require some form of an effective conductivity value for evaluating the heat flux, and Zhou et.al.[172] suggest the use of $\frac{1}{K_p} = \frac{1}{K_{p1}} + \frac{1}{K_{p2}}$ for the same.

The effect of the impact durations on the heat transfer is further incorporated by Sun & Chen[147], where, using Hertzian contact mechanics principles, the expression for heat exchange between particles due to impact is characterized in terms of the flux $\mathcal{Q}_{ij}$ given by:

$$\mathcal{Q}_{ij} = \frac{0.87\left(T_{0j} - T_{0i}\right) A_c \sqrt{\delta t}}{\left(\rho_1 C_{p1} K_{p1}\right)^{-1/2} + \left(\rho_2 C_{p2} K_{p2}\right)^{-1/2}} \tag{2.124}$$

It is to be noted that the expression in Equation 2.124 was originally derived for low Fourier numbers, which in turn indicate high thermal conductive transport rates. To extend the formulation for more general cases, Sun & Chen[147] provided numerically obtained values for a constant $C_{\mathcal{Q}}$ that can be multiplied with $\mathcal{Q}_{ij}$ as presented in Equation 2.124. In a more detailed, finite element based analysis of heat exchange between particles during

impact, [171] extends this idea and provides an expression for the constant $C_{\mathcal{Q}}$ based on the finite element results as follows:

$$C_{\mathcal{Q}} = \frac{0.435\left(\sqrt{C_2^2 - 4C_1\left(C_3 - Fo\right)} - C_2\right)}{C_1} \tag{2.125}$$

$$C_1 = -2.3\left(\frac{\rho_1 C_{p1}}{\rho_2 C_{p2}}\right)^2 + 8.909\left(\frac{\rho_1 C_{p1}}{\rho_2 C_{p2}}\right) - 4.235 \tag{2.126}$$

$$C_2 = 8.169\left(\frac{\rho_1 C_{p1}}{\rho_2 C_{p2}}\right)^2 - 33.77\left(\frac{\rho_1 C_{p1}}{\rho_2 C_{p2}}\right) + 24.885 \tag{2.127}$$

$$C_3 = -5.758\left(\frac{\rho_1 C_{p1}}{\rho_2 C_{p2}}\right)^2 + 24.464\left(\frac{\rho_1 C_{p1}}{\rho_2 C_{p2}}\right) - 20.511 \tag{2.128}$$

where $Fo = \frac{K_{p1}\delta t}{\rho_1 C_{p1} r_c^2}$ is the particle based Fourier number characterizing the transient heat exchange. The expressions presented by Zhou et.al.[171] can be used as a good approximation for a wide range of transient heat exchange phenomena between dissimilar particles impacting with a finite impact duration δt. In another work aimed at obtaining the effective thermal conductivity of a packed granular bed, Cheng at.al.[26] illustrate the use of Voronoi polyhedra based calculation of particle-particle heat transfer and heat transfer between particle and interstitial fluid. Such an approach would be very suitable for calculations of particle systems primarily in static, enduring contact. Yet another approach towards heat transfer in particle systems has been presented by Hunt[69] where a combination of discrete element simulation techniques and kinetic theory applied to particle systems is used to characterize the effective conductivity of the particulate system. While Hunt[69] does not actually provide expressions for the flux term $\mathcal{Q}$ to be used in Equation 2.117, their approach provides an alternative method of characterizing the heat transfer by means of macroscopic homogenized effective conductivities and diffusivities. In their analysis, they also remark on the dependence of the ratio between discrete element and kinetic theory based values of conductivities on the Biot and Fourier numbers.

An intermediate approach to discrete particle media and continuum field partial differential equations was presented using a network model for packed particles by Siu & Lee[140] which models each particle as an element with a certain thermal resistance. The particles in contact form a network of thermal resistances which can then be solved using ordinary differential equations to obtain the temperature of each particle. The limitations of the requirement that the particles be isothermal is overcome in a similarly motivated approach presented by Feng et.al.([43] and [44]) called the Discrete Thermal Element Method. The method utilizes the analytical integral solution for the temperature distribution in a circle

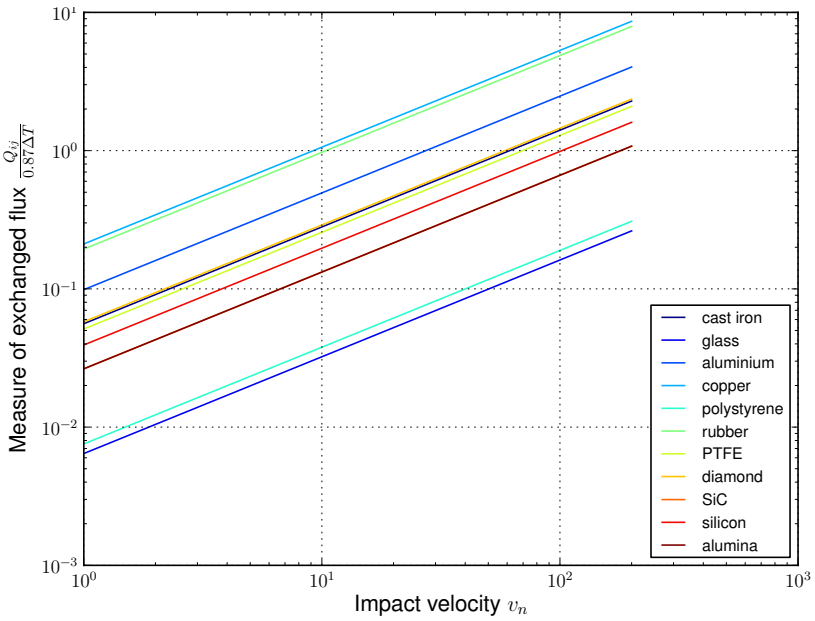

Figure 2.7: *A comparison of heat flux between particles of millimeter radius for different material properties, illustrating how thermal exchange during impact is governed by mechanical parameters.*

with Neumann boundary conditions. The particle or element equations resemble a finite element like discretized system, but with the unknowns being the average temperatures over the contact regions for all the other particles that are in contact with the particle. Such methods have been dominantly used in two-dimensional dense packings of particles, but references in the literature to applying such techniques to three-dimensional problems are rare.

For particulate systems, an alternative approximation to the heat exchange flux between a collection of particles in contact has been presented by Zohdi[179] which makes use of a Fourier law representation of the particle heat fluxes, and performs a discretization of the heat flux based on the particle positions, assuming that for small Biot number the temperature variations within the bulk of the particles is negligible. The generalized form for this flux contribution for particle-particle thermal conduction is given as follows:

$$mC_p\frac{d\theta}{dt} = K_p\sum_{j=1}^{N_c}\frac{\theta_j-\theta_i}{\parallel \mathbf{r}_j-\mathbf{r}_i \parallel}^2 \tag{2.129}$$

where N_c is the number of particles in contact, and the summation is done over all particle contact pairs. In another work by the same author, referred here as Zohdi[175], additional mechanisms of heat exchange are incorporated into the model for the flux represented in Equation 2.129.

Chapter 3

Fluid-Particle Interaction Modeling

3.1 Introduction

Particle laden fluid flows are ubiquitous in a wide spectrum of applications that include transport systems, fluidized beds, manufacturing and materials processing technologies, energy conversion and propulsion technologies, sprays, jets and slurry flows. A broad overview of industrial applications of particle-laden, multi-phase flows can be found in Crowe et.al.[29]. Primarily such flows comprise of a carrier fluid medium in which small (compared to the fluid flow scales) particles, droplets, or bubbles are dispersed - hence the alternative term dispersed multiphase flows. Such flows can appear in multiple regimes dependent on the volume fraction of the particles, Φ_p, with varying levels of phase interactions. They can also be categorized into flows where the background fluid is laminar and where it is turbulent. The complex physics of turbulence, along with such interactions, lend formidable complexity to the physics of particle-laden turbulent flows. The main advances in both experimental and computational work in particle laden flows have been in the two-way coupling regime of dilute suspensions as a result of the computational complexity in evaluating dense suspensions and the negligible effects that very dilute particles have on the flow as discussed in Elghobashi[36]. Our focus in this chapter will be to present a broad overview of the physics and techniques of particle-laden flows - both laminar, and turbulent. Following which, we will outline a suitable method that we have incorporated into the discrete particle simulation framework - the basis of which is one-way coupling models. For reference throughout the section, we define the particle response number τ_p as:

$$\tau_p = \frac{2\rho_p R^2}{9\mu_f} \tag{3.1}$$

which is a measure of how quickly a particle responds to changes in the luis flow around it. We would also like to point out to the reader that our objective and the scope of this

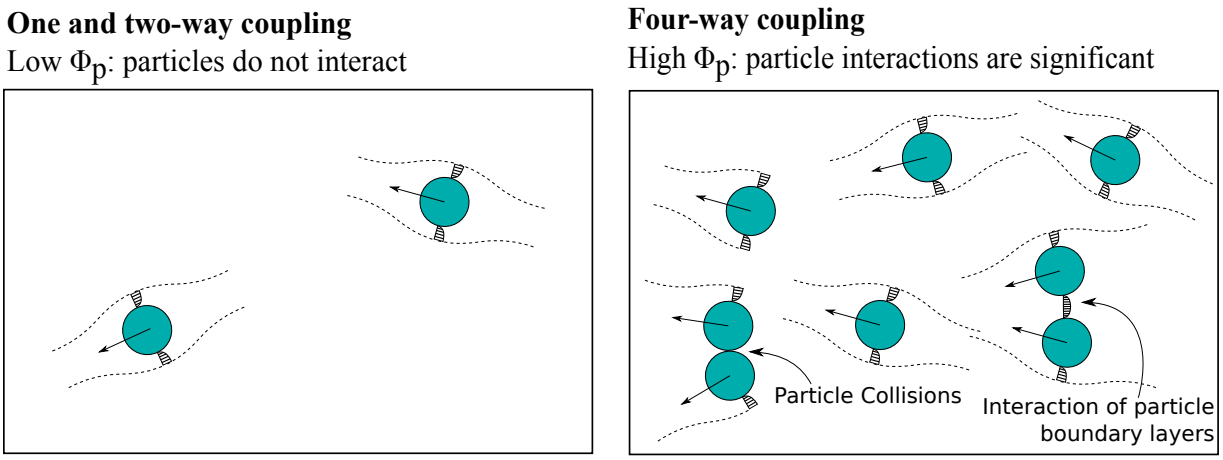

Figure 3.1: *A representation of the different ways in which the dispersed and the carrier phase interact while transitioning from two-way to four-way coupling regimes*

dissertation does not include a detailed resolution of the fluid-particle interactions and the effect on turbulence. Such an investigation would require a further intense set of algorithmic formulations and numerical computations.

3.2 Overview of the underlying physics

The physics of particle-laden turbulent flows comprises a broad spectrum of important length and time scales - which in turn makes it difficult to provide a unified theory explaining all related phenomena for such flows. A number of researchers have reviewed the underlying physical mechanisms, and we refer the interested reader to the work of Hetsroni [68], Elghobashi [36] and Balachandar & Eaton [9]. Perhaps the most important physical aspect that complicates our understanding of such flows is the nature of the fluid flow around the dispersed phase ('particles'). The microscale flow around these particles is very hard to measure experimentally due to limitations of available experimental tools, and a direct computation of the flow is not possible using available computing resources. To cite an example, Elghobashi [36] demonstrates that for an engineering application of $Re \approx 10^3$ the computational complexity scales to $\mathcal{O}(10^9)$ for just one field variable component. Hence a range of studies have been done to gain a more fundamental understanding of how the different phases interact with each other through momentum and energy coupling and how the interaction between these phases modulates the flow. The existing studies clearly demarcate a relationship between the physical phenomena and both the particle response times, τ_p (or it's non-dimensional form, the Stokes Number St_p), and the dispersed phase volume fraction, Φ_p. In his review, Elghobashi [36] provides a mapping of phase coupling and turbulence

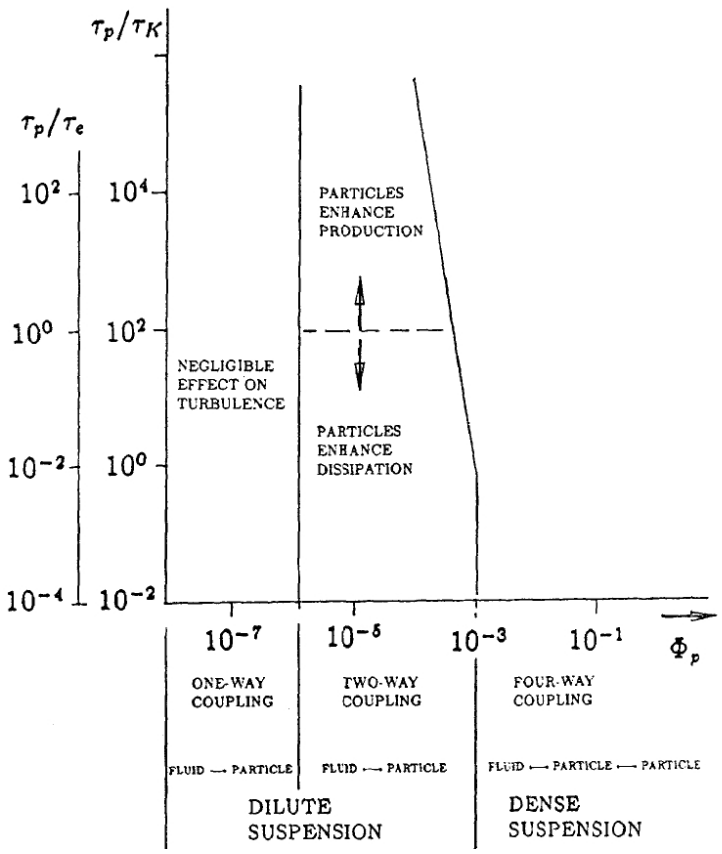

Figure 3.2: *Mapping of phase coupling and turbulence modulation in terms of Stokes Number and volume fraction from Elghobashi (1994)*

modulation in terms of these two parameters in Figure 3.2.

If the particle length-scales are small compared to the dominant length scales of the flow or if Φ_p is very low, then the overall effect of the dispersed particles on the carrier flow is negligible (although there maybe local modifications to the flow near the particle). Such a regime is referred to as *'One-way coupling'*. As the concentration is further increased - the global characteristics of the flow start getting affected. This is referred to as the *'Two-way coupling'* regime and the particles have a significant effect on the carrier phase - but the inter-particle interactions are deemed negligible (see Figure 3.1 for a schematic representation). The particulate phase now starts affecting the carrier phase turbulence and can lead to both enhancement or dissipation of turbulent energy. Of the different mechanisms that have been proposed for turbulence modulation (see Balachandar & Eaton [9]) - the most prominent ones are represented schematically in Figure 3.3.

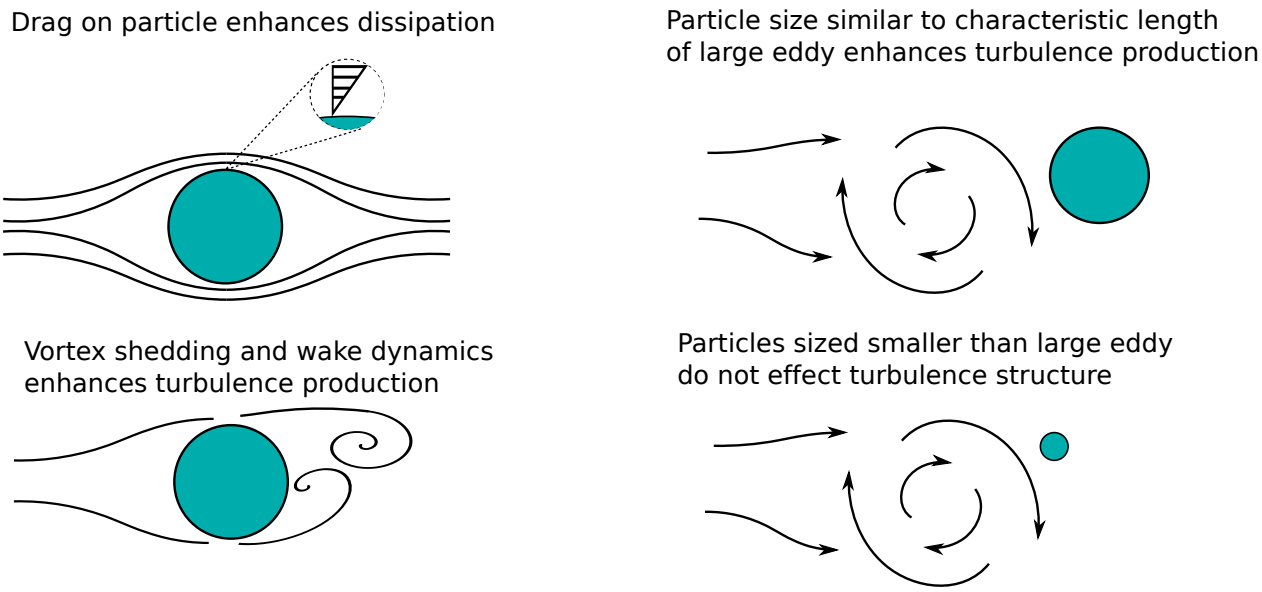

Figure 3.3: *A schematic representation of turbulence modulation mechanisms*

When the particle Stokes number is small, the corresponding particle length-scales are small which thereby corresponds to a higher surface-to-volume ratio. The viscous stresses along the surface of the particles cause dissipation of the turbulence energy - and with increased surface-to-volume ratio there is an increased dissipation of turbulence. On the other hand, as the particle length-scale increases, the corresponding particle Reynolds number also increases and can lead to the onset of vortex shedding. Addition of these vortices into the flow field thereby enhances the turbulence of the carrier phase flow. As Φ_p increases even further, the effects of the particles colliding with each other, and the interaction of the microscale flows around the particles and the wakes behind the particles can become a dominant factor. This is referred to as the *'Four-way coupling'* regime, and the turbulence modulation in this regime is still not very well understood. Intuitively, as Φ_p keeps increasing further, it can be imagined that there will be a limit wherein the carrier phase will simply be an interstitial fluid amidst the particles. From this regime until $\Phi_p = 1$ is typically referred to as dry granular flow.

It must be noted, however, that from the vast amount of existing studies in the literature - there have been ample evidences of other possible mechanisms of turbulence modulation. For example, turbulence can be enhanced by buoyancy induced instabilities caused when there are density variations induced by variable particle concentrations in different regions of the flow. On the other hand, turbulence can be dissipated by enhanced inertia of the multiphase media, and increased effective viscosity of the combined fluid. Oftentimes there is evidence of a competition between these different mechanisms in the literature - or other

phenomena (for example particle-wall collisions in a closed channel flow) that may explain some of the data. Such aspects of turbulence modulation are, however, still not very well understood. Along the same lines, existing literature indicates that it can be hard to demarcate a well-defined regime for characterizing turbulence modulation. There have been attempts by Elghobashi [36], Tanaka & Eaton[151], and Balachandar & Eaton[9] to characterize the regimes based on scaling or self-similarity considerations. A recent categorization by Tanaka & Eaton [151] was presented in terms of a non-dimensionalized *Particle Moment Number*(Pa_{St}) defined as: $Pa_{St} = \frac{1}{54\sqrt{2}} \frac{Re_L^2}{St^{1/2}} \left(\frac{\rho_p}{\rho_f}\right)^{3/2} \left(\frac{d_p}{L}\right)^3$.

The fluctuations in the velocity field of the carrier media add a stochastic component to the forces on the particles, and an interesting phenomena that originates from this is that of turbulent diffusion of the particle phase. The particles, acted upon by a stochastic loading, tend to follow a random excursion - particularly for low inertia particles. This phenomena causes a dispersion of the particle concentration spatially - a phenomena which is much like molecular diffusion, except that the origins of this are not the thermal agitations at the molecular level, but the fluctuations of a turbulent flow field. In his classical work, Taylor [154] provided a theoretical basis for analysing this phenomenon - and as per his theory, the effective particle diffusivity behaves linearly with time for short time-scales, and is constant for long time-scales. This is in contrast to molecular diffusivity - which does not have any time-scale dependence. The simulation or measurement of diffusivity becomes harder as Φ_p increases, since there are chances that inter-particle interactions and carrier turbulence modulation will significantly affect diffusion of the particles.

Another interesting phenomenon in dispersed multi-phase flows is that of preferential concentration of particles (see for example Squires & Eaton [144]). Such a phenomenon causes the particle distribution to be non-uniform even in an isotropic turbulent flow. The primary physics behind this is that low inertia particles tend to be drawn towards the core of a vortical flow field owing to centripetal effects, while higher inertia particles tend to be thrown out of the vortices and end up concentrating in regions of low vorticity. At the largest inertial scale, the particles are unaffected by vortices in the flow. Existing studies (see for example Aliseda et.al.[3], and more recently Pozorski & Apte[123]) show evidence of preferential concentration through both experiments and simulations, and of key interest is to observe the effect of particle Stokes number on the distribution of particles.

3.3 Brief review of available computational techniques

A wide variety of computational methods have been studied and documented for dispersed multiphase flows. Their range of applicability is strongly dependent upon the particle Stokes' numbers (St_p), and the particle volume fractions (Φ_p). Comprehensive reviews of such meth-

Method/Approach	Contributors/References	Remarks
Dusty Gas approach	Marble[91], Marble[92], Monaghan[107]	assumes particle follows fluid perfectly, most simple formulation for low Φ_v flows
Equilibrium Eulerian method	Ferry & Balachandar[46], Ferry et.al.[47]	works for low particle response times, no need to solve PDE to get particle velocities
Deterministic Two Fluid method	Crowe et.al.[29], Druzhinin & Elghobashi[34], Fevrier et.al.[49], Fox et.al.[51]	dispersed phase treated as a continuum (averaged over a control volume), *'cloud'* of particles are tracked instead of individual
Statistical Two Fluid method	Buyevich[20], Buyevich[21], Reeks[130], Reeks[131], Reeks[132]	continuum modelling of dispersed phase, but dispersed phase equations derived from transport equations of phase probability density function
Lagrangian particle methods	Elghobashi & Truesdell[38], Squires & Eaton[142], Ferrante & Elghobashi[45], Berlemont et.al.[13], Yamamoto et.al.[168]	small (point) particles tracked individually using Newton's laws, handles polydispersity and even collisions easily, hard to determine coupling between phases
Fully resolved DNS	Elghobashi & Truesdell[37], Mclaughlin[99], Squires & Eaton[143], Burton & Eaton[19]	all scales of fluid flow, and flow induced by particles' presence is resolved, computationally heavily intensive, impossible to perform for larger Φ_v systems

Table 3.1: *A brief summary of computational modeling approaches highlighting their main feature, and a mix of canonical and key recent literature. The categorization of the references are from the authors' survey of the literature.*

ods have been presented by Elghobashi [36], Crowe et.al.[29], and Balachandar & Eaton[10] and extensive details on the mathematical formulations of each approach can be found in these reviews. From amongst the existing literature that the authors surveyed, a very broad summary has been provided in Table 3.1 for a concise reference for the interested readers. In their review, Balachandar & Eaton [10] have also presented a classification of applicability of these methods based on St_p and Φ_p.

At low Stokes number regimes approaches like the *'Dusty Gas approach'*, and the *'Equilibrium Eulerian approach'* are useful tools - primarily because of the simplicity that they lend by assuming that the particles are not affecting the fluid flow - and their velocities are either the same as (for the former), or simple functions of (for the latter) the fluid velocities. By this assumption, these methods do not require explicit solutions of differential equations for the particle phase. However, as St_p and Φ_p increase, this simple approximation about the particle phase ceases to be applicable. Eulerian approaches that consider the two-phases to be interpenetrating fluids - and uses averaging techniques to derive transport equations for the particles - can be used for such cases (see Table 3.1). The particle concentration and the velocity fields now need to be evolved along with the carrier phase velocity and pressure fields - leading thereby to a coupled set of eight PDE's to be solved. Elghobashi[36] comments upon the differences between the averaging techniques to obtain the transport equations - and also describes significant advantages of evolving the particle phase equations in terms of their probability density functions - particularly in terms of it's ability to correctly deal with boundary conditions, and establishing a natural length-scale (that of the mean free path of particles) that can be used to validate simple gradient diffusion. Note that in such cases, deriving an appropriately accurate transport equation for the turbulence Reynolds stresses is a major issue, one that has been addressed in mathematical detail, for example, by Elghobashi & Abou-Arab [39].

In contrast with Eulerian methods, the Lagrangian particle tracking methods solve for the trajectories of individual particles and thereby essentially don't suffer from any restrictions on maximum Stokes number they can simulate, or in terms of not being able to handle particle phase polydispersity. The basis of much of this work is to identify an equation for individual particle in a fluid - the most famous version being the one proposed by Maxey & Riley[96] which was later corrected by Kim et.al.[82]. The effect of the turbulent velocities can be usually included in this equation by solving for the mean velocities and adding a random fluctuation component - typically from a normal distribution with zero mean, and variance proportional to the turbulence kinetic energy. See Berlemont et.al.[13] for a detailed description of incorporating the turbulent velocities into the particle trajectory equations. As the number of particles keep increasing, these methods become computationally expensive - and requires usage of efficient data structures and memory handling. Some such techniques can be found in the literature for granular flows (see Poschel & Schwager[122]). As the parti-

cle size increase, however, these methods are physically inaccurate and require fully resolved DNS or LES simulations. The accurate implementation of the back coupling of the particles to the fluid is also a problem for such methods.

To perform simulations of size greater than or comparable to the smaller scales of carrier flow, any approximations such as the ones discussed so far, will not be correct and the only option left is to perform fully resolved simulations using DNS. Such calculations are computationally intensive even for a small number of particles, and low Reynolds numbers (see Elghobashi[36] for a discussion on their computational complexity) - and existing studies in the literature have reported simulations of up to $\mathcal{O}(10^3)$ particles using intensive computational resources. Given that most engineering or real-world applications involve much larger numbers of particles, a fully resolved DNS for realistic problems is still an impossible task even with the rapid strides being made in the field of parallel computations and efficient memory management techniques. In the subsequent sections we will present a Lagrangian particle tracking based approach to incorporate fluid-particle interactions within the discrete particle simulation framework developed as a part of this research. We will also, for the sake of the rest of the dissertation, assume that the fluid-particle interaction is only one-way coupled - that is, the particles do not affect the fluid.

3.4 Motion of a particle in a fluid

As discussed, a fully resolved solution of the flow around a sphere is computationally intensive proposition. Hence, an alternative approach of characterizing the unsteady motion of a particle in a fluid is provided by deriving an equation for the particle motion by superposing the steady and unsteady forces due to the fluid on the particle. The earliest of these equations was provided by Basset, Boussinesq, and Oseen who provided a solution of Navier-Stokes equation for creeping flow. Much later, Maxey & Riley [98] rederived the motion equations for non-uniform, creeping flow by considering the forces from the background fluid flow, and the perturbed flow created by the presence of the moving sphere. The full form of their equation can be presented as follows:

$$m_i \frac{d\mathbf{v}_i}{dt} = \underbrace{6\pi\mu_f R_i \left(\mathbf{u} - \mathbf{v}_i + \frac{1}{6}R_i^2\nabla^2\mathbf{u}\right)}_{\text{viscous and pressure drag}} + \underbrace{\frac{1}{2}m_{fluid}\frac{d(\mathbf{u} - \mathbf{v}_i + \frac{1}{10}R_i^2\nabla^2\mathbf{u})}{dt}}_{\text{added mass}} + \underbrace{m_{fluid}\frac{D\mathbf{u}}{dt}}_{\textbf{undisturbed flow}}$$
$$+ \underbrace{6R_i^2\sqrt{\pi\mu_f\rho_f}\int_0^t \frac{d(\mathbf{u} - \mathbf{v}_i + \frac{1}{6}R_i^2\nabla^2\mathbf{u})/d\tau}{\sqrt{t-\tau}}d\tau}_{\text{Basset history force}} + \underbrace{(m_i - m_f)\mathbf{g}}_{\text{weight, buoyancy}} \tag{3.2}$$

where the fluid velocities are represented using $\mathbf{u}$. The terms involving $\nabla^2\mathbf{u}$ are due to the

Faxen type forces accounting for non-uniform free stream velocity (see the work by Rallison [125] for details). The term m_{fluid} refers to the mass of fluid displaced by the particle. Oftentimes, a Saffman type lift force is also added to the above equation (as discussed in Elghobashi [36]). A widely used variant of the original Maxey-Riley equation presented in Equation. 3.2 for many practical engineering applications can be obtained by neglecting the Faxen forces, and rewriting the drag force in the more general form as follows (see for example Balachandar & Eaton[9], Yuu et.al.[170], and Berlemont et.al.[13] amongst other works):

$$m_i \frac{d\mathbf{v}_i}{dt} = \frac{1}{2}\rho_f C_D\left(Re_i\right)\left(\pi R_i^2\right)\left|\mathbf{u}-\mathbf{v}_i\right|\left(\mathbf{u}-\mathbf{v}_i\right) + \frac{1}{2}m_{fluid}\frac{d(\mathbf{u}-\mathbf{v}_i)}{dt} + m_{fluid}\frac{D\mathbf{u}}{dt} + 6R_i^2\sqrt{\pi\mu_f\rho_f}\int_0^t \frac{d(\mathbf{u}-\mathbf{v}_i)/d\tau}{\sqrt{t-\tau}}d\tau + (m_i - m_f)\mathbf{g} \tag{3.3}$$

thereby relaxing the creeping flow assumption in an ad hoc manner. If the particle starts moving in the fluid with an initial velocity that is different from the carrier fluid velocity then the motion equations need to be modified further - and Maxey [97] gave the correction term for this effect as $6R_i^2\sqrt{\pi\mu_f\rho_f}\left[\mathbf{u}(0)-\mathbf{v}_i(0)\right]/\sqrt{t}$. Another version of the equation for spherical particle motion was proposed by Mei [100] and Mei & Adrian [101] which is applicable to finite Reynold's number flows, and has been validated against experiments over a broad range of Reynold's numbers. Their equation is presented as follows:

$$m_i \frac{d\mathbf{v}_i}{dt} = \frac{1}{2}\rho_f C_D\left(Re_i\right)\left(\pi R_i^2\right)\left|\mathbf{u}-\mathbf{v}_i\right|\left(\mathbf{u}-\mathbf{v}_i\right) + \frac{1}{2}m_{fluid}\left(\frac{D\mathbf{u}}{Dt} - \frac{d\mathbf{v}_i)}{dt}\right) + m_{fluid}\frac{D\mathbf{u}}{dt} + 6\pi\mu_f R_i\int_{-\infty}^t K(t-\tau,\tau)\frac{d(\mathbf{u}-\mathbf{v}_i)}{d\tau}d\tau + \left(m_i - m_{fluid}\right)\mathbf{g} \tag{3.4}$$

where the correction for initial velocity difference has to be added on, and the integral kernel for the history force term is given as follows:

$$K(t-\tau,\tau) = \left[\left[\frac{\pi(t-\tau)\nu_f}{R_i^2}\right]^{1/4} + \left[\frac{\pi|\mathbf{u}(\tau)-\mathbf{v}_i(\tau)|^3}{2R_i\nu_f f_H^3(Re_\tau)}(t-\tau)^2\right]^{1/2}\right] \tag{3.5}$$

$$f_H(Re_\tau) = 0.75 + 0.105Re_\tau(\tau) \tag{3.6}$$

$$Re_\tau = \frac{|\mathbf{u}(\tau)-\mathbf{v}_i(\tau)|2R_i}{\nu_f} \tag{3.7}$$

From a detailed theoretical derivation, and numerical results for the Navier-Stokes, Kim

et.al. [82] provided another modified version of the equation that performed well when compared to other prescribed equations over a broad range of Reynolds numbers. Their modification was primarily in terms of the integral kernel used to model the history force, and the equations can be summarized as follows:

$$\begin{aligned} m_i\frac{d\mathbf{v}_i}{dt} &= \frac{1}{2}\rho_f C_D\left(Re_i\right)\left(\pi R_i^2\right)|\mathbf{u}-\mathbf{v}_i|\left(\mathbf{u}-\mathbf{v}_i\right)+\frac{1}{2}m_{fluid}\left(\frac{D\mathbf{u}}{Dt}-\frac{d\mathbf{v}_i)}{dt}\right)+m_{fluid}\frac{D\mathbf{u}}{dt} \\ &+6\pi\mu_f R_i\int_{0^+}^{t}K(t-\tau,\tau)\frac{d(\mathbf{u}-\mathbf{v}_i)}{d\tau}d\tau+\left(m_i-m_{fluid}\right)\mathbf{g} \\ &+6\pi\mu_f R_i K_1(t)\left[\mathbf{u}(0^+)-\mathbf{v}(0^+)-\mathbf{u}(0^-)+\mathbf{v}(0^-)\right] \end{aligned} \tag{3.8}$$

where the modified form of the integral kernel can be described as follows:

$$K(t-\tau,\tau)=\left[\left[\frac{\pi(t-\tau)\nu_f}{R_i^2}\right]^{1/2c_1}+G(\tau)\left[\frac{\pi|\mathbf{u}(\tau)-\mathbf{v}_i(\tau)|^3}{2R_i\nu_f f_H^3(Re_\tau)}(t-\tau)^2\right]^{1/c_1}\right]^{-c_1} \tag{3.9}$$

$$G(\tau)=\frac{1}{1+\beta\sqrt{M_{A1}(\tau)}} \tag{3.10}$$

$$\beta=\frac{c_2}{1+\phi_r\phi_r^{c_4}/\left[c_3\left(\phi_r+\phi_r^{c_4}\right)\right]} \tag{3.11}$$

$$f_H=0.75+c_5 Re_t(\tau) \tag{3.12}$$

where $M_{A1}=\frac{2R_i}{|\mathbf{u}-\mathbf{v}_i|^2}|\frac{d|\mathbf{u}-\mathbf{v}_i|}{dt}|$ is the dimensionless relative acceleration between the particle and the fluid. The dimensionless parameter ϕ_r is defined as M_{A2}/M_{A1}, where the numerator is another dimensionless parameter that involves the second derivative of the relative velocity between the particle and the fluid, defined as $M_{A2}=\frac{4R_i^2}{|\mathbf{u}-\mathbf{v}_i|^3}|\frac{d^2|\mathbf{u}-\mathbf{v}_i|}{dt}|$.

$$K_1(t)=\left[\left[\frac{\pi t\nu_f}{R_i^2}\right]^{1/2c_1}+G_1\left[\frac{\pi|\mathbf{u}(0)-\mathbf{v}(0)|^3}{2R_i\nu_f f_H^3 Re_0}\right]^{1/c_1}\right]^{-c_1} \tag{3.13}$$

$$G_1=\frac{1}{1+c_6 Re_0^{-1/4}\left(\rho_i/\rho_f+0.5\right)^{-1/2}} \tag{3.14}$$

where ρ_r is the ratio of the density of the particle to that of the fluid. In their original article [82], the values of the six coefficients fitted from numerical results and some scaling analysis have been tabulated, which is reproduced here for the sake of completion as follows:

$$c_1 = 2.50, c_2 = 22.00, c_3 = 0.07$$
$$c_4 = 0.25, c_5 = 0.126, c_6 = 17.8 \tag{3.15}$$

We remark that the modifications to the integral kernel made in Equations 3.4, and 3.8 are such that for high-frequencies of oscillations (that is, for short times) of the spherical particle they attain the same mathematical form as the original integral kernel proposed by Basset, as included in Equation 3.2.

Additionally, we remark that owing to the underlying superposition idea and the additive nature of the interaction terms in the equation, it is possible, as a first order approximation, to include further particulate interaction contributions to the Equations 3.2, 3.3, 3.4, and 3.8. For example lift forces due to particle rotations (otherwise referred to as Magnus forces), and lift due to shear in the carrier flow (otherwise referred to as Saffman lift forces) can be incorporated as and when required. It is also worthwhile to make a few remarks on the relative importance of the various force terms that were assembled in the equations presented here. For many practical applications, the density ratio between particles and fluid (ρ_r) is reasonably large. Under such a condition, it can be seen that the added mass contribution, the history force contribution, and the pressure gradient contributions will all be negligible, leading to a relatively simple form of the motion equation given as follows;

$$m_i \frac{d\mathbf{v}_i}{dt} = \frac{1}{2}\rho_f C_D\left(Re_i\right)\left(\pi R_i^2\right)\left|\mathbf{u}-\mathbf{v}_i\right|\left(\mathbf{u}-\mathbf{v}_i\right)\left(m_i - m_f\right)\mathbf{g} \tag{3.16}$$

Such applications may include macroscopic, solid particles carried in a gaseous media, or even molten metal droplets (which owing to their high surface tension, does not lead to major oscillations of the free surface, and deformations). The Basset history force term incorporates the gradual development of the boundary layer around the particle as it moves through a transient field - and as such is important in highly transient fluid flows, or turbulent flows. Hence, in many applications involving unsteady effects and reasonably low values of the density ratio ρ_r, often the history terms can be neglected as a first-order approximation towards integrating the particle motion equation.

3.5 Drag coefficient for a sphere

From the discussions presented in Sections 3.2, and 3.4, the drag force can be seen to be the most dominant interaction that is present in a broad range of applications. Hence a correct estimate of the drag force is crucial to resolving the dispersed particulate phase behavior. Using the standard form of the drag force, this would then require a reasonably accurate

estimate of the drag coeficient $C_d(Re_p)$. There are numerous correlations available in the existing literature and the reader is referred to the works by Crowe et.al.[29], Fritsching[53] and Bailey & Hiatt[8] amongst others. Of these, the correlation presented by Haider & Levenspiel[62] finds applicability over a broad range of Reynolds numbers, and also has a very low mean square error when compared to values of drag coefficients obtained from available experimental data - and hence has been the dominant choice for the simulation libraries developed as a part of this research. Their correlation can be numerically expressed as follows:

$$C_D\left(Re_p\right) = \frac{24}{Re_p}\left(1 + 0.1806 Re_p^{0.6459}\right) + \frac{0.4251}{1 + \frac{6880.95}{Re_p}} \tag{3.17}$$

3.6 Rotational momentum transfer

The interactions between a particle and its surrounding fluid can affect the rotational momentum of the particle as well. There are relatively fewer studies on the torque transferred to a particle by the carrier fluid over a broad range of Reynolds numbers. The problem of a spinning sphere in a viscous fluid at low Reynolds number regimes was analytically studied by Rubinow & Keller [133]. Their expression for the torque due to the Stokes flow on the sphere can be presented as follows:

$$\tau_i = -8\pi\mu_f R_i^3 \omega \tag{3.18}$$

In a later work by Feuillebois & Lasek [48], the above expression was extended to the non-stationary Stokes flow regime, and the modified equation for the fluid rotational motion was derived to be of the following form:

$$\begin{aligned} I_i \frac{d\omega_i}{dt} = \tau_{ext} - 8\pi\mu_f R_i^3 \omega - 8\pi\mu_f R_i^3 \left(\frac{R_i}{3\sqrt{\pi\nu_f}} \int_0^t \frac{d\omega_i}{dt} \frac{dt^*}{\sqrt{t - t^*}}\right) \\ + \frac{8\pi\mu_f R_i^3}{3} \left[\int_0^t \frac{d\omega_i}{dt} \exp\left(\frac{\nu_f (t - t^*)}{R_i^2}\right) \operatorname{erfc}\left(\sqrt{\frac{\nu_f (t - t^*)}{R_i^2}}\right) dt^*\right] \end{aligned} \tag{3.19}$$

where the viscous history forces on the particle (as discussed in Section 3.4) account for the modifications to the total torque.

3.7 Integration of history forces

A salient feature of the particle motion equations presented in Section 3.4 is the presence of a history force term, which can render considerable computational challenges to solving the particle equation for a large number of particles dispersed in a fluid - since the storage requirements for the convolution term (that is, the relative acceleration) is going to be very high. An additional issue with the form of the chosen kernel is the singularity as $t \to \tau$ (see Equations 3.2, 3.4, and 3.8).The history forces are important for many highly transient, unsteady flow applications, and as such an accurate estimation of this force is quite critical. Vojir & Michalides [161] present a discussion on the conditions under which the history contributions are signficant, while Van Hinsberg et. al. [158] mention more recent findings on applications where history forces are significant contributors. Hence, there have been many alternative approaches proposed to particularly deal with the estimation of the history force. The particular issue for dealing with the singularity in the integral kernel can be dealt with by specialized numerical quadrature formulae like the Euler-MacLaurin summation formulae. The evaluation of the history term was approached using expressing the term using semi derivatives or fractional derivatives by Tatom [153]. For the original Basset term as in Equation 3.2, this entails writing the history term using the following:

$$\int_a^t \frac{d(\mathbf{u}-\mathbf{v})/d\tau}{\sqrt{t-\tau}} d\tau = \Gamma\left(\frac{1}{2}\right) \frac{d^{-0.5}\left(d(\mathbf{u}-\mathbf{v})/dt\right)}{\left[d(t-a)\right]^{-0.5}} \tag{3.20}$$

The term on the right-hand side is a fractional derivative, and for a general function f, a fractional derivative of fractional order q can be expressed in terms of a series expansion as follows:

$$\frac{d^q f}{[d(t-a)]^q} = \lim_{N\to\infty}\left[\left(\frac{t-a}{N}\right)^{-q} \frac{1}{\Gamma(-q)} \sum_{k=0} N-1 \frac{\Gamma(k-q)}{\Gamma(k+1)} f\left(t-\frac{k(t-a)}{N}\right)\right] \tag{3.21}$$

where f can be replied by the relative acceleration. While Tatom's work did not provide further analysis on evaluation of the history term, in a recent work Bombardelli et. al. [16] provided a detailed discussion on using the semi-derivative approach to calculate the Basset history forces on colliding particles for sediment transport problems. Their examples, however, are based on approximated forms of the relative acceleration terms in form of simple trigonometric and algebraic functions - and hence the issue of implementation for more generalized calculation for unsteady relative motion velocity profiles is not completely clear. Another solution technique of particle equation with the history force was proposed by Mei et. al. [102] where the equation for a gravitationally settling particle in the Stokes flow regime was solved in the frequency domain. A similar approach was presented by Michaelides [103] where Laplace transform techniques are used to convert the original Maxey-Riley form

of the particle motion integro-differential equation into a higher-order ordinary differential equation, where the particle velocities are no longer the part of an integral kernel. It is not very clear as to whether the extensions of these approaches would hold for the case of complex multi physically interacting particles in a flow - however, they can definitely form very good starting points for undertaking detailed calculations for particles dispersed in a flow.

An alternative to the aforementioned methods was provided by Dorgan & Loth [2] where a strategy to reduce the cost of storage for evaluating the history force is provided by means of modifying the integral kernel to be defined over a specified temporal window as follows:

$$K_{mod}(t-\tau) = \begin{cases} K_{history}(t-\tau) & \forall\ \tau \in (t - t_{window}, t) \\ 0 & \forall\ \tau < t - t_{window} \end{cases} \tag{3.22}$$

where the functional form for t_{window} can be obtained by using scaling arguments with an appropriate particle flow time-scale τ_p as follows:

$$t - t_{window} = \max(0, t - \beta\tau_p) \tag{3.23}$$

with β being a factor obtained by an integration of the history kernel for a chosen particle phase Reynolds number. This formulation was further modified in a more recent work by Van Hinsberg et. al. [158] where the tail of the kernel is no longer set to 0 as in Equation. 3.24, but set to a particular functional form as follows:

$$K_{mod}(t-\tau) = \begin{cases} K_{history}(t-\tau) & \forall\ \tau \in (t - t_{window}, t) \\ K_{tail}(t-\tau) & \forall\ \tau < t - t_{window} \end{cases} \tag{3.24}$$

where [158] proposes a choice of the approximated tail to be $K_{tail} = \sqrt{\frac{e}{t_{window}}} \exp\left(-\frac{t}{2t_{window}}\right)$. The numerical integration of the history term can now be performed using the modified kernels, by discretizing the integral over intervals over the window duration t_{window}, and expressing the relative acceleration as a linear interpolation function over the discretized intervals.

3.8 Convective heat transfer

In continuation with the discussions presented in section 3.4, the thermal interactions between a particle and the carrier fluid are also assumed to be one-way coupled. Analogous to the mechanical interactions and flow velocities, a complete resolution of the heat exchange with the micro scale flow around the particles is not pursued here. Instead, the interactions are modeled through a direct convective heat transfer, and the total convective heat flux

from the particle to the fluid is then given by (see Crowe et. al.[29]):

$$\mathcal{Q}_{i,conv} = \pi R_i^2 h_{conv} \left(\theta_{fluid} - \theta_i\right) \tag{3.25}$$

where the convective transfer coefficient h_{conv} can be more conveniently represented in terms of the fluid thermal conductivity (K_f) using the definition of the non-dimensional Nusselt number (Nu)as follows:

$$Nu = \frac{h_{conv} 2R_i}{K_f} \Rightarrow \mathcal{Q}_{i,conv} = \frac{1}{2}\pi Nu K_f R_i \left(\theta_{fluid} - \theta_i\right) \tag{3.26}$$

The Nusselt number is typically estimated indirectly from the particle phase based Reynolds number and the fluid phase Prandtl number ($Pr = C_f \mu_f / K_f$) using the Ranz-Marshall correlations [128] which can be given in the following form:

$$Nu = 2.0 + 0.6 Re^{0.5} Pr^{0.33} \tag{3.27}$$

Further details on modified Ranz-Marshall correlations can be found in the work by Fritsching [53] and Crowe et. al. [29]. Along the same idea of expressing the Nusselt number using the Reynolds and Prandtl numbers, Acrivos & Taylor [1] provided a solution of the heat transfer due to a single sphere in the Stokes flow regime, and developed an expression of the Nusselt number in terms of the dimensionless Peclet number (Pe), which is defined to be the product of Reynolds and Prandtl numbers for heat transfer. Their result can be summarized as follows:

$$Nu = 2 + 0.5Pe + 0.25Pe^2 \log Pe + 0.03404 Pe^2 + 0.0625 Pe^3 \log Pe \tag{3.28}$$

An alternative approach towards understanding heat transfer between sphere and the carrier fluid was given in a later work by Michaelides & Feng [104] where they perform a basic derivation of the energy equation for a spherical particle in a manner analogous to that presented by Maxey & Riley [98]. The equation for the rate of change of temperature of the spherical particle obtained from this derivation is presented as follows:

$$\begin{aligned} m_i C_i \frac{d\theta_i}{dt} = m_f C_f \frac{D\theta_f}{Dt} &- 4\pi R_i K_f \left(\theta_i - \theta_f - \frac{1}{6} R_i^2 \nabla^2 \theta_f\right) \\ &- 4\pi R_i^2 K_f \int_0^t \frac{\frac{d}{d\tau}\left(\theta_i(\tau) - \theta_f(\tau) - \frac{1}{6} R_i^2 \nabla^2 \theta_f(\tau)\right)}{\sqrt{\frac{\pi K_f}{\rho_f C_f}(t-\tau)}} d\tau \end{aligned} \tag{3.29}$$

where the effect of the history terms have been explicitly taken into account. There are not many discussions on utilizing such an equation for multiple particles dispersed in a carrier fluid, and from our review of the existing literature, utilizing correlation based estimates for

convective heat transfer seems to be the more widely used alternative.

3.9 A simple treatment for isotropic turbulence

A significantly detailed discussion on modeling the effect of flow turbulence in particle laden fluid flows will be remarkably extensive, and deserves, in our opinion, separate attention. Hence for the scope of the current work, such a discussion is not pursued. However, since turbulent phenomena play a crucial role in transport of the dispersed, particle phase - we include in our simulation library, a simplistic approach to be able to provide some qualitative simulation capabilities for indicating the potential effects of turbulence. This is done by re-writing the particle motion equations presented in Section 3.4 in an abstract form as follows:

$$m_i \frac{d\mathbf{v}_i}{dt} = \mathcal{F}(\mathbf{v}_i, \mathbf{u}_i) \tag{3.30}$$

where, it is noted that $\mathbf{u}_i$ is the instantaneous velocity of the fluid at the location of the particle indexed by i. Keeping consistent with our assumption of a one-way coupled modeling approach, the velocity $\mathbf{u}_i$ has been assumed to be unaffected by the particle motion. In more detailed simulation of two way coupling - it is typical to evolve the fluid flow field and the particle motion in a staggered or partitioned manner, and in such cases, for the staggered update of the particle motion as well the aforementioned assumption will hold. More details on staggering has been presented in Chapter 4, Section 4.2. The simplest approximation that can be performed now to obtain the velocity $\mathbf{u}_i$ is to represent it as:

$$\mathbf{u}_i = \mathbf{U}_i + \mathbf{u}'_i \tag{3.31}$$

where $\mathbf{U}_i$ is the time-averaged velocity field (obtained either from known data, or additional computations), and $\mathbf{u}'_i$ is a fluctuating component of velocity. Additionally, it is typical to assume that the fluctuations are sampled randomly from a Gaussian distribution with zero mean and variance equal to the fluid turbulent intensity $2k_t/3$. Such a sampling method produces a homogenous, isotropic turbulent flow field only (see Elghobashi [36] for detailed review on such methods). A particle in a certain turbulent eddy will now continue to see this modified velocity until it resides in the eddy or the eddy decays. The size of the large energy containing eddies - also referred to as the integral length scale (see for example Davidson[31] for theoretical details) can be obtained to be

$$l_0 = \int_0^\infty \frac{Q_{xx}(r)}{\langle u^2 \rangle} dr \tag{3.32}$$

where Q_{xx} is the velocity correlation function. The corresponding integral time-scale can be simply then given by $T_l = l_0/u$ (see the works by Corrsin [28] and Snyder & Lumley [141]). in terms of the viscous dissipation ϵ we can express the integral length scale as

$l_0 \propto \frac{k_t^{3/2}}{\epsilon}$ and the time scale as $T_l \propto \sqrt{\frac{3}{2}}\frac{k_t}{\epsilon}$. The correlation functions are usually the subject of experimental measurements and examples of such measurements can be found in Snyder & Lumley [141] amongst others. Thus as a basic approximation to the particle motion, it can be assumed that as it travels across an eddy of size l_0 and life-time T_l it experiences a fluctuating fluid velocity obtained from sampling from a distribution with variance proportional to k_t. This process is schematically illustrated in Figure 3.4.

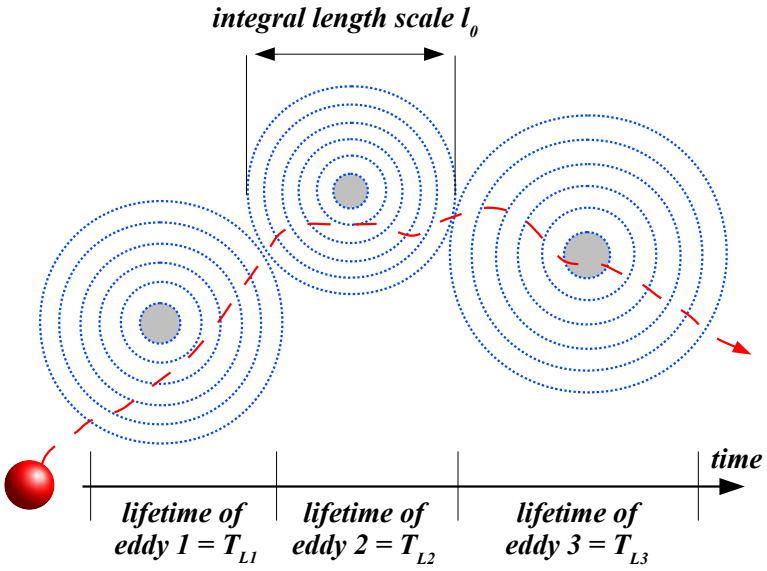

Figure 3.4: *Schematic representation of a discrete element moving across a series of eddies in a turbulent flow field.*

The implementation of this simplified idea by itself is not effective other than basic illustration of the dynamics of a particle ensemble in a fluctuating flow field. Advanced modeling techniques based on this idea has been devised in the works by Picart et. al. [120], Berlemont et. al. [13], the work by Macinnes & Bracco [90], an approach based on Langevin dynamics presented by Pozorski & Minier [124] and a detailed review on Lagrangian techniques by Gouesbet & Berlemont [57]. The main technique behind these is to obtain a fluid velocity correlation and then use the correlation to obtain fluctuating velocity components at the location of the particle, and update the velocities of both phases with time.

Chapter 4

Algorithmic considerations for discrete particle simulations

4.1 Introduction

In this chapter we focus on assembling the particle-particle, particle-surface, and particle-fluid interaction models into a framework for numerical computation of the dynamics of a collection of particles or discrete elements, which we shall refer to as a particle ensemble. This notion of an ensemble may seem somewhat similar to that encountered in statistical mechanics - however, we would like to note that there are critical differences that stem from the fact that for an ensemble of macroscopic particles the randomness in the phase space is introduced by some non-thermal mechanism, and is thereafter typically sustained by collisions and other interactions. A detailed review of granular physics in this context can be found in Duran[35] for example. Analogously, the degrees of freedom of each particle - positions, velocities, angular velocities and orientations - will be referred to as the phase-space for that particle. Various algorithmic consideration for numerically updating the dynamic variables of the ensemble phase-space have been presented in the remaining sections of this Chapter - and each aspect has been illustrated using appropriate pseudocodes wherever detailed clarification of the implementation was found necessary. Note that the pseudocode implementations were all programmed into the various modules of the simulation library developed as part of this research.

4.1.1 Brief note about interpreting the algorithms presented

In the pseudocodes presented in the following sections, the usual programming constructs (for example, for-loops, while-lops etc) should be interpreted as the way they have been written. Wherever specific calculations are to be noted, they have been explicitly typed out, otherwise, they have just been verbally described. The idea being that in a program, there

will be a corresponding function/subroutine that will perform the task described (and the details of how it is done is unimportant for the context). Wherever particular references were required to a category of physics subroutines to be invoked, they have been done in capitalized phrases that describe the subroutines. For example, to evaluate inter-particle contact forces, using any of the broad range of models specified in Chapter 2, the name $EVALUATE-PARTICLE-PARTICLE-CONTACT$ will be used as the place-holder.

4.2 Time-stepping for system dynamics

We begin our discussion by modifying the particle dynamics equations presented at the beginning of Chapter 2 so as to represent the contact interactions appropriately:

$$m_i \frac{d\mathbf{v}_i}{dt} = \sum_{j=1}^{N_s} \mathcal{I}(i,\mathcal{S}_j)\left[\mathbf{F}_{ijs,contact} + \mathbf{F}_{ijs,adh}\right] + \sum_{j\neq i,j=1}^{N_p} \mathcal{I}(i,j)\left[\mathbf{F}_{ij,contact} + \mathbf{F}_{ij,adh}\right] + \mathbf{F}_{i,fluid} + \mathbf{F}_{i,em} \tag{4.1}$$

$$\frac{d\mathbf{x}_i}{dt} = \mathbf{v}_i \tag{4.2}$$

$$m_i C_i \frac{d\theta_i}{dt} = \sum_{j=1}^{N_s} \mathcal{I}(i,\mathcal{S}_j)\mathcal{Q}_{is} + \sum_{j\neq i,j=1}^{N_p} \mathcal{I}(i,j)\mathcal{Q}_{ij} + \mathcal{Q}_{i,conv} + \mathcal{H}_i + \mathcal{Z}_i \tag{4.3}$$

where only the translational motion equations have been written out in detail. The function $\mathcal{I}$ is an indicator function for contact occurrence. For example $\mathcal{I}(i,\mathcal{S}_j)$ is equal to unity if the i'th particle and the surface $\mathcal{S}_j$ are in contact, and zero otherwise. Similarly, $\mathcal{I}(i,j)$ is unity if the i'th and j'th particles are in contact, and zero otherwise. The heat fluxes during particle-particle contact, particle-surface contact, and through particle-fluid convective transfer are represented using $\mathcal{Q}_{ij}$, $\mathcal{Q}_{is}$, and $\mathcal{Q}_{i,conv}$ respectively.

The time integration of such coupled ordinary differential equations involving short-range interactions like contact with a steep gradient is an issue that has been discussed by many researchers. A detailed treatment of construction and analysis of numerical integration schemes for the generalized N-body problem can be found in Leimkuhler & Reich[85]. More specific discussions on the integration of motion equations for particles using the Verlet type integration schemes can be found in Frenkel & Smit [52]. Such algorithms have been developed and analyzed in great detail for molecular dynamics applications - for instance, we refer the interested reader to the work by Swope & Andersen[149] on a modification to the Verlet algorithm called the Velocity Verlet algorithm, the work by VanGunsteren & Berendsen[157] on modified higher-order Leap-Frog methods for particle systems behaving

stochastically. A detailed discussion on the usage of predictor-corrector type schemes (Gear algorithm) for such systems can be found in Poschel & Schwager[122]. It can be seen that the exact schemes for the popular Verlet type algorithms for motion equations are all essentially one-step difference schemes. The usage of multi-step schemes for simulating dynamics of ensembles of particles is limited by their high storage requirements for storing dynamic variables at previous time-steps. One-step schemes with multi-stage approximations to the derivatives - which are commonly referred to as Runge-Kutta(RK) methods - are on the other hand a useful choice, and the reader is referred to the text by Leimkuhler & Reich[85] and the work by Blanes & Moan[15] for examples on using RK methods for N-body dynamics.

For the rest of the present discussion, further details of the various possible numerical schemes for integrating the particle equations is not presented. Instead, we will outline in sufficient detail, three important aspects, that were found to be critical to performing computer simulations of multi-particle ensembles. These aspects are:

- Staggered, iterative computations for multi-field, coupled phenomena
- Resolution of collisions in a time-step
- Algorithmic treatment of time-step adaptivity

4.2.1 Staggered, iterative computations for multi-field, coupled phenomena

Let us consider the scenario where the coupled mechanical and thermal equations of a particle are to be simultaneously solved. We represent the equations for the updated velocities, positions, and temperatures in the following abstracted form:

$$\mathbf{v}_i^{N+1} = \mathcal{G}_1\left(\mathbf{v}_i^{N+1}, \mathbf{x}_i^{N+1}, \theta_i^{N+1}\right) + \mathcal{R}_1 \tag{4.4}$$

$$\mathbf{x}_i^{N+1} = \mathcal{G}_2\left(\mathbf{v}_i^{N+1}, \mathbf{x}_i^{N+1}, \theta_i^{N+1}\right) + \mathcal{R}_2 \tag{4.5}$$

$$\theta_i^{N+1} = \mathcal{G}_3\left(\mathbf{v}_i^{N+1}, \mathbf{x}_i^{N+1}, \theta_i^{N+1}\right) + \mathcal{R}_3 \tag{4.6}$$

where the function $\mathcal{G}_i$ and $\mathcal{R}_i$ are derived from the corresponding operators for numerical discretization of the ordinary differential equations. The solution of the system above can be possibly performed monolithically using an appropriate implicit time-stepper. However, owing to the underlying physics of the different phenomena captured in the equations, the convergence characteristics of each equation may be different. Furthermore, staying consistent with the central idea of having a computational tool that can be easily linked to other available solvers for applications in potentially complicated fluid-particle interaction problems, and combined finite-discrete element type problems - it is advantageous to partition

the system physics and solve for the different dynamic physical variables in a staggered manner. Such staggered schemes have been investigated and implemented by many researchers and the interested reader is referred to the extensive review and tutorial article by Felippa et.al.[42], a discussion on staggered solution schemes formulated for two-field coupled problems by Felippa & Park[41], the implementation of staggered solution schemes for solving non-linear, transient, fluid-structure interaction problems associated with flutter of wings by Farhat & Lesoinne[40], the work by Zienkiewicz et.al.[173] on solving fluid-soil-pore interaction problems using such methods, and the work by Schrefler[137] on a staggered simulator of a geothermal reservoir. Specifically for the case of discrete particle systems, if we are concerned only with the dynamic fields of the particles then the updates to field variables will have to be staggered and iterative - and a detailed formulation of such techniques has been presented for discrete particle simulations by Zohdi (see [174], [175], and [179]). The same formulation is also extended to coupled fluid-particle systems in the work by Zohdi[178]. We remark here that, for fluid-particle or fluid-continuum or particle-continuum type coupled problems - the individual subsystems that are staggered can be solved using appropriate available methods (explicit/implicit or discrete/finite element/finite volume) and software tools - with the subsystems exchanging information with each other through interaction terms. This aspect will not be addressed herein, but has been identified as a topic for future research and investigations.

We now seek to demonstrate the implementation of the staggered, iterative formulation for discrete particle systems as presented by Zohdi[174] etc. For this purpose, we chose a one-step ϕ-trapezoidal method given as follows (a choice consistent with the popular Verlet type schemes which have been extensively studied for the related application of simulation of molecular systems):

$$\mathbf{v}_i^{N+1} - \mathbf{v}_i^N = \frac{\Delta t}{2m_i}\left[\phi \mathbf{F}_i^{N+1} + (1-\phi)\mathbf{F}_i^N\right] \quad \text{etc.} \tag{4.7}$$

where the superscripts N and $N+1$ denote the values at the current and the future time-steps respectively. From the discussions presented in Chapters 2 and 3, it is clear that $\mathbf{F}_i$ is in reality a complicated function of the particle velocities and positions, hence we do not write the explicit dependence on $\mathbf{v}_i^{N+1}$ and $\mathbf{v}_i^N$ in the terms on the right hand side of Equation. 4.7. Therefore, following the notation of Equations 4.4, 4.5, and 4.6, we can write for the ϕ-trapezoidal method the following forms of $\mathcal{G}_i$, and $\mathcal{R}_i$:

$$\mathcal{G}_1 = \frac{\Delta t}{2m_i}\phi \mathbf{F}_i^{N+1}, \qquad \mathcal{R}_1 = \mathbf{v}_i^N - \frac{\Delta t}{2m_i}(1-\phi)\mathbf{F}_i^N \tag{4.8}$$

$$\mathcal{G}_2 = \frac{\Delta t}{2}\phi \mathbf{v}_i^{N+1}, \qquad \mathcal{R}_2 = \mathbf{x}_i^N - \frac{\Delta t}{2}(1-\phi)\mathbf{v}_i^N \tag{4.9}$$

$$\mathcal{G}_3 = \frac{\Delta t}{2m_i C_i}\phi \mathcal{Q}_i^{N+1}, \quad \mathcal{R}_3 = \theta_i^N - \frac{\Delta t}{2m_i C_i}(1-\phi)\mathcal{Q}_i^N \tag{4.10}$$

The idea behind implementing this scheme now has been illustrated in detail in form of a pseudocode presented in Algorithm 1. The form of the iteration function $\mathcal{G}_i$ also plays a major role in controlling iteration error, and extensive discussion of using the iterative error estimate to perform time-step adaptivity has been presented by Zohdi[174].

4.2.2 Resolving collisions in a time-step

Let us consider the numerically discretized time-interval $(t, t+\Delta t)$, and assume in general that for a single particle, a collision event occurs over time interval $(t^*, t^*+\delta t)$. The time instant t^* is the moment of collision detection. Tracking the exact collision time t^* within a single time-step is a computationally intensive task, thereby motivating a simplifying assumption that shifts (as an approximation) the instant t^* to either the beginning or the end of the time-step. Hence, the computation of position and velocity updates occur by identifying which particles undergo a collision over a certain interval i and allowing the collision updates to occur first at the beginning of the $i+1$'th interval, followed by updates due to all other forces. With this context, we can envisage two distinct cases of time-step selection.

First, let us consider the case that $t^* \in (t, t+\Delta t)$ and $\Delta t > \delta t$. The sequence of dynamic events within this time-step can then be decomposed as follows:

$$m_i \mathbf{v}_i(t^*) - m_i \mathbf{v}_i(t) = \int_t^{t^*} \mathbf{F}_{i,non-contact} dt \tag{4.11}$$

$$m_i \mathbf{v}_i(t^*+\delta t) - m_i \mathbf{v}_i(t^*) = \int_{t^*}^{t^*+\delta t} \left(\mathbf{F}_{i,contact} + \mathbf{F}_{i,non-contact}\right) dt \tag{4.12}$$

$$m_i \mathbf{v}_i(t+\Delta t) - m_i \mathbf{v}_i(t^*+\delta t) = \int_{t^*+\delta t}^{t+\Delta t} \mathbf{F}_{i,non-contact} dt \tag{4.13}$$

Shifting $t^* \to t$ allows us to have a collision event for a duration δt, followed by streaming motion of particles under the action of external, non-collisional forces. Therefore, such a scenario is useful for implementing an impulse-based approach to treat collisions as discussed in

Algorithm 1 *A pseudocode to illustrate the implementation of time-stepping with staggered, iterative updates for integrating particle equations using the one-step trapezoidal scheme as performed in the developed simulation library.*

EVALUATE-PARTICLE-PARTICLE-CONTACT($particles$)
EVALUATE-PARTICLE-SURFACE-CONTACT($particles$, $surfaces$)
EVALUATE-PARTICLE-FLUID-INTERACTION($particles$, $fluid$)
EVALUATE-PARTICLE-EM-INTERACTION($particles$, $EMfields$)
for $i = 1, N_p$ **do**
  $\mathbf{F}_i^N \leftarrow$ sum of all forces, $\mathcal{Q}_i^N \leftarrow$ sum of all fluxes
  $\mathbf{v}_i^N \leftarrow$ store current velocity, $\mathbf{x}_i^N \leftarrow$ store current position
  $\theta_i^N \leftarrow$ store current temperatures
  set initial guess for velocity $\rightarrow \mathbf{v}_i^{N+1,0}$, set initial guess for position $\rightarrow \mathbf{x}_i^{N+1,0}$
  set initial guess for temperature $\rightarrow \theta_i^{N+1,0}$
  update dynamic variables $\mathbf{v}_i$, $\mathbf{x}_i$, θ_i
end for
while $err_{vx} \geq err_{TOL}$ **do**
  EVALUATE-PARTICLE-PARTICLE-CONTACT($particles$)
  EVALUATE-PARTICLE-SURFACE-CONTACT($particles$, $surfaces$)
  EVALUATE-PARTICLE-FLUID-INTERACTION($particles$, $fluid$)
  EVALUATE-PARTICLE-EM-INTERACTION($particles$, $EMfields$)
  for $i = 1, N_p$ **do**
    $\mathbf{F}_i^{N+1,K} \leftarrow$ sum of all forces
    $\mathbf{v}_i^{N+1,K+1} = \mathbf{v}_i^N + \frac{\Delta t}{2m_i}\left[\mathbf{F}_i^{N+1,K} + \mathbf{F}_i^N\right]$
    $\mathbf{x}_i^{N+1,K+1} = \mathbf{x}_i^N + \frac{\Delta t}{2}\left[\mathbf{v}_i^{N+1,K+1} + \mathbf{x}_i^N\right]$
    update dynamic variables $\mathbf{v}_i$, $\mathbf{x}_i$, retain θ_i
  end for
  $err_{vx} = \sum_i \frac{\|\mathbf{v}_i^{N+1,K+1} - \mathbf{v}_i^{N+1,K}\| + \|\mathbf{x}_i^{N+1,K+1} - \mathbf{x}_i^{N+1,K}\|}{\|\mathbf{v}_i^{N+1,K+1} - \mathbf{v}_i^{N+1,0}\| + \|\mathbf{x}_i^{N+1,K+1} - \mathbf{x}_i^{N+1,0}\|}$
end while
while $err_\theta \geq err_{TOL}$ **do**
  EVALUATE-PARTICLE-PARTICLE-CONTACT($particles$)
  EVALUATE-PARTICLE-SURFACE-CONTACT($particles$, $surfaces$)
  EVALUATE-PARTICLE-FLUID-INTERACTION($particles$, $fluid$)
  for $i = 1, N_p$ **do**
    $\mathcal{Q}_i^{N+1,K} \leftarrow$ sum of all fluxes
    $\theta_i^{N+1,K+1} = \theta_i^N + \frac{\Delta t}{2m_i C_i}\left[\mathcal{Q}_i^{N+1,K} + \mathcal{Q}_i^N\right]$
    update dynamic variables θ_i, retain $\mathbf{v}_i$, $\mathbf{x}_i$
  end for
  $err_\theta = \sum_i \frac{\|\theta_i^{N+1,K+1} - \theta_i^{N+1,K}\|}{\|\theta_i^{N+1,K+1} - \theta_i^{N+1,0}\|}$
end while

Chapter 2, Sections 2.3. The forces from the collision can be also averaged over the time-step to obtain momentum conservation as mentioned in Section 2.3. It must be noted however that as an artifact of the way collisions are dealt with, there could be cases where colliding particles have a delay in responding to the collision event, and they end up penetrating each other further than realistically allowed. During the time step they are then allowed to resolve the collisions. Therefore this method can be very useful for collisionally dominant systems, but can lead to erroneous particle configurations with unrealistic penetrations for particle systems undergoing enduring contact.

For particle systems with enduring contacts, we consider the case where $t^* \rightarrow t$ and $\Delta t < \delta t$, such that the contact events for every particle level contact are resolved within the time-scale of the contact lifetime. From the theoretical discussion on force-deformation relations for deformable contacts presented in Chapter 2, Section 2.2, it can be seen that such models are well suited to deal with this particular scenario. During the course of developing algorithms for integrating such equations, we found that a choice of time-step such that $N_{div}\Delta t = \delta t$ with $N_{div} \approx 3 - 5$ can capture dynamics reasonably well - although the choice of N_{div} is an issue completely dependent on the problem and the user.

For the sake of completion, we discuss two further specific cases that can be obtained from the decomposition of physical events presented in Equations 4.11, 4.12, and 4.13. The first one is the specific case where the sum of all non-contact external forces acting on the particle $\mathbf{F}_{i,non-contact}$ is either zero or a constant. Under such a scenario, the particle motion is collisionally driven, and the non-collisional motion of the particles is easily integrable and gives the following:

$$\mathbf{v}_i^{N+1} = \mathbf{v}_i^N + \frac{\mathbf{F}_{constant}}{m_i}\Delta t \tag{4.14}$$

$$\mathbf{x}_i^{N+1} = \mathbf{x}_i^N + \mathbf{v}_i^N\Delta t + \frac{\mathbf{F}_{constant}}{2m_i}(\Delta t)^2 \tag{4.15}$$

This provides a direct way of estimating when two particles would collide by solving a quadratic equation involving particle positions and the time interval Δt - and allows for a discrete event based treatment of collisions where the velocities get updated during collisions whenever they occur, and particles follow Equations 4.14 and 4.15 otherwise. This is the main idea behind Event-driven Particle Dynamics Simulations and a very detailed review of existing techniques and applications for this technique can be found in Poschel & Schwager[122].

Along similar lines, a second technique can be motivated by considering the case where

$\delta t << \Delta t$, and revisiting the Equations 4.11-4.13. Shifting the collision instant to the beginning of the time-step, and using the assumption of very short impact durations, the time-step can be decomposed into a collision step where the particle velocities are directly updated post-collision, and the updated velocities are then used to propagate the particle under the action of non-contact forces for the rest of the time-duration Δt. This leads to the premise of a 'Collide and Stream' type calculation - which is usually employed in Lattice-Boltzmann type calculations (see Sukop & Thorne[146] for a detailed discussion on such methods).

$$m_i \mathbf{v}_i(t+\delta t) - m_i \mathbf{v}_i(t) = \langle \mathbf{F}_i^c \rangle \delta t + \langle \mathbf{F}_i^e \rangle \delta t \qquad \text{Collide step} \tag{4.16}$$

$$m_i \mathbf{v}_i(t+\delta t) - m_i \mathbf{v}_i(t+\Delta t) = \int_{t+\delta t}^{t+\Delta t} \mathbf{F}_i^e dt \qquad \text{Stream step} \tag{4.17}$$

It must be remarked furthermore, that since the 'Collide step' only lasts physically until the collision event gets over, the positions of the colliding bodies will not get updated during the collide step. Hence with the post-collisional velocities the positions and future velocities get updated together in the stream step - making the collide step behave mathematically more like an operator that modifies the momenta.

4.2.3 An example of time-step adaptivity

The computation of the dynamic variables of a particle ensemble can be made more efficient if the time-step sizes are allowed to vary based on a control strategy. Specifically for discrete particle simulations, there could be distinct time-scales of the physical interactions during a single simulation - dynamic variables could vary slowly during certain durations, and rapidly during others. We present here an example of time-step adaptivity using Runge-Kutta methods, which are, as mentioned earlier, higher-order accurate, one-step methods that can be represented typically using the following tableaux representation called the Butcher array:

$$\begin{array}{c|ccc} c_1 & a_{11} & \dots & a_{1s} \\ \vdots & \vdots & & \vdots \\ c_s & a_{s1} & \dots & a_{ss} \\ \hline & b_1 & \dots & b_s \end{array} \tag{4.18}$$

where s is the number of stages used for approximating the derivatives. The updates to the primary variable in an ordinary differential equation of the form $y = \frac{d}{dt} f(y,t)$ is given using the coefficients as follows:

$$k_i = f\left(t_n + c_i\Delta t, y_n + \Delta t \sum_{j=1}^{s} a_{ij}k_j\right) \tag{4.19}$$

$$y_{n+1} = y_n + \Delta t \sum_{j=1}^{s} b_j k_j \tag{4.20}$$

The typical approach for time-step adaptivity is to seek a measure of the error in the solution, and the conventional approach is to use the one-step error also called the local truncation error τ_n. For a numerical discretized scheme of order p, τ_n has an asymptotic behavior as follows:

$$\tau_n \approx C\Delta t^{p+1} \tag{4.21}$$

where C is a constant dependent on the discretization. simple way of estimating this error can be proposed by considering now the solutions obtained through successively refining the time-step size. Considering time-step size to be Δt, let us consider two successive refinements in time-step as $\alpha\Delta t$ and $1-\alpha\Delta t$ (with $\alpha \in (0,1)$). Writing the exact solution at the instant $n+1$ going from n to be $\bar{y}_{n+1}$, and the original and refined solutions to be y_{old} and y_{ref} respectively, we can write the following:

$$y_{old} = \bar{y}_{n+1} + C\left(\Delta t\right)^{p+1} + \mathcal{O}\left(\Delta t^{p+2}\right) \tag{4.22}$$

$$y_{ref} = \bar{y}_{n+1} + C\left(\alpha^{p+1}\Delta t^{p+1}\right) + C\left((1-\alpha)^{p+1}\Delta t^{p+1}\right) + \mathcal{O}\left(\Delta t^{p+2}\right) \tag{4.23}$$

$$\text{subtract} \Rightarrow C = \frac{\parallel y_{ref} - y_{old} \parallel}{\left[1-\alpha^{p+1}-(1-\alpha)^{p+1}\right]\Delta t^{p+1}} \tag{4.24}$$

Plugging this value of C back into Equation. 4.23, an estimate of the error can be obtained now as follows:

$$\tau_n = \frac{\left[\alpha^{p+1}+(1-\alpha)^{p+1}\right]}{\left[1-\alpha^{p+1}+(1-\alpha)^{p+1}\right]} \parallel y_{ref} - y_{old} \parallel \tag{4.25}$$

For the particle dynamics Equations 4.1 and 4.3, now, the function f in the above discussion, will be replaced by $\frac{\mathbf{F}_i}{m_i}$ and $\frac{\mathcal{Q}_i}{m_i C_i}$ respectively. Assuming that higher order accurate Runge-Kutta methods are used, the fact that the function f is evaluated three times for getting the error estimate makes this a computationally expensive procedure. To estimate the error more efficiently therefore, a specialized class of such methods called the embedded Runge-Kutta methods can be used. In such methods, two embedded discretizations one of order p (say) and the other of order $p+1$ are chosen such that they have the same stage

derivatives k_i - which avoids recalculation of the complicated force and flux terms in our simulation framework. Assuming the solution obtained from the lower and higher order discretizations to be y_p and y_{p+1} respectively, we have the following:

$$C\Delta t^{p+1} = y_p - y_{p+1} \tag{4.26}$$

$$= y_n + \Delta t \sum_{j=1}^{s} b_j^p k_j - y_n - \Delta t \sum_{j=1}^{s} b_j^{p+1} k_j \tag{4.27}$$

$$= \Delta t \sum_{j=1}^{s} \left(b_j^p - b_j^{p+1}\right) k_j \tag{4.28}$$

Assuming now that the objective of the control strategy is to keep the error within a tolerance TOL, the folioing can be written for the optimal step-size Δt_{opt}:

$$C\left(\Delta t_{opt}\right)^{p+1} = TOL \Rightarrow \Delta t_{opt} = \Delta t \left(\frac{TOL}{\Delta t \sum_{j=1}^{s} \left(b_j^p - b_j^{p+1}\right) k_j} \right)^{1/p+1} \tag{4.29}$$

In reality, the time-step sizes for a simulation will always have to be bound between a chosen maximum and minimum step-size which are dictated by either simulation time or other physical time-scale requirements or both. Also, to obtain the estimated error, it is typical practice to scale the error measure with a constant factor less than 1. Using the discussions presented here, the implementation of a control strategy ported into the developed simulation library, has been illustrated in form of a simple pseudocode in Algorithm 2.

4.3 Pre-processing - generation of initial ensemble configurations

At this point in our discussion, having explored the issue of integrating the motion equations, we focus on specifying the initial conditions for these motion equations - since essentially we are solving an initial value problem for each particle in the ensemble. In the context of discrete particle simulations, specification of initial conditions entail the generation of an initial configuration of a required number of particles. The classical method for generating an arbitrary configuration of spheres is the Random Sequential Addition algorithm proposed by Widom [165]. The central idea of this method is to place non-overlapping spheres at random locations within a specific domain - and the implementation of the algorithm has been illustrated using a flowchart in Figure 4.1.

While essentially simple to implement, such an algorithm cannot computationally generate volume fractions beyond a certain threshold ($\approx$ 0.35-0.40 in 3D). To provide for a

Algorithm 2 *The pseudocode sequence illustrating the implementation of a simple time-step adaptivity algorithm based on Equation 4.29*

obtain values of $\mathbf{v}_i^N$, θ_i^N, Δt, TOL
calculate updated solution using Equation 4.19, 4.20
$error = \Delta t \sum_{j=1}^{s} \left(b_j^p - b_j^{p+1}\right) k_j$
if $error \leq TOL$ **then**
    accept the step-updated solution $\mathbf{v}_i^{N+1}$, θ_i^{N+1}
    $\Delta t_{new} = \beta_{safe} * \Delta t \left(\frac{TOL}{\Delta t \sum_{j=1}^{s} \left(b_j^p - b_j^{p+1}\right) k_j} \right)^{1/p+1}$
    if $\Delta t_{new} \geq \Delta t_{max}$ **then**
        $\Delta t_{new} = \Delta t_{max}$
    else if $\Delta t_{new} \leq \Delta t_{min}$ **then**
        $\Delta t_{new} = \Delta t_{min}$
    end if
else
    reject the step-updated solutions
    $\Delta t_{new} = \beta_{safe} * \Delta t \left(\frac{TOL}{\Delta t \sum_{j=1}^{s} \left(b_j^p - b_j^{p+1}\right) k_j} \right)^{1/p+1}$
    if $\Delta t_{new} \geq \Delta t_{max}$ **then**
        $\Delta t_{new} = \Delta t_{max}$
    else if $\Delta t_{new} \leq \Delta t_{min}$ **then**
        $\Delta t_{new} = \Delta t_{min}$
    end if
    reiterate, goto Step 2
end if

technique to generate higher packing volume fractions, Lubachevsky & Stillinger [88] proposed an alternative algorithm based on concurrent collision and growth of an ensemble of randomly located particles. According to the original version of this algorithm, after every impact the velocities of the particles are modified as follows:

$$\mathbf{v}_i = \mathbf{v}_{i,n} + h \frac{\mathbf{x}_i - \mathbf{x}_j}{\| \mathbf{x}_i - \mathbf{x}_j \|} + \mathbf{v}_{i,t} \tag{4.30}$$

$$\mathbf{v}_j = \mathbf{v}_{j,n} + h \frac{\mathbf{x}_j - \mathbf{x}_i}{\| \mathbf{x}_j - \mathbf{x}_i \|} + \mathbf{v}_{j,t} \tag{4.31}$$

where the subscripts n and t represent the velocity components normal and tangential to the plane of contact. The post-impact velocities are augmented with additional energy in

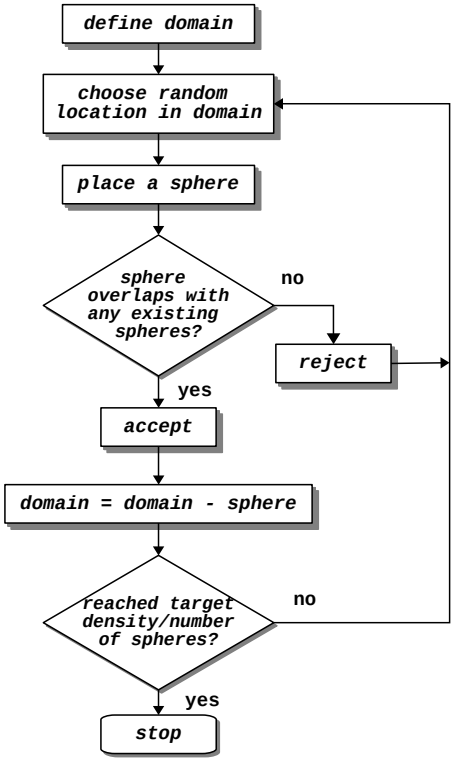

Figure 4.1: *A flowchart illustrating the algorithm for random sequential addition of spheres to a domain*

form of an added velocity component of magnitude h. This addition of energy to the particles is justified by the fact that at each step the radius of the particles are also increased by a simple law:

$$\frac{dR_i}{dt} = \lambda_i \tag{4.32}$$

and the growth of particles therefore causes particle surfaces to approach each other faster than the particle centers. The original form of the growth rate was simply a constant. In a later modification to this algorithm Kansal et. al. [81], improved upon the statistical properties of the packing obtained by making the growth rate proportional to the initial radius of the particles. This will still be a constant for the case of a monodisperse ensemble, but will ensure a uniform increase in mean particle volume with simulation time for polydisperse ensembles as well. Kansal et. al. [81] further discuss aspects of the addition of energy to the particles. It must be noted here that an increase in energy with time for the particles may cause increasingly diverging collision rates, and leads to scenarios that are numerically difficult to tackle. Appropriate strategies have been provided in both Lubachevsky & Still-

inger [88], and Kansal et.al.[81]. The original form of the algorithm uses an event-driven simulation algorithm - but keeping with the current work on force based simulations, we present in Algorithm 3 a modified form of the algorithm that has been implemented and included in the libraries developed as a part of this work - where the ensemble growth and energy addition both continue up until the time in the simulation when the ensemble volume fraction reaches very close to the desired volume fraction. The criteria can be based solely on the energy addition as well - such modifications can be easily made if required.

Algorithm 3 *A pseudocode illustrating the implementation of a modified form of the concurrent growth based algorithm for generating a high density ensemble of spheres.*

GENERATE-RANDOM-SEQUENTIALLY-ADDED-ENSEMBLE(N_p)
for $i = 1, N_p$ **do**
    assign small initial velocity $\rightarrow \mathbf{v}_i$
    $\lambda_i \leftarrow R_i$
end for
while $volfrac \leq desired$ **do**
    EVALUATE-PARTICLE-PARTICLE-ELASTIC-CONTACT(*particles*)
    if *boundary condition* = *hard wall* **then**
        EVALUATE-PARTICLE-SURFACE-ELASTIC-CONTACT(*particles*, $surfaces$)
    end if
    for $i = 1, N_p$ **do**
        update particle velocities $\rightarrow \mathbf{v}_i$
        add energy to particles $\mathbf{v}_i \leftarrow \mathbf{v}_i + \left[\frac{\lambda}{\sqrt{3}}, \frac{\lambda}{\sqrt{3}}, \frac{\lambda}{\sqrt{3}}\right]$
        $R_i \leftarrow R_i + \lambda_i \Delta t$
        if *boundary condition* = *periodic* **then**
            APPLY-PERIODIC-BOUNDARY-CONDITION(*particles*)
        end if
        calculate and update $volfrac$
    end for
end while

The implementation of these two algorithms has also been illustrated in Figure 4.2 where an ensemble with a low volume fraction was initially generated using an RSA algorithm, and thereafter, was grown using the LS type algorithm as presented in Algorithm 3 up until a desired higher volume fraction value was attained. Further discussions on advanced algorithms for generating particle ensembles using a modified random sequential addition algorithm can be found in the work of Torquato et. al. [155]. However since the objective here is to create an initial configuration for a more detailed calculation of particle dynamics, and not the accurate estimation of statistics of packed spherical or ellipsoidal particles - such

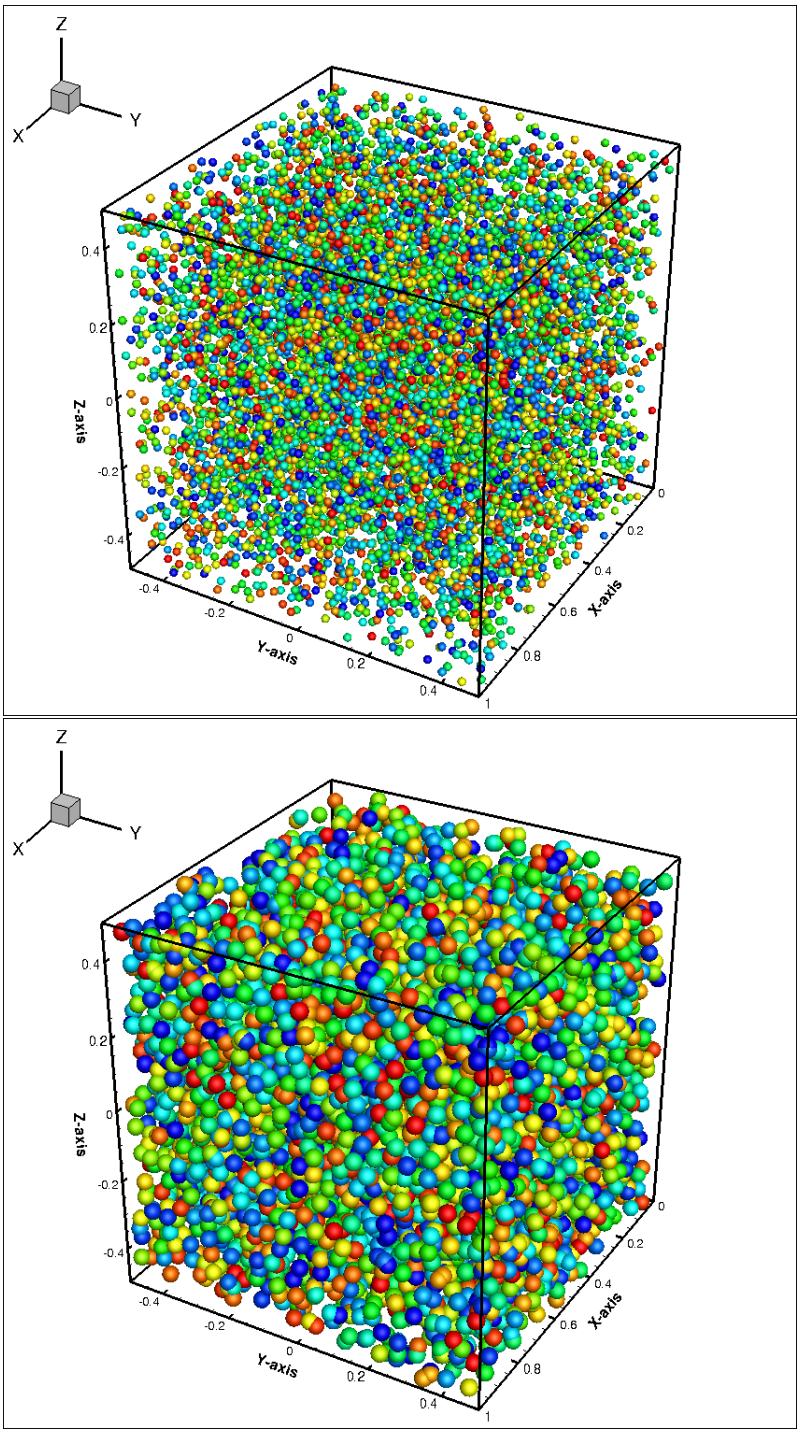

Figure 4.2: *An example of a low volume fraction (top) ensemble created using a random sequential addition implementation, and a high volume fraction (bottom) created using a concurrent growth algorithm as presented in Algorithm 3*

algorithms will not be explored in detail here.

The generation of an initial configuration also involves the assignment of an initial velocity (and angular velocity if needed) to each particle. For most applications this velocity can be set based on the kind of problems being addressed. For example, for particulate spray applications, it is typical practice to set the particulate initial velocities based on the exit velocities from the spray nozzle (see for example the work by Fritsching [53] for further details and examples). For granular beds and silo flows on the other hand, typically the particles are all started from rest (see the examples presented in Poschel & Schwager[122] for details). For a broad range of applications, the particle velocities can also be set to be randomly sampled from an underlying distribution with a mean value and variance that is characteristic to the problem being addressed. Particularly interesting is the case of assigning random initial velocities to the particles such that the particles all have constant energy. For translational motion, this entails sampling $v_{i,x}, v_{i,y}, v_{i,z}$ such that:

$$\frac{1}{2}m_i\left(v_{i,x}^2 + v_{i,y}^2 + v_{i,z}^2\right) = E_0 \qquad \forall i = 1, \cdots, N_p \tag{4.33}$$

This essentially entails choosing points on a sphere with radius $E_0/2m_i$. Such problems of choosing random points on an N-dimensional hypersphere have been studied extensively and the interested reader is referred to the works by Muller [109], Sibuya [139], and Tashiro [152], and the review by Saff & Kuijlaars [135]. The simplest approach, as cited in Muller [109] is to generate normal random variates $x_k, k = 1, 2, 3$, and then obtain the velocities as

$$v_k = \frac{x_k}{\sqrt{x_1^2 + x_2^2 + x_3^2}}\sqrt{2m_i E_0} \tag{4.34}$$

4.4 Neighbor-lists for contact checks

From Equation 4.1 and 4.3, the evaluation of the contact forces involve a detection of contact between particles (that is to say, evaluation of the indicator function $\mathcal{I}(\cdot,\cdot)$). While for spherical particles, the check for contact between particles is a simple geometric criteria given by:

$$(R_i + R_j) - \parallel \mathbf{x}_i - \mathbf{x}_j \parallel \geq 0 \tag{4.35}$$

a naive evaluation of this criteria for all possible pairs in a system of N_p particles involves $0.5N_p(N_p - 1)$ operations, and turns out to be the most expensive step for the computation (scaling with system size asymptotically as $\mathcal{O}\left(N_p^2\right)$). To deal with this check in an efficient manner, it is noted that contact interactions (and other similar short-range interactions) for any particle will be restricted mainly within other neighboring particles in close vicinity. Therefore, ideas based on partitioning of particles in the domain, and maintaining a list

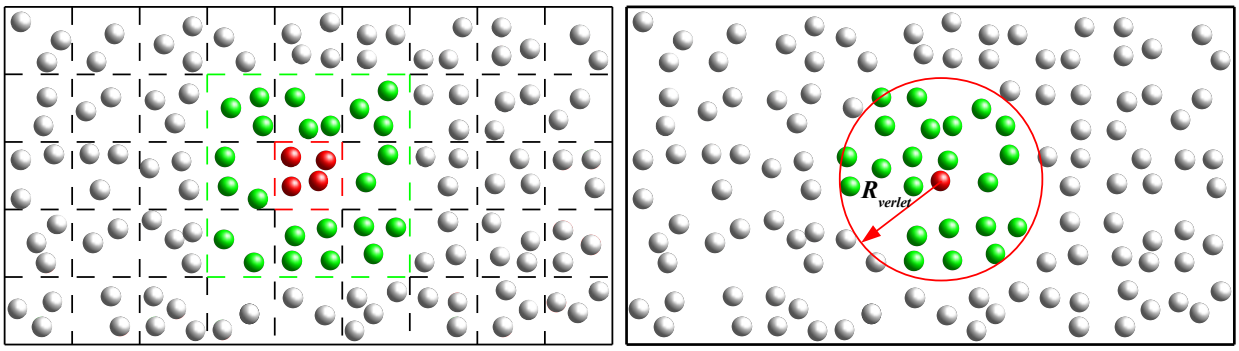

Figure 4.3: *Schematic representation of creating neighbor lists for efficient detection of contact pairs for a particle ensemble. For binned domain (left) the red particles in a bin interact with other red and surrounding green particles. For Verlet list (right), particles within a cut-off distance from the red particle are in the neighbor list.*

of close neighbors will reduce contact checks and make the computations more efficient. The classical form of such a neighbor list was introduced by Verlet [159] in a work on molecular systems driven by Lennard-Jones type interactions, where a bookkeeping technique for maintaining a list of particles within a specified cut-off distance from a given particle was introduced. Such lists are named Verlet lists, and the basic idea is illustrated in Figure 4.3 (right hand side). The lists are created for each particle based on inter-particle separations, and therefore need to be updated if particles are displaced appreciably since the time the lists were constructed last. The interested reader is referred to the works by Frenkel & Smit [52], and Poschel & Schwager [122] for implementation details. Since the Verlet lists are created based on inter-particle separations, a naive implementation of the algorithm would again require $\mathcal{O}\left(N_p^2\right)$ operations to initialize the lists every time. An alternative method - also referred to as Cell-List method, or Linked-Cell method or simply Binning method - overcomes this by partitioning the particles into grids or bins in the domain, and seeking contact pairs for a particle in its own bin, and all of its neighboring bin. The basic idea has been illustrated also in Figure 4.3 in the second panel. From a simple analysis of the number of operations, it can be claimed that the number of operations required to initialize the bins will be approximately equal to the number of particles (and hence asymptotically scale as, $\mathcal{O}\left(N_p\right)$). If we consider that on an average, there are N_b bins, and each bin gets N_p/N_b particles then a simple estimate of the total operation count for contact checks can be given to be (for a single simulation time-step):

$$N_{contact} = \mathcal{O}\left(N_p\right) + \mathcal{O}\left(\left(\frac{N_p}{N_b}\right)^2 N_b\right) \approx \mathcal{O}\left(N_p\right) \tag{4.36}$$

Identifying this advantage in computational effort Auerbach et. al. [6] combined the two

Algorithm 4 *The pseudocode illustrating a binning algorithm implementation used for the simulation libraries for DEM described in this work. It is assumed that each bin is of dimension $\Delta_x \times \Delta_y \times \Delta_z$. The variables are self-explanatory.*

```
for i = 1, N_p do
    bin_x = int((x_i − x_0)/Δx) etc.
    place particle i in bin indexed by (bin_x, bin_y, bin_z)
end for
for b = 1, N_b do
    P_b ← number of particles in bin b
    for i = 1, P_b do
        for j = i + 1, P_b do
            Evaluate-Particle-Particle-Contact(i, j)
        end for
    end for
    Nbr ← number of neighbors of bin b
    for n = 1, Nbr do
        P_nor ← number of particles in bin b
        for i = 1, P_b do
            for j = 1, P_nbr do
                Evaluate-Particle-Particle-Contact(i, j)
            end for
        end for
        delete n from the list of neighbors of b
        delete b from the list of neighbors of n
    end for
end for
```

implementations to provide a fast way of initializing the Verlet lists while retaining the update scheme - an implementation that has also been discussed in detail by Poschel & Schwager [122]. In order to illustrate the implementation details, a variant of the Binning algorithm used to develop the simulation libraries for this work has been illustrated in Algorithm 4. Further references on expanding such algorithms into parallel computing applications can be found in the works of Chialvo & Debenedetti [27], Grest et. al. [59], and Sutmann & Stegailov [148].

Chapter 5

Representative Simulations of Spray Dynamics and Particulate Flow

5.1 Introduction

In this chapter we present representative numerical simulations performed using the computer simulation library developed based on the ideas presented in Chapters 2, 3, and 4. The objective of the examples presented here is to demonstrate, in general, the utility of such simulations in analyzing dynamics of granular and particulate media for a broad range of applications, and also specifically to demonstrate the capabilities of the simulation libraries developed. In particular, our focus has been on loosely flowing particulate media for manufacturing applications. Particulate media enjoy substantial prominence in a vast range of modern manufacturing processes - spray-forming, abrasive finishing, and additive manufacturing to name a few. Such processes essentially involve coupled multi-physical phenomena in media comprising discrete particles or grains surrounded by a fluid. The interested reader is referred to the works by Martin (see [93] and [94]) for a detailed overview about a broad range of such processes for deposition and surface engineering, the work by Fritsching [53] for spray process engineering, the work by Luo & Dornfeld[89] and Arbelaez & Zohdi [4] on the abrasive polishing of surfaces using chemical-mechanical planarization, and the review on additive manufacturing technologies by Kruth et.al.[84] and Gu et.al.[60]. In the following sections, two representative case-studies have been discussed in detail. The first example presented in Section 5.2 is that of a stream of abrasive particles impacting a porous composite material layer. This is a problem of interest in polishing and abrasive finishing processes, and in the analysis of performance and durability of an engineered surface coating against abrasive wear. The second example presented in Section 5.3 is that of a spray of particles being deposited on a target surface. For both examples, the insights provided through a detailed resolution of discrete particle dynamics, as compared to a continuum based approach will be illustrated in sufficient detail.

5.2 Dynamics of a Jet Impacting a Porous Surface

5.2.1 Simulation configuration

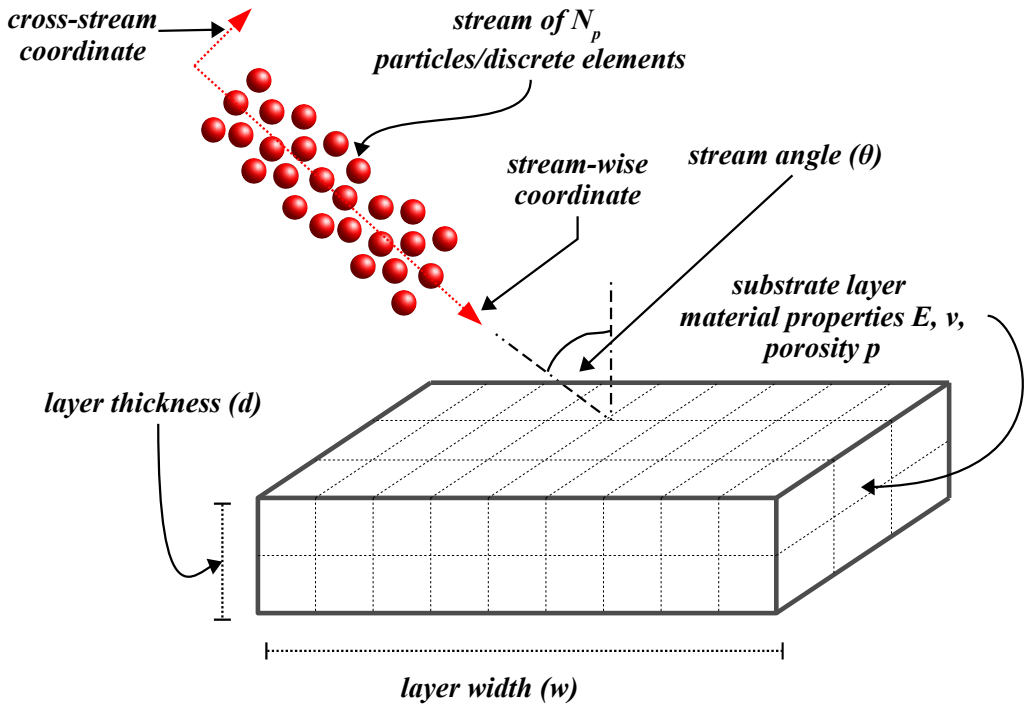

Figure 5.1: *Schematic representation of the simulation set-up for analysis of the impact of a stream of particles impacting a material layer of thickness d and width w such that both $d, r \ll$ particle radius.*

The schematic of the simulation configuration is presented in Figure 5.1, where a stream of loose, non-bonded particles are propagating towards a surface which can be either porous or heterogeneous (or both) in terms of its microstructure. The particle ensemble is generated using pre-processing algorithms as presented in Section 4.3. The domain is binned into subdomains for checking for possible contacts. The actual computation domain being much bigger than the cross-span dimensions of the particle stream, so as to capture the dynamic spreading of the stream after collision with the surface. Any particle that exits the computation domain is taken out of the simulation data structures. For the examples presented here, the impulse-momentum form of the contact law has been used. To account for stream angle, the impact forces are transferred to the surface using appropriate coordinate transformations. The details of stress-calculation and damage evolution have been discussed separately in the subsequent sections - and together, they can be thought of to be a naive implementation of a coupling technique between discrete particles and a material continuum.

5.2.2 Stress calculation

The translation of the contact forces into stresses in the surface material can be approached by considering the surface being impacted to be a semi-infinite half-space, and considering the contact forces to be applied surface tractions, as explained in the schematic in Figure 5.2. This is a good abstraction for cases where the contact does not involve extensive deformations as compared to the dimensions of the surface - which is a reasonably good approximation for erosive wear of surfaces under impact by abrasive particles. Semi-analytical solutions for the sub-surface stresses obtained using Boussinesq potential functions for point and distributed tractions on a semi-infinite elastic half-space are used for the applied surface tractions. For the sake of a concise presentation the detailed expressions for the solutions for stress components are not provided here, and the interested reader is referred to Johnson[77] for the details of the derivation and the explicit expressions for point tractions, and Hamilton[64] for the explicit expressions for Hertzian tractions distributed over the contact area between a sphere and a half-space. A fully detailed analysis of the deformations and stresses would require a finite element type calculation over a discretized mesh of the bulk of the particle-surface combination - as found in Camacho & Ortiz[22] and more recently in Ramanujam & Nakamura[126].

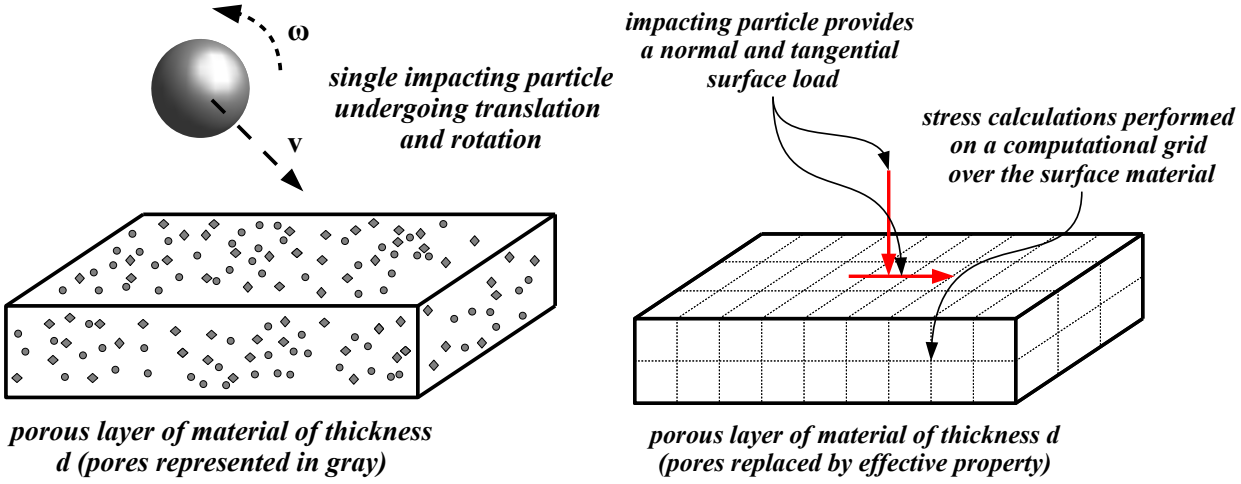

Figure 5.2: *A schematic representation of the translation of impact loads and material porosity into a simple stress-calculation framework over the material continuum.*

In order to incorporate the surface material porosity and microstructure in the calculations, without a detailed mesh-discretized resolution of the microstructure - we approximate the effective material properties of the surface material using analytical approaches involving variational bounds on the properties as presented by Hashin & Shtrikman[66], and Hashin & Shtrikman[65]. Such an approach has been used by Zohdi[177] for rapid parametric initial design investigations for tailoring microstructures to obtain desired effective properties -

and is advantageous owing to its minimal requirement of computational effort. The Hashin-Shtrikman bounds for material bulk modulus and shear modulus for a two-phase material are given by:

$$\kappa^{*,-} = \kappa_1 + \frac{v_2}{\frac{1}{\kappa_2-\kappa_1} + \frac{3(1-v_2)}{3\kappa_1+4\mu_1}} \leq \kappa^* \leq \kappa_2 + \frac{1-v_2}{\frac{1}{\kappa_1-\kappa_2} + \frac{3v_2}{3\kappa_2+4\mu_2}} = \kappa^{*,+} \tag{5.1}$$

$$\mu^{*,-} = \mu_1 + \frac{v_2}{\frac{1}{\mu_2-\mu_1} + \frac{6(1-v_2)(\kappa_1+2\mu_1)}{5\mu_1(3\kappa_1+4\mu_1)}} \leq \mu^* \leq \mu_2 + \frac{1-v_2}{\frac{1}{\mu_1-\mu_2} + \frac{6v_2(\kappa_2+2\mu_2)}{5\mu_2(3\kappa_2+4\mu_2)}} = \mu^{*,+} \tag{5.2}$$

where κ_1, κ_2 are the bulk moduli of the two-phases, and μ_1, μ_2 are the shear moduli of the two phases (with $\kappa_2 > \kappa_1$ and $\mu_2 > \mu_1$). For isotropic microstructure with isotropic effective properties, these bounds are the tightest provided no additional micro-topological information is available. A reasonably good approximation of the overall effective property can now be constructed using a convex combination of the bounds as follows:

$$\kappa^* = \phi\kappa^{*,+} + (1-\phi)\kappa^{*,-}, \quad \mu^* = \phi\mu^{*,+} + (1-\phi)\mu^{*,-} \tag{5.3}$$

In order to incorporate the porosity, we assume that the material is effectively a multi-phase composite, with the pores and voids making up phase 1 - such that $\kappa_1 = C\kappa_2$, and $\mu_1 = C\mu_2$, where C is a very small number. This can be plugged into Eq. 5.1, 5.2, 5.3 to obtain the effective mechanical properties of the porous material. It was found from repeated numerical experimentation that the property estimates are insensitive to changes in the value of C beyond $\approx 10^{-4}$. Clearly then the porosity(p) is going to be given by $p = v_1$, and we can plug in $v_2 = 1 - p$ in Eq. 5.1 and 5.2.

5.2.3 Damage evolution

The characterization of damage due to particle erosion and material removal has received much attention from both experimental and modeling perspectives. The earlier works by Finnie[50] and Bitter[14] characterized a series of erosive wear phenomena, and for ductile and brittle materials, they outlined the different causes of erosive wear. In a later work on ceramic coatings, Nicholls et.al.[114] further explored the characterization of erosive material loss from these coatings upon impact by particles. For brittle materials, Finnie[50] described the mechanics of crack induced damage and the propagation of circumferential ring cracks - whose diameter was explicitly reported to be dependent on the normal impact velocity as $d_{crack} \propto v_n^{0.4}$. The detailed analysis of the evolution of these cracks and the characterization of material removal will however require fully resolved analysis of the material continuum. For the current example, we incorporate a simplified damage criteria based on an appropriately defined equivalent stress. This is a non-local form of characterizing the potential damage a

particle impact can induce and in order to do so, we define (as per the discussions presented in the work by Lemaitre & Desmorat[86]) the triaxiality function R_ν as follows:

$$R_\nu = \frac{2}{3}(1+\nu) + 3(1-2\nu)\left(\frac{\sigma_{dil}}{\sigma_{vm}}\right)^2 \tag{5.4}$$

where σ_{dil} is the total dilatational stress, and σ_{vm} is the Von Mises effective stress. The criteria for non-local damage can now be stated in terms of an equivalent stress σ_{eq} that can be written as:

$$\sigma_{eq} = \sigma_{vm}\sqrt{R_\nu} \geq \sigma_0 \tag{5.5}$$

where σ_0 is an effective stress threshold, and can be set to be the yield stress or ultimate stress depending on the kind of material. The function R_ν relates to the strain energy density release rate (see Chaboche[23] and also Lemaitre & Desmorat[86] for details on the derivations) thereby providing a thermodynamic basis for utilizing such a criteria. It can be shown that the value of σ_{eq} as presented above is often quite different from the Von Mises stress - and could lead to a less conservative estimate of the extent of material damaged. In order to use this equivalent stress to estimate the evolution of damage across the continuum of the material the following variable is defined:

$$\Sigma = \frac{\sigma_{eq} - \sigma_0 + \parallel \sigma_{eq} - \sigma_0 \parallel}{2\sigma_0} \tag{5.6}$$

This variable is a non-dimensional indicator of damage initiation, and is zero for all cases where the equivalent stress is lesser than the critical. The potential damage at a certain location in the material continuum can be tracked by the number of times during the simulation that Σ exceeds zero - that is, by tracking the number of occurrences of high damage equivalent stresses at a location.

5.2.4 Simulation results

The simulation parameters used for the examples presented here have been summarized in Table 5.1. The results for the simulation can be discussed from the perspective of the dynamics of the particle ensemble, and the evolution of stresses and damage in the material being impacted. For the former, snapshots of the particle ensemble at various instants during the process of impact have been compiled in Figure 5.3. All particles have been colored based on their energy content. Even though the incident velocities are all normal to the surface, the inherent randomness of the particle initial configuration, causes a significant number of oblique inter-particle collisions that lead to a spread pattern of the particle jet as observed here. In order to demonstrate the corresponding dynamics for a oblique incidence of the particle ensemble on the surface - the snapshots of the particle ensembles for a stream angle

of $\theta = 30$ degrees has also been presented in Figure 5.4. The side view of the stream dynamics is presented for this case so as to emphasize on the spread pattern upon oblique impact - which is driven by both oblique particle particle collisions, and by oblique particle surface collisions.

Parameter	**Assumed values**
Material bulk modulus (both surface and particle)	100 GPa
Poisson ratio (both surface and particle)	0.30
Particle density	8500 kg/m^3
Impact velocity range	80 - 90 m/s
Porosity range	0.10 - 0.40
Friction coefficients (static, dynamic)	0.55, 0.50

Table 5.1: *Simulation parameters for the examples of abrasive jet impacting a porous surface*

The evolution of the accumulated damage due to the normal incident stream of particles has been shown in Figure 5.5, and it can be seen that the accumulated damage spreads radially outward from the centerline of the stream. The corresponding evolution of the damage equivalent stress σ_{eq} as defined in 5.5 has also been compared in Figure 5.6 for normal vs oblique incidence, and for varying levels of material porosity at a point very close to the centerline of the stream, located across the thickness (that is, $z = d$, for the snapshots presented in Figure 5.5). The corresponding accumulated damage shows a direct correlation of increased accumulated damage due to increased porosity, and a lower level of damage sustained due to an oblique impact - particularly as is evident from the sample results on accumulated damage due to a jet impacting at 80 m/s as presented in Figure 5.6 (bottom). The stress-signatures (presented in Figure 5.6 top) indicate an interesting feature of a sharper rise in the stresses immediately when impact initiates, followed by a reduced level of stresses as the impact progresses on. This reduction can be explained by a retardation of the incident stream of particles owing to collisions with reflected particles from the surface. Since each collision will involve some energy losses, the energy with which the stream impacts the surface therefore reduces after the first set of particles impact the surface. In this regard, it is remarked that further modifications to the simulations can be done in terms of boundary conditions to maintain a constant mass flow rate of particles. To do this, for every particle that leaves the computation domain as the stream spreads out post-impact, another particle of equal mass has to be entered into the domain from the stream inlet. Although this has not been implemented here, such modifications are easy to perform given that explicit tracking of particles entering and leaving the computation domain is already being performed as a part of binning the computation domain.

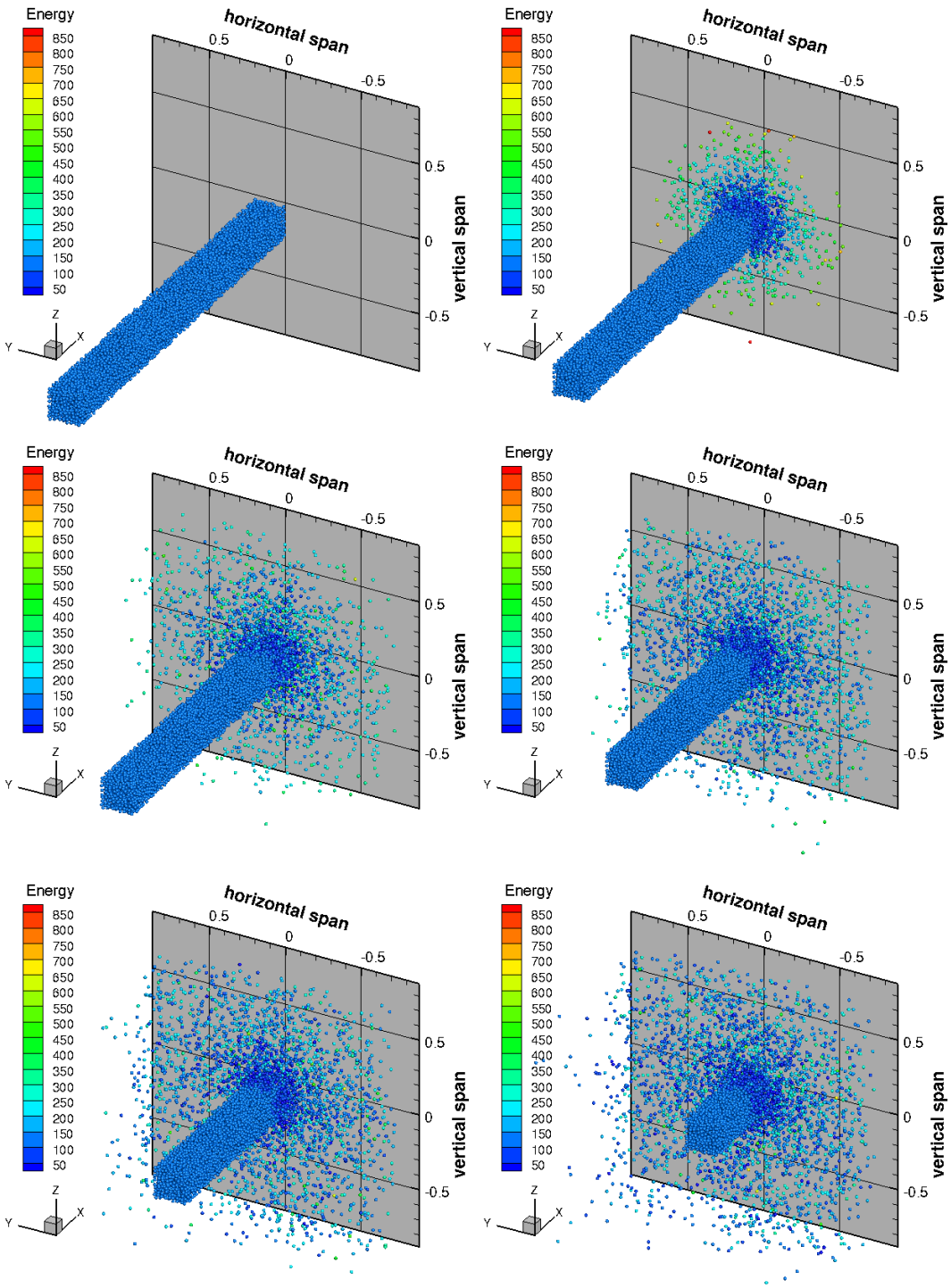

Figure 5.3: *Snapshots of the particle stream dynamics for normally incident stream*

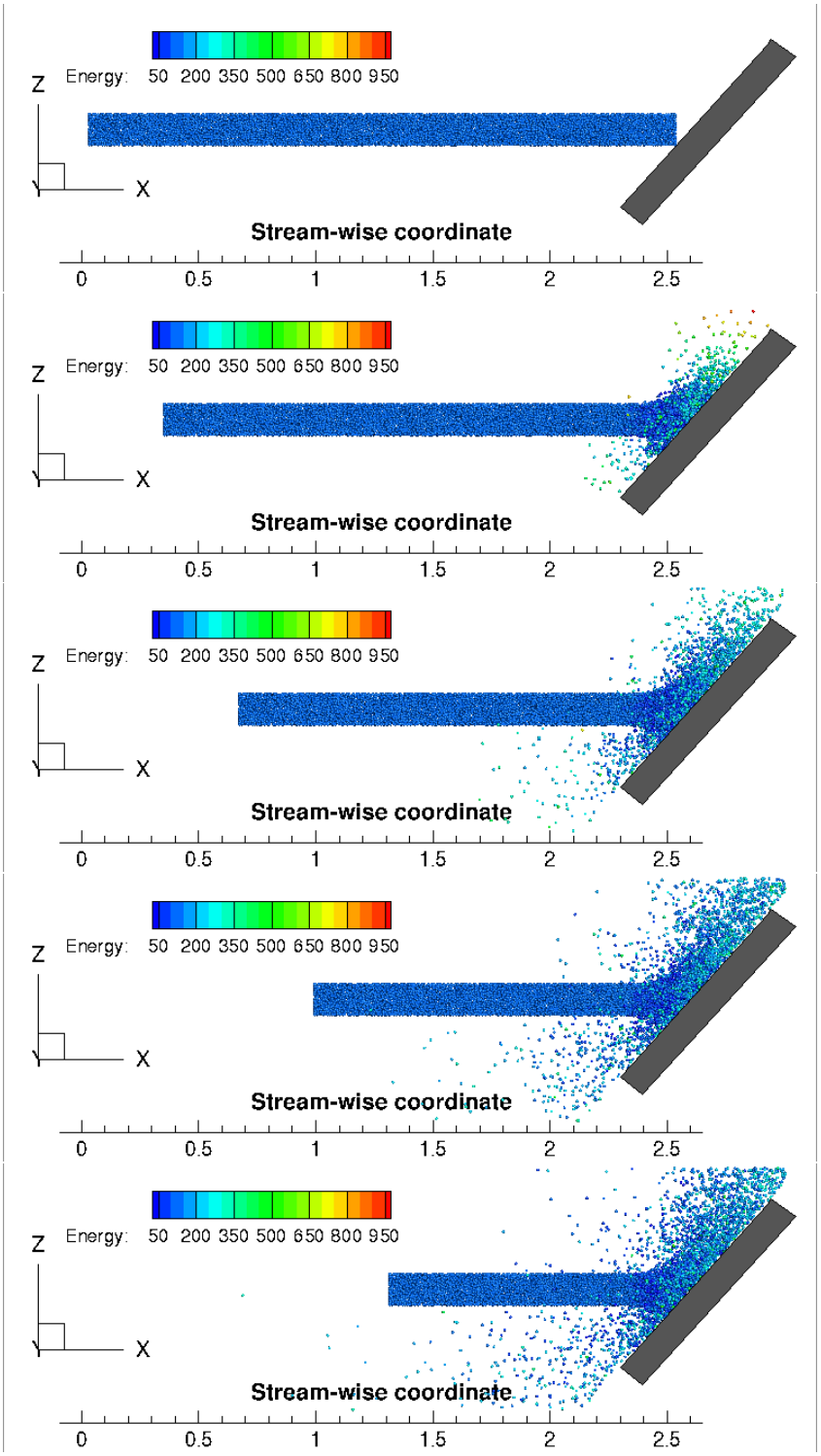

Figure 5.4: *Snapshots of the particle stream dynamics for an obliquely incident stream*

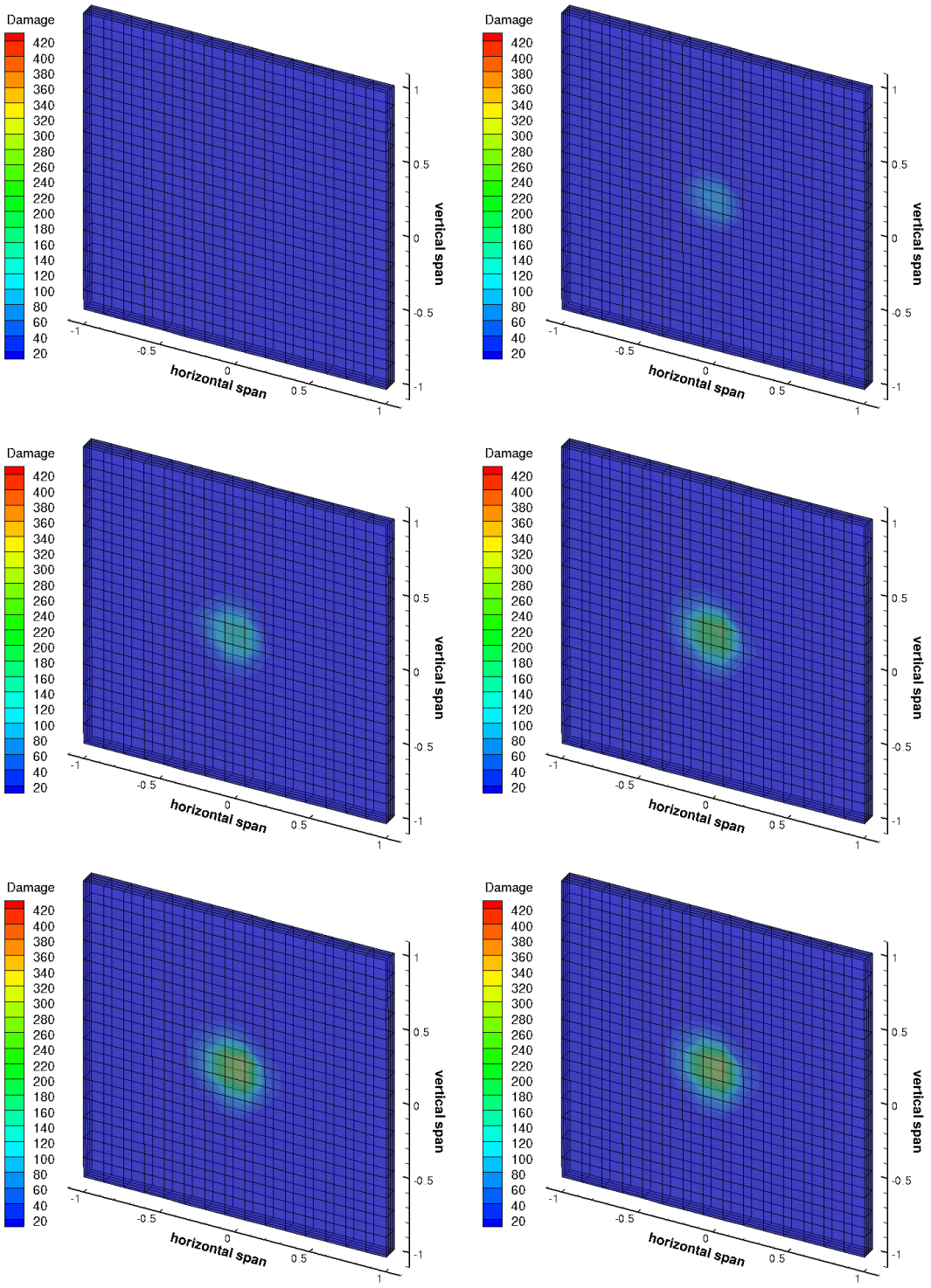

Figure 5.5: *Snapshots of evolving accumulated damage across the material*

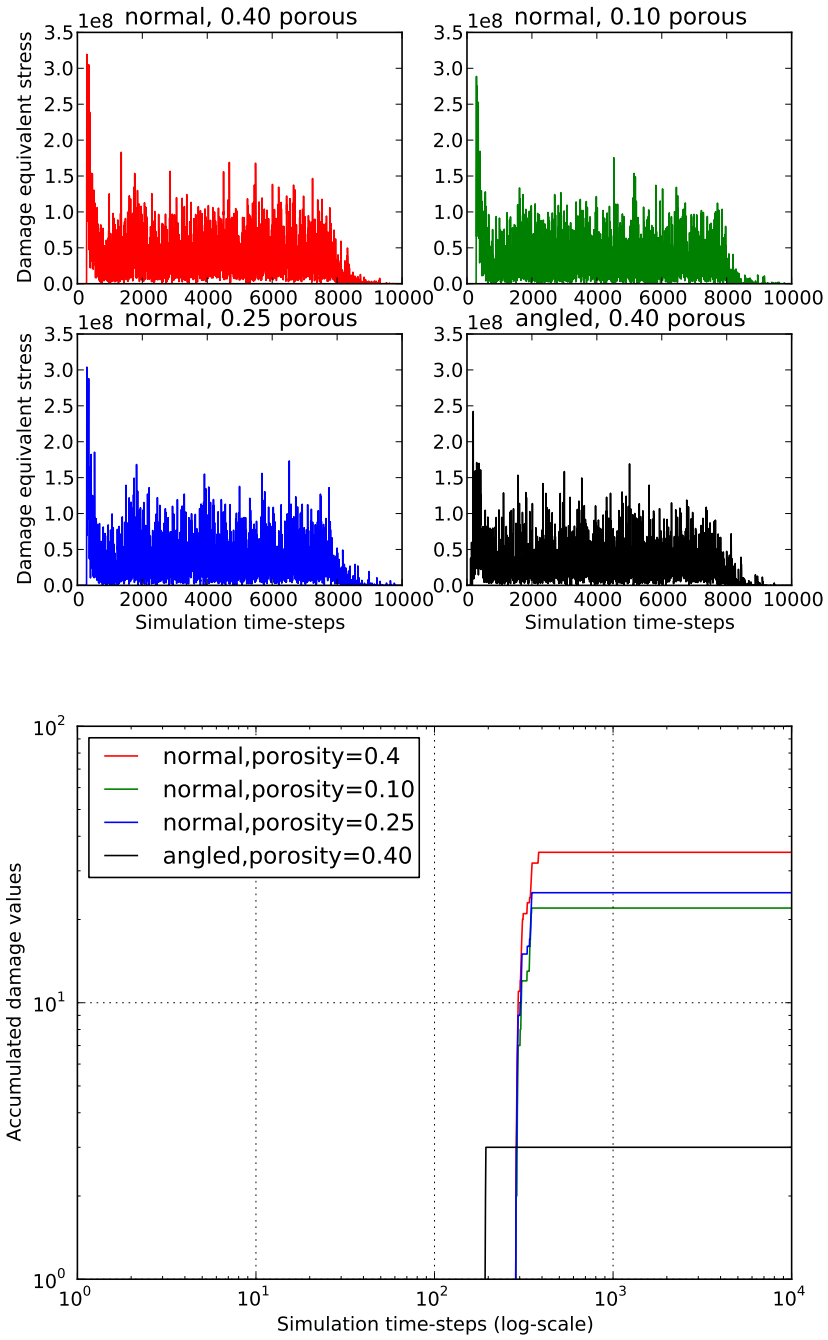

Figure 5.6: *A comparison of stress levels and accumulated damage at a point located across the depth of the layer of material, at a location very close to the centerline of the stream. The stress signatures for varying angles and porosity are shown on top, and comparison of accumulated damage at this location is shown in bottom.*

5.3 Dynamics of Spray Deposition

5.3.1 Simulation configuration

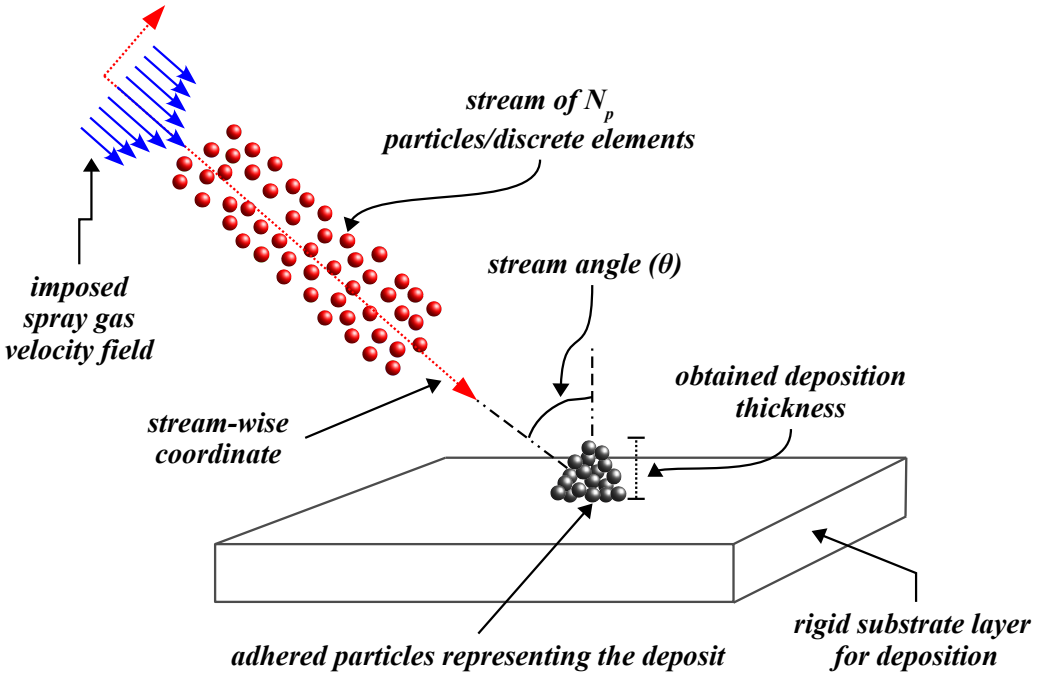

Figure 5.7: *Schematic representation of the simulation set-up for analysis of spray deposition. The lines in blue indicate an imposed background gas velocity field, and the already deposited particles have been indicated in gray.*

The schematic of the simulation configuration set-up for analysis of spray dynamics and deposition is presented in Figure 5.7, where similar to the previous example a stream of loose, non-bonded particles are propagating towards a surface for deposition. The particle ensemble is treated in the same manner as in the previous example. We are concerned here with the combined mechanics of collision and adhesion at the surface, and not the sub-surface stresses. A simple criteria to algorithmically model the deposition phenomena based on near-field, adhesive effects is presented in the next section. It must be noted that inter-particle adhesive interactions that could lead to particle agglomeration while in flight has not been incorporated here. As the particles are released into the spray gas stream emanating from the nozzle, the dynamic interactions of the particles with the gas are modeled using the discussions presented in Section 3.4. An appropriately imposed fluid velocity field is a necessary boundary condition for such one-way coupling analysis, and this has also been discussed in the subsequent sections. The exact mechanism of introducing the particles

into the spray-stream is not important here. The simulation parameters for the examples presented here have been summarized in Table 5.2.

Parameters	**Assumed values**
Particle radius	80 μm
Particle density	5680 kg/m^3
Particle bulk modulus	167 GPa
Particle shear modulus	77 GPa
Particle yield stress	200 MPa
Particle surface energy	46 mJ/m^2
Surface bulk modulus	160 GPa
Surface shear modulus	80 GPa
Surface surface energy	1100 mJ/m^2
Fluid density	1.1 kg/m^3
Fluid viscosity	25e-6 m^2/s
Average nozzle velocity	20 - 30 m/s
Assumed α for adhesion	5000

Table 5.2: *Simulation parameters for the spray deposition examples*

5.3.2 Deriving a simple criteria for deposition

The exact mechanism of deposition is a complicated aspect of the governing physics of spray manufacturing technologies - and as such, deposition can result from chemical reactions, solidification of molten droplets, physical bonding, or ionic/electrostatic mechanisms. For a detailed review on these various processes the reader is referred to the work by Martin [94], and the discussions presented by Fritsching [53]. For the current example, it is sought to have a simple model to treat the basic process of a flowing discrete element sticking to a surface - which can then be hierarchically integrated into a large-scale simulation to understand global system behavior. To do this, we refer to the macroscopic force of adhesion between a sphere and a surface at very small distances as presented in Section 2.6. Using the Derjaguin Approximation for forces between a sphere and a flat surface, the adhesion force can be written as in terms of the particle-surface interface energy (γ_{12}) as:

$$F^{adh} = -4\pi\gamma_{12}R \tag{5.7}$$

with $\gamma_{12} \approx 2\sqrt{\gamma_1\gamma_2}$ (see Equation 2.74 in Section 2.6). Referring to Figure 5.8 on the left, and using the expression for the final velocity as in Equation 2.25, it can be seen that

$$v_{cn}(t+\delta t) = -ev_{cn}(t) + \frac{1}{m}F_n^{adh}(\delta t - \delta t_1) - \frac{e}{m}F_n^{adh}\delta t_1 \tag{5.8}$$

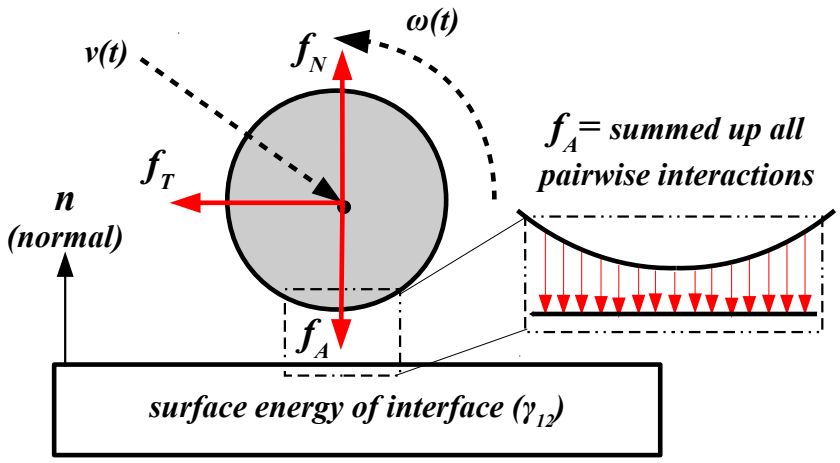

Figure 5.8: *Schematic for the derivation of a velocity dependent adhesion criteria.*

Let us consider $v_{cn}(t) = -v_0$, and $\mathbf{F}^{adh} = -F^{adh}\hat{\mathbf{n}}$, which is consistent with Figure 5.8. Furthermore, since the fundamental assumption is that of a nearly-rigid collision, with very small time-scales of collision that do not overlap the simulation time-steps, it will be expected that within one time-step of the simulation, the final velocity $v_{cn}(t + \delta t)$ should be positive if adhesive effects have not dominated the collision. On the other hand, if $v_{cn}(t + \delta t)$ is negative, then the above assumptions are contradicted, and adhesion effects are dominant - and appropriate physical bonding interactions are established. Therefore, if $v_{cn}(t + \delta t) < 0$ it is assumed that the particle sticks to the surface, and assumes the same velocity as the surface. With the further consideration that purely elastic collisions will occur at very low velocities for all practical purposes (which leads to lower collision forces, and more adhesion dominant collisions), it can be assumed that this criteria on final velocity be applied in the regime of inelastic collisions, which then gives us the following final criteria after some algebra:

$$\begin{aligned} 0 &> -ev_0 - \frac{1}{m}F^{adh}(1.2e\delta t_1) + \frac{e}{m}F^{adh}\delta t_1 \\ v_0 &< \frac{0.2F^{adh}\delta t_1}{m} \end{aligned} \tag{5.9}$$

where we have used the discussions presented in Section 2.4 for the relative magnitude of compression and recovery times in inelastic collision. Note that as particle sizes keep getting bigger, the particle mass increases, thereby leading to very low upper bounds for impact velocities to induce complete adhesion - which is consistent with the physical behavior of such systems. Furthermore, the effect of temperature can be incorporated into this criteria using the discussions presented in Setion 2.6.2, in particular Equation 2.77. In accordance with this, as temperature rises, there is an increase in interface energy required, thereby requiring

higher upper bounds on impact velocities to complete adhesion. This is also physically consistent with the physical behavior of such systems. The simple form of Equation 5.9 also allows for a simple integration into simulation algorithms.

5.3.3 Jet velocity profile for one-way coupling

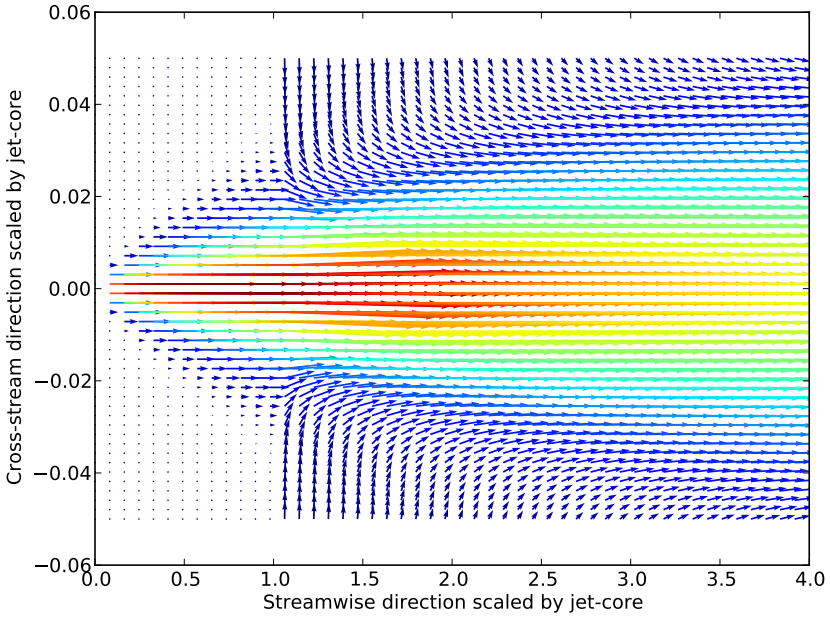

Figure 5.9: *A vector plot in two dimension representing the flow velocity profile used in the one-way coupling simulations demonstrated here.*

For the examples presented here, a simple jet velocity profile has been assumed as follows:

$$u_f = \frac{C_1}{x^{1/3}} \operatorname{sech}^2\left(\frac{C_3 y}{x^{2/3}}\right) \tag{5.10}$$

$$v_f = \frac{C_2}{x^{2/3}}\left[2\frac{C_3}{x^{2/3}} \operatorname{sech}^2\left(\frac{C_3 y}{x^{2/3}}\right) - \tanh\left(\frac{C_3 y}{x^{2/3}}\right)\right] \tag{5.11}$$

For three-dimensional simulation, the assumption of axi-symmetry is invoked, and y is replaced by the radial cross-span coordinate location, and x becomes the stream-wise coordinate location (as represented in Figure 5.7). The obtained velocity distribution is illustrated in 5.9 for a two-dimensional cross-section of the flow. In consistent with free jet-flow from a nozzle, a small region of flow with no entrainment has been assumed near the nozzle exit - which is referred to as core in the Figure. Other possible forms of velocity

profiles appropriate for spray dynamics have been discussed in detail by Pawlowski [119], and Fritsching [53], and Yuu et. al. [170], and can be imported into the simulation framework easily if required.

5.3.4 Simulation results

The three dimensional dynamics of the particulate spray under the combined action of particle collisions and fluid particle interactions has been demonstrated by means of snapshots taken from the side (along the full length of the stream-wise coordinate axis) at different instants of simulation time in Figure 5.10. A close analysis of the Figures will reveal two physical mechanisms that compete with each other. The nature of the imposed fluid velocity as presented in Equations 5.10 and 5.11 is such that the particles away from the centerline move much slower than the particles closer to the centerline. However, since the particle length scales (and correspondingly their response times) are small, they respond to the entrainment velocities very quickly, thereby leading to some non-uniformity in the cross-span particle velocities. Further non-uniformities could be introduced from the mechanism by which the particles are introduced into the spray gas - which has been incorporated in the present example by assigning each particle a small random cross-span velocity component. The combined action of these cross-span velocities therefore leads to inter-particle collisions, and causes the flow pattern as observed in Figure 5.10. Such an effect can lead to an increased scattering of the particles as they are deposited onto the surface, thereby causing non-uniformities in the deposition. It would be expected then that for a reduced number density of particles, and for reduced non-uniformities in cross-span velocities, the flow pattern will show reduced scattering due to collisions. This is indeed the case, as can be seen from the snapshots for a different configuration of spray particulate stream presented in Figure 5.11 - where the number of particles is 8000 as compared to 20000 for the previous case, and the cross-span velocity non-uniformities are very low. Furthermore, from the data presented in the simulation parameter list in Table 5.2, the calculated density ratio ρ_f/ρ_p is found to be 1.95×10^{-4}, and the particle response time can be given to be $\tau_p \approx 55\mu s$. For this configuration, by analyzing the particle motion equations in Section 3.4, it can be seen that the unsteady terms involving added mass and pressure gradient are insignificant owing to the low density ratio. Also, the drag forces turn out to be more dominant than the history forces for this regime, owing to the small particle sizes.

As an example of translating the particulate flow analysis to a metric for deposition, simple metrics for deposit pattern analysis can be augmented with the simulations. For the purpose of the examples presented here, it is assumed that once a particle satisfies the deposition criteria and gets adhered, it is removed from the set of dynamic particles in the system, and therefore remains adhered permanently during the simulation lifetime. Given that the list of particles that are stuck to the target surface can be represented using the list

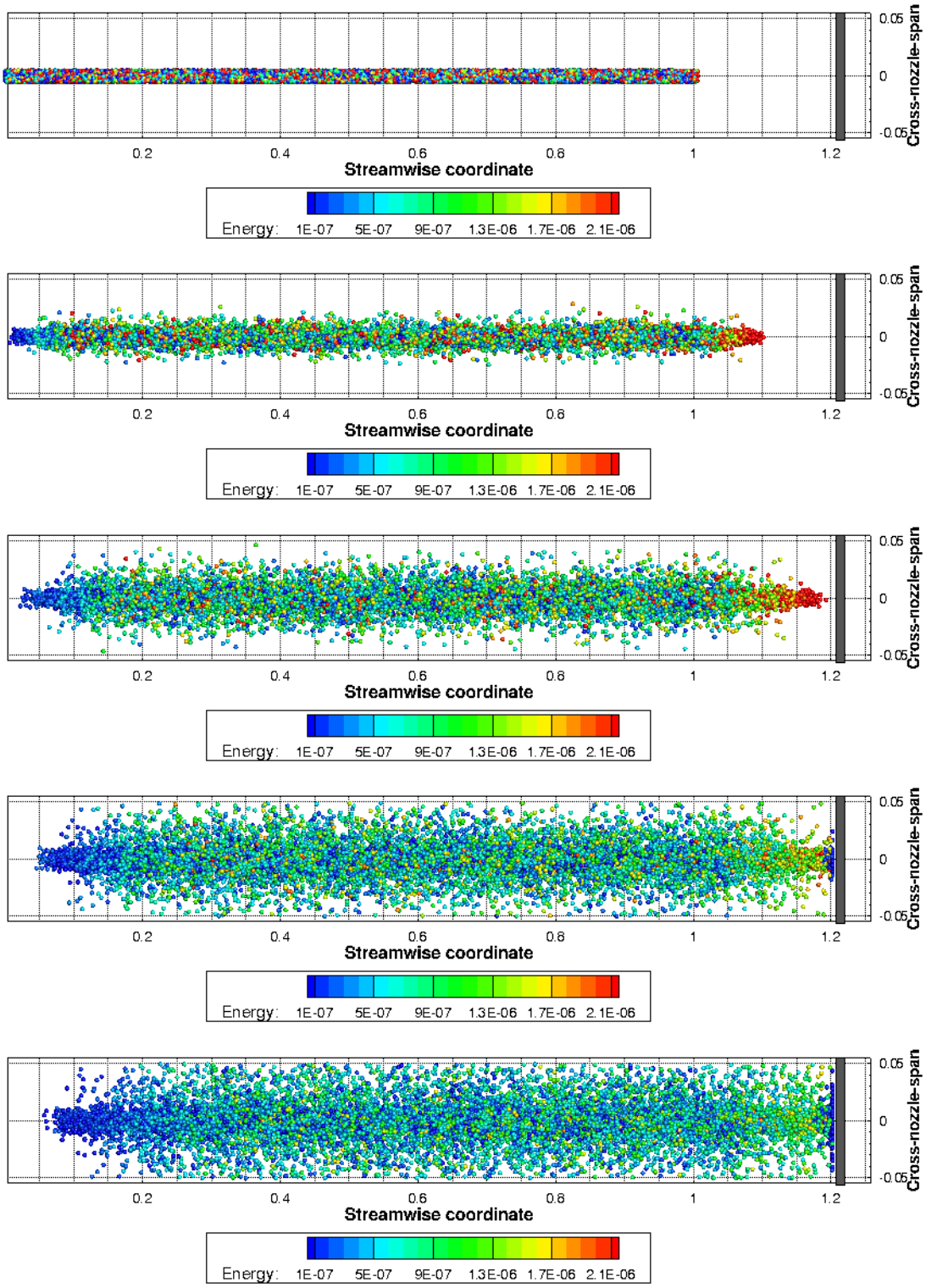

Figure 5.10: *Snapshots for the simulated dynamics of a high number density spray plume*

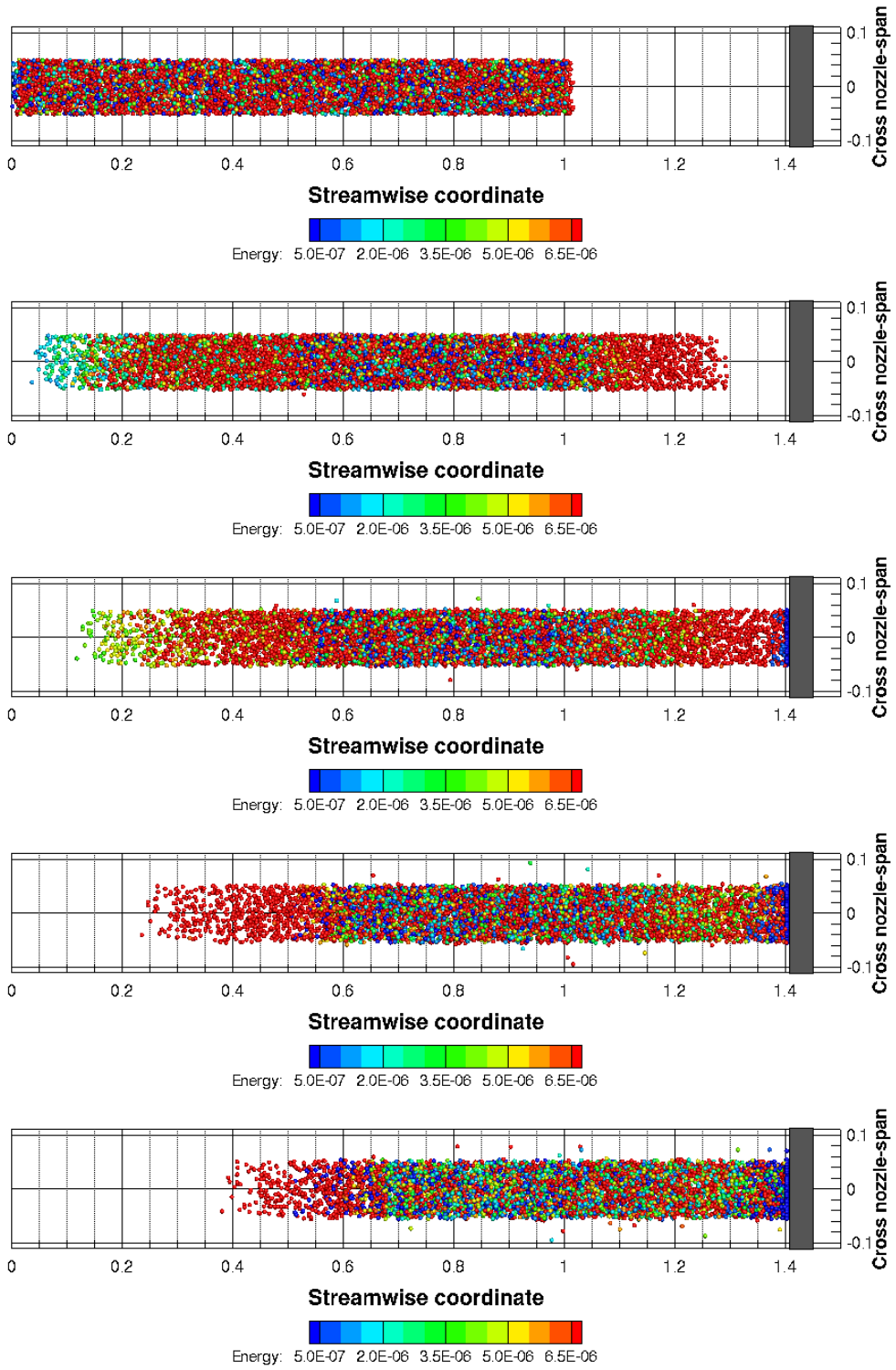

Figure 5.11: *Snapshots for the simulated dynamics of a lower number density spray plume*

Simulation conditions	h_{dep}/nozzle radius	n_{dep}
20000 particles, non-zero cross-span velocities	0.0391	0.0932
20000 particles, zero cross-span velocities	0.0601	0.1449
8000 particles, non-zero cross-span velocities	0.0049	0.3718
8000 particles, angled at 5 degrees	0.0050	0.3755

Table 5.3: *Sample results for analysis of deposit metrics presented in Equation 5.12 for processing spray simulation data*

$\mathcal{P}_{stuck}$, we can define a representative deposit height h_{sep}, and a proportion of the number of particles that adhered during the simulation life-time as n_{sep} as follows:

$$h_{dep} = (x_{max} + R_{av}) - (x_{min} - R_{av}),\ n_{dep} = N_{stuck}/N_p \tag{5.12}$$

where x_{max}, x_{min} represent the maximum and minimum height at which an individual particle is located at the location of the deposit, R_{av} represent the average particle radius. A calculation of these deposit metrics for four different representative simulation runs have been summarized in Table 5.3. A higher number density causes more scatter in deposition at the target surface, and hence results in a lower proportion of deposit particles, as compared to lower number density. However, there being more particles overall that get deposited at the deposit location, the average deposits will be thicker for the former. Additionally, for a certain spray particle number density, reduced cross span velocities cause lesser collisions and better deposition as is reflected from the first two entries in Table 5.3. Furthermore, it is also important to note that there could be scatter introduced in the deposit pattern due to collisions between the collection of already deposited particles which is growing with time, and the incoming particles from the spray-plume. In order to illustrate this mechanism, simulations of deposition from a particle spray with a lot of inter-particle collisions and scatter has been compared with those of deposition from a spray where the inter-particle collisions before impact with the deposit on the target surface were algorithmically restricted. Representative deposit growth patterns for 20,000 particles have been presented for these two cases in Figure 5.12. While the latter case does show more uniform and efficient deposition pattern, there are variabilities seen in Figure 5.12 on the bottom which are entirely due to collisions between the incoming particle stream and the growing deposit of particles.

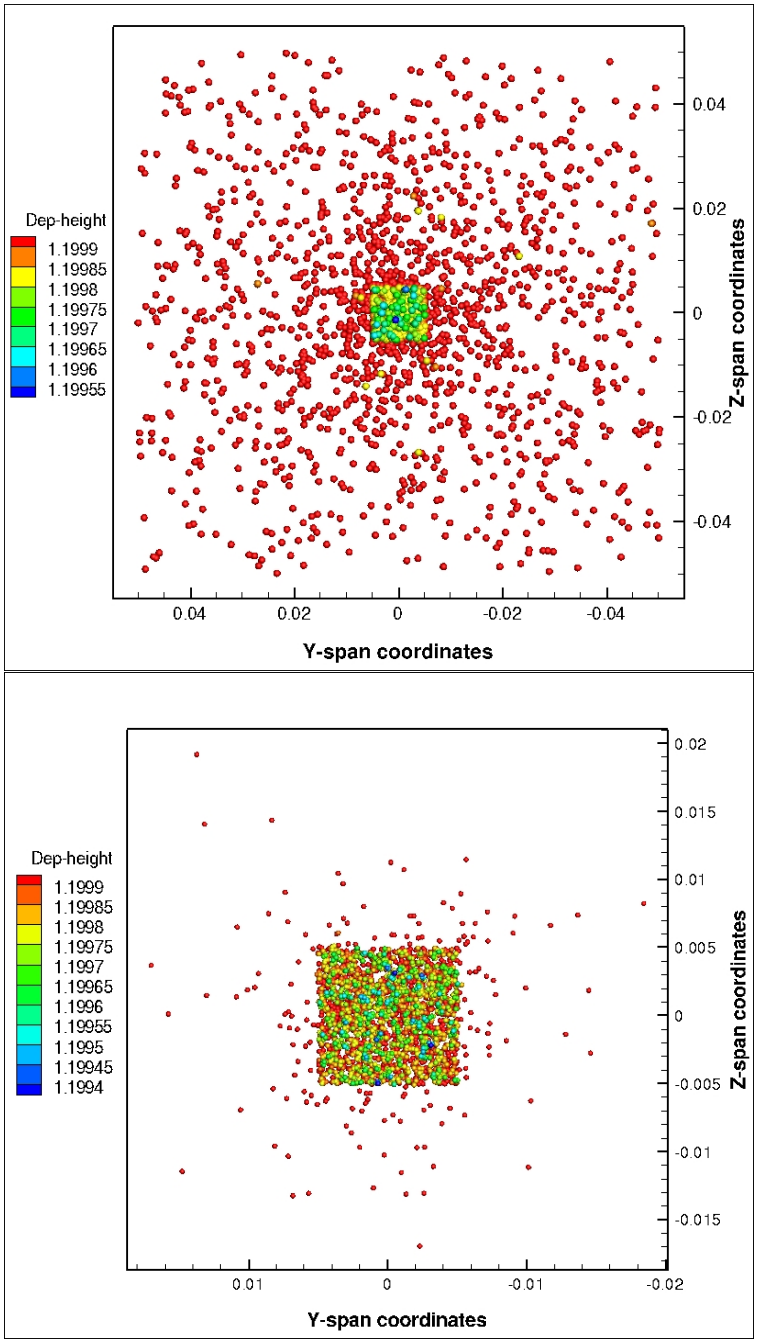

Figure 5.12: *Deposit patterns for a highly scattered spray plume, and a plume generated by restricting all scatter due to inter-particle collisions in the propagating spray*

Chapter 6

Conclusions and Future Work

6.1 Concluding Remarks

In this dissertation, the computational modeling and simulation of flowing particulate and granular media was addressed using discrete element method and collision driven particle dynamics type models. The particular focus of the discussions presented here was on the hierarchical modeling of coupled multi-physical phenomena that are common in many applications involving particulate media. While a comprehensive list of all possible interaction models and their details cannot be provided in a dissertation or monograph, an attempt has been made to present a broad and representative collection of physical models, numerical techniques, and their algorithmic implementations under a single research and development exercise. The frameworks discussed herein, were used to develop a research purpose computer simulation library named SLIDES (acronym for *'Software Library for Discrete Element Simulations'*) for reference and continued future development - which was the end product of the research and development exercise presented in this dissertation. The library has been developed in Fortran (2003 standard) using an object oriented architecture, and is capable of performing fully three-dimensional particle dynamics simulations. The capabilities of the simulation tool, and the utility of such modeling frameworks have been illustrated using two particular case-studies. In both examples, the treatment of individual particle motions revealed information on system behavior that would be otherwise hard to obtain using a continuum based approach.

The first case-study presented was on the analysis of a flowing particulate stream impacting a surface at high velocities. The analysis was motivated by the analogous real-world problem of erosive wear of engineered surface coatings. The example demonstrated the calculation of the impact forces and spread patterns of the impacting particle stream, and the translation of impact loads into stresses and damage. The explicit resolution of collisions provided the exact variation of stresses with time, and also allowed a resolution of the re-

tardation effect due to collisions between incident and reflected particles from the surface. The second case-study presented was on the analysis of particulate media propagating towards a surface carried by a carrier fluid. This analysis was motivated by the analogous real-world problem of spray-deposition based manufacturing of a surface coating. The example demonstrated the utility of such models in hierarchically representing the deposition phenomena and derive a velocity based criteria for particle deposition. The calculations also provided valuable insights into the dynamics of the spray plume as it propagates from the spray-nozzle towards the target surface. Particularly, it was possible to see the effects of particle number-density, and inter-particle collisions on the scattering of the spray-plume and the variabilities in the deposit pattern. Both case studies involved simulations performed using the developed software libraries, and were performed within reasonable computation time on readily available computing resources. For most of the models presented here, only very few phenomenological modeling constants appear. For many other case, however, it may be of interest to include further interaction physics into the simulations through simple phenomenological models. The constants and parameters for these can only be validated by a systematic comparison with available experimental data. The generalized problem of parameter estimation can then be formulated as an Inverse problem to find the set of parameters that best match available predictions - and such problems have been addressed by Zohdi([177] and [176]). To keep with the scope of the current discussion, further details on construction of inverse problems for parameter estimation have not been discussed here.

6.2 Future Research Directions

In closing, we remark on a few important aspects that are relevant to the ideas discussed in this dissertation, and that can be discussed in specific detail as future research objectives now that a developed simulation framework exists. The first of these is the issue of a detailed resolution of the fluid-particle coupling phenomenon. The combined interaction of collisions, steady and unsteady forces on the particle due to the fluid, steady and unsteady heat transfer, and presence of a turbulent flow field can make a detailed analysis of the flows quite complicated (even in the one way coupling regime). A consistent resolution of this interaction, combined with the already developed simulation framework, will then provide for a probe into phenomena like the role of collisions in turbulent diffusion of particles, and their preferential concentration. In fact, with existing fluid dynamics solvers, better approximations of the carrier flow velocity fields can be obtained for more complex flow configurations, which can then be linked to the discrete particle frameworks developed here directly.

Continuing along the same idea, we remark also that even further utility can be rendered to such simulations if the more complex problem of particle-continuum coupling is considered. While the example on erosive wear calculations due to impact by a stream of particles did

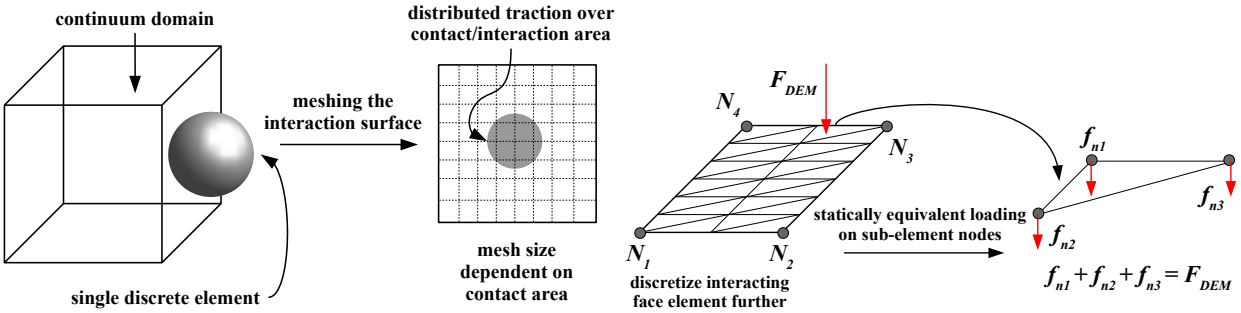

Figure 6.1: *An illustration of coupling between a discrete particle/element and a finite element mesh*

provide a naive implementation of such a coupling - this topic can be further explored. A simple way of making the discrete elements talk to a finite element mesh is to represent the interactions through applied surface tractions - similar to the erosive wear example - and convert the tractions on the mesh into nodal loads for augmenting the global system matrix equations. A schematic of this is shown in Figure 6.1.

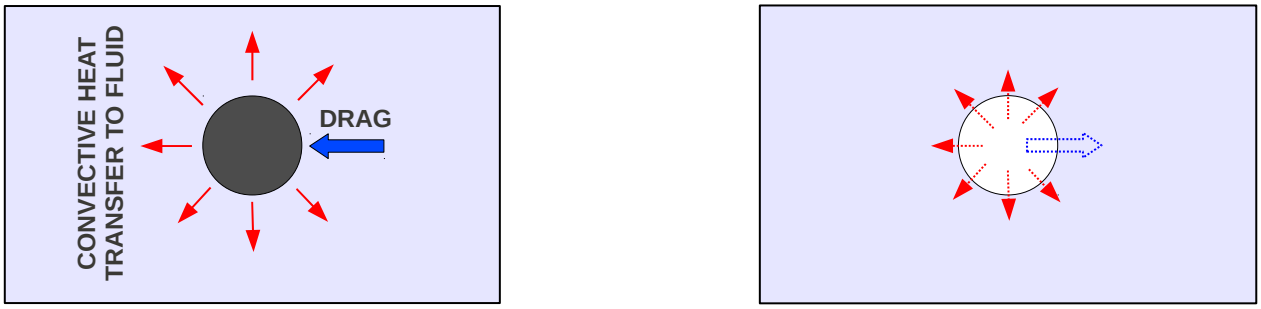

Figure 6.2: *An illustration of incorporating two-way coupling between fluid and particle within a continuum volume element of fluid.*

For the two-way coupled fluid-particle interaction, if we consider a single computational cell of the fluid continuum, then the presence of the particle will lead to addition of a source term for the momentum and the energy equation for that computational cell. This is the main concept behind a series of methods called Particle Source In a Cell (see Crowe et. al. [29]), and the concept has been illustrated in Figure 6.2. The presence of the demonstrated simulation capabilities for discrete elements, and already existing algorithms and software tools for finite elements/finite volume allow for detailed exploration of such coupled problems - which has been identified as a broad topic for future research.

Appendix A: Details on the software library for discrete element simulations

The models and algorithms described in the dissertation were utilized to construct the basic layer of a computer simulation library for discrete particle simulations called *'Software Library for Discrete Element Simulations'* (in short, SLIDES). The development of the software has been an integral part of the research documented in this dissertation. At the time of compiling the dissertation, the first stage of development has been completed and primary architecture, multi-physics libraries, and data structures have been developed and tested - examples of which have been presented in the dissertation. The libraries have a modular, object-oriented design with the flexibility of adding more functionalities and also using the existing functionalities as basic API's for scripting simulations. The programs have all been written in FORTRAN with many 2003 standard features incorporated. Therefore a FORTRAN 2003 standard compatible compiler is a necessary system requirement. The SLIDES library is not meant to be a full-service commercial package. Instead, it is intended to be a flexible, general purpose research tool that can be used to model and simulate a wide range of discrete particle dynamics based phenomena. Many such modeling aspects have been discussed in detail in this dissertation. This appendix will provide a brief description of the design details and usage of the libraries. A comprehensive user manual (both offline, and navigable html format) is also being developed, and can be provided upon request.

Program structure

The main architecture of the library has already been presented in Figure 1.3. The directory structure for the simulation library files has been presented in Figure 3. This structure can be modified- but it is advisable to keep the sources and applications directories unchanged unless necessary. The generic structure of a simulation script that can be used as a basic layout for using the library functionalities has been presented in form of a sequence of instructions in Algorithm 5. These may be translated into relevant sequences of FORTRAN syntax. The script being written in FORTRAN, the general syntax rules of the language apply throughout. All data structures have accessor functions or subroutines whose names

begin with *'get...'* and *'set...'*. The execution of the script is usually done in the following format:

```
./sampleSimulationScript.out <command-argument-1>
    <command-argument-2> ....  <command-argument-N>
```

The standard of the library is to place the name of the input file as the first command-line argument. The input file is to be prepared by the user, and essentially the problem parameters and their values can be typed into a formatted data file - an example of which, with a brief explanation of the relevance of each problem parameter has been presented separately in Appendix B. In order to explain the way in which sequence of instruction flows occur in a typical simulation that involves the library subroutines - a sample call-graph generated using Doxygen for the erosive jet application discussed in this dissertation has been presented in Figure 4. The graph indicates set of possible alternative flow of instructions, and in a way is a representation of the static dependency of procedure calls, since every call relationship that may occur (that is, every possible run of the program) is indicated.

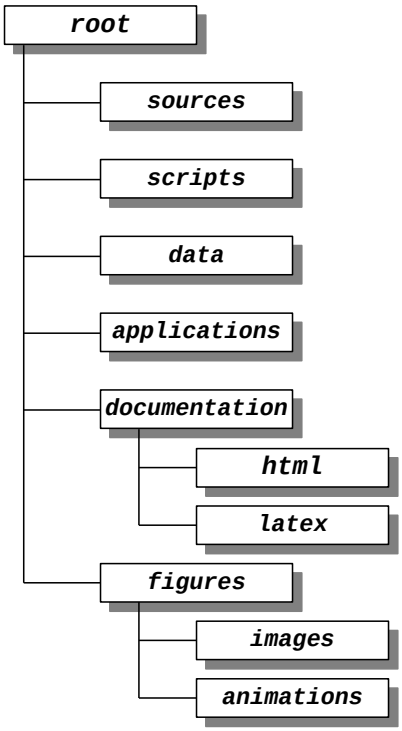

Figure 3: *The directory structure of the discrete particle simulation libraries*

Algorithm 5 *The sequence of instructions that can be used to script a simulation using the simulation library*

```
define and declare all local variables
read and parse all command-line arguments
read input data from input file provided as first command-argument
allocate all data structures
initialize particle configuration and particle data
if control surfaces are needed then
    initialize control surface data
end if
if fluid media is needed then
    initialize fluids data
end if
if domain requires binning then
    bin domain and sort particles
end if
while time ≤ simulation time do
    integrate system using a time-stepper of choice
    if time since last output dump ≥ dump-interval then
        write phase-space and other dynamics data to output files
    end if
    if time since last bin sort operation ≥ bin-interval then
        bin domain and sort particles
    end if
end while
clear all allocated memory
```

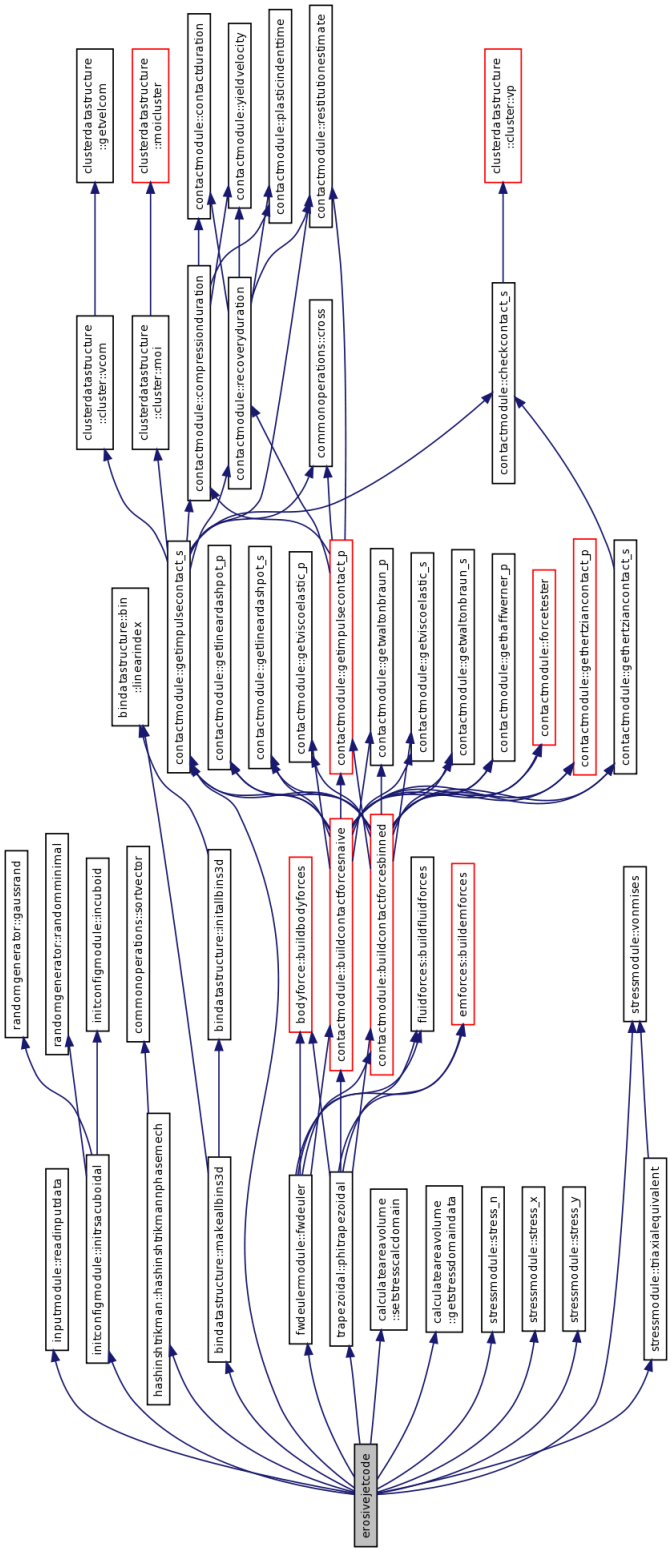

Figure 4: *The detailed call-graph for the erosive jet application example presented in Chapter 5.*

Scripting and compilation

In order to avoid complications owing to complication cascades and creating and executing simulation scripts, the compilation and execution tasks have been outlined clearly in form of a pseudocode sequence in Algorithm 6. These tasks can either be scripted (for example, using shell-scripts in Unix), or the user can manually execute the sequence of tasks. The function names in capitals are just presented as place-holders for the actions to be performed on the input arguments specified in the pseudocode. The 'dump' directory refers to a temporary directory that can be named according to user convenience. There may be other possible ways of achieving the same using other similar techniques.

Algorithm 6 *The pseudocode sequence that can be used to execute simulations using the compiled simulation libraries*

1: enter root-level
2: compile all sources
3: create temporary dump directory
4: COPY-TO-DUMP(*compiled application*)
5: COPY-TO-DUMP(*user input data*)
6: execute simulation from dump directory
7: COPY-FROM-DUMP(*simulation output data*)
8: delete temporary dump directory
9: jump back to root-level

Further development plans

As mentioned earlier, at the current stage of development the basic layer of simulation libraries have been developed. Possible extensions to the current libraries will include the following steps in the subsequent stages of development:

- more application specific physics modules that can expand the applicability of the simulation tool to a broader range of research problems.
- making the front-end of the application more graphical - possibly using a Python based graphical interface.
- making the compilation and application generation more generic for cross-platform application development.

Appendix B: A sample documented user-input file

```
DOMAIN-DATA
&ComputationDomain  isDomainCuboid  = .true.,    !< Boolean choice variable for
                                                 !! cuboidal starting domain
                    isDomainCylinder= .false.,   !< Boolean choice variable for
                                                 !! cylindrical starting domain
                    isRegularArray  = .false.,   !< Boolean choice variable for
                                                 !! a regular lattice starting domain
                    isBinDomain     = .false.,   !< Boolean choice variable for
                                                 !! binning the domain
                    domainRadius    = 0.0d0,     !< Radius of cylindrical domain
                    domainLength    = 0.0d0,     !< Length of cylindrical domain
                    domainX         = 0.0d0,     !< X-coordinate length of cuboidal domain
                    domainY         = 0.0d0,     !< Y-coordinate length of cuboidal domain
                    domainZ         = 0.0d0,     !< Z-coordinate length of cuboidal domain
                    NX              = 10,        !< Number of bins along X direction
                    NY              = 10,        !< Number of bins along Y direction
                    NZ              = 10,        !< Number of bins along Z direction
                    outerBinX       = 0.0d0,     !< Outer span of binned computation domain
                                                 !! along the X direction
                    outerBinY       = 0.0d0,     !< Outer span of binned computation domain
                                                 !! along the Y direction
                    outerBinZ       = 0.0d0,     !< Outer span of binned computation domain
                                                 !! along the Z direction
                    XYZ0            = 0.0d0, 0.0d0, 0.0d0 / !< Reference coordinate for
                                                            !! locating the domain origin

PARTICLE
&ParticleInitialise  numPart         = 1,     !< Number of particles in the system
                     radiusMean      = 0.0d0, !< Mean particle radius
                     radiusVar       = 0.0d0, !< Variance of particle radius
                     isMonoDisperse  = .true. / !< Boolean choice variable for
                                                !! handling particle monodispersity
&ParticleMaterial    densityP        = 0.0d0, !< Density of the particles
                     elasticityP     = 0.0d0, !< Elasticity modulus of the particles
                     poissonP        = 0.0d0, !< Poisson ratio of the particles
                     shearP          = 0.0d0, !< Shear modulus of the particles
                     bulkP           = 0.0d0, !< Bulk modulus of the particles
                     yieldP          = 0.0d0, !< Yield strength for particles
                     surfaceEnergyP  = 0.0d0, !< Surface energy of the particles
                     conductivityP   = 0.0d0, !< Thermal conductivity of particles
                     specifHeatP     = 0.0d0, !< Specific heat capacity of the particles
                     multiParticleInit = 'file.dat' / !< Filename for initialising particles
                                                      !! using pre-processed particle data
```

```
SURFACE
&SurfaceMaterial  numSurf        = 0,      !< Number of control surfaces/boundaries
                  elasticityS    = 0.0d0,  !< Elasticity modulus for surface
                  poissonS       = 0.0d0,  !< Poisson ratio for surface
                  shearS         = 0.0d0,  !< Shear modulus for surface
                  bulkS          = 0.0d0,  !< Bulk modulus for surface
                  yieldS         = 0.0d0,  !< Yield strength for surface
                  conductivityS  = 0.0d0,  !< Thermal conductivity for the surface material
                  surfaceEnergyS = 0.0d0 / !< Surface energy for surface material

FLUID
&FluidMaterial  densityF      = 0.0d0,    !< Density of the fluid medium
                viscosityF    = 0.0d0,    !< Dynamic viscosity of fluid medium
                conductivityF = 0.0d0,    !< Thermal conductivity of fluid medium
                specifHeatF   = 0.0d0,    !< Specific heat capacity of fluid medium
                isTurbulent   = .false. / !< Boolean choice variable for performing
                                          !! a turbulent flow simulation

CONTACT
&Contact  statFric  = 0.0d0,  !< Static friction coefficient between particles and surfaces
          dynFric   = 0.0d0,  !< Dynamic friction coefficient between particles and surfaces
          restCoeff = 0.0d0,  !< Restitution coefficient for normal inelastic impact
          collideT  = 0.0d0,  !< Estimate of the total collision duration
          recoveryT = 0.0d0,  !< Estimate of the recovery duration of the collision
          compressT = 0.0d0,  !< Estimate of the compression phase duration of the collision
          alphaRest = 0.0d0,  !< Modelling constant for the restitution coefficient
          alphaYRest= 0.0d0,  !< Modelling constant for the restitution coefficient
          isRestVary= .true., !< Boolean choice variable for modelling
                              !! restitution dependent on velocity
          isGeneralRestModel = .false., !< Boolean choice variable for modelling
                                        !! restitution for general materials
          isFricRegularized  = .true.,  !< Boolean choice variable for modelling
                                        !! a regularised friction law
          fricRegP    = 0.0d0, !< The regularization parameter for friction stick-slip law
          modelChoice = 1,     !< Choice for contact model methods
          isContactImplementUsingPointers = .false., !< Choice for code feature to select
                                                     !! contact models using a pointer
                                                        implementation
          contactPenalty = 0.0d0,        !< Model parameters for a penalty based
                                         !! contact law for simple cases
          linearDashpot  = 0.0d0, 0.0d0, !< Free parameters for linear dashpot normal force
          viscoElastic   = 0.0d0,        !< Free parameters for viscoelastic normal force
          waltonBraun    = 0.0d0, 0.0d0, 0.0d0, 0.0d0,!< Free parameters for walton-braun's
                                                       !! complete force model
          haffWerner     = 0.0d0,  !< Free parameters for haff-werner's tangential force
        cundallStrack    = 0.0d0 / !< Free parameters for cundall-strack's tangential force

E-AND-M
&EMFields EField = 0.0d0, 0.0d0, 0.0d0,  !< Externally applied electric field
          BField = 0.0d0, 0.0d0, 0.0d0 / !< Externally applied magnetic field

BODY-FORCE
&Body  BFDensity   = 0.0d0,                !< Body force density
       BFDirection = 0.0d0, 0.0d0, 0.0d0 / !< Body force orientation

ADHESIVE-PAR
&Adhesives  alphaDep = 0.0d0,  !< Parameter for particle-surface adhesion for deposition
            alphaAgg = 0.0d0 / !< Parameter for particle-particle adhesion for agglomeration
```

```
TIME-STEP
&TimeStepper startTime      = 0.0d0,  !< Simulation starting time
             stopTime       = 0.0d0,  !< Simulation ending time
             stepSize       = 0.0d0,  !< Simulation step-size
             stepErrtol     = 0.0d0,  !< Error tolerance for adaptivity
             stepSizeMax    = 0.0d0,  !< Maximum step size selection
             stepsizeMin    = 0.0d0,  !< Minimum step size selection
             schemeChoice   = 'FWD',  !< Time stepping scheme choice
             isAdaptiveStep = .false. / !< Boolean choice variable for an adaptive time-
                 stepper

STRESS-ANALYSIS
&StressCalculator isMultiComposite = .false., !< Choice variable for composite
                                              !! or porous materials
                  porosity         = 0.0d0,   !< Specific value for the porosity
                  numStressPoints  = 0, 0, 0, !< Number of grid points in each direction
                                              !! for stress analysis
                  stressAddDomainX = 0.0d0,   !< Extending X direction to bound the x domain
                  stressAddDomainY = 0.0d0,   !< Extending Y direction to bound the y domain
                  stressAddDomainZ = 0.0d0,   !< Extending Z direction to bound the z domain
                  probeStress      = 0.0d0, 0.0d0, 0.0d0 / !< Specified probe point
                      coordinates
                                                          !! for stress calculation

END-OF-INPUT
```

Bibliography

[1] A Acrivos and TD Taylor. Heat and Mass Transfer from Single Spheres in Stokes Flow. *Physics of Fluids*, 5(4):387–394, 1962.

[2] a.J. Dorgan and E. Loth. Efficient calculation of the history force at finite Reynolds numbers. *International Journal of Multiphase Flow*, 33(8):833–848, August 2007.

[3] A Aliseda, A Cartellier, F Hainaux, and J C Lasheras. Effect of preferential concentration on the settling velocity of heavy particles in homogeneous isotropic turbulence. *Journal of Fluid Mechanics*, 468(1):77–105, 2002.

[4] D. Arbelaez, T. I. Zohdi, and D. a. Dornfeld. Modeling and simulation of material removal with particulate flows. *Computational Mechanics*, 42(5):749–759, March 2008.

[5] P Attard and Jl Parker. Erratum: Deformation and adhesion of elastic bodies in contact. *Physical review. E, Statistical physics, plasmas, fluids, and related interdisciplinary topics*, 50(6):5145, December 1994.

[6] D. J. Auerbach, W. Paul, a. F. Bakker, C. Lutz, W. E. Rudge, and Farid F. Abraham. A special purpose parallel computer for molecular dynamics: motivation, design, implementation, and application. *The Journal of Physical Chemistry*, 91(19):4881–4890, September 1987.

[7] JS Bader and D Chandler. Computer Simulation Study of the Mean Forces Between Ferrous and Ferric Ions in Water. *The Journal of Physical Chemistry*, 96(15), 1992.

[8] AB Bailey and J Hiatt. Sphere drag coefficients for a broad range of Mach and Reynolds numbers. *Aiaa Journal*, 10(11):1436–1440, 1972.

[9] S Balachandar and J K Eaton. Turbulent dispersed multiphase flow. *Annual Review of Fluid Mechanics*, 42:111–133, 2010.

[10] S. Balachandar and John K. Eaton. Turbulent Dispersed Multiphase Flow. *Annual Review of Fluid Mechanics*, 42(1):111–133, January 2010.

[11] GK Batchelor and RW O'Brien. Thermal or electrical conduction through a granular material. *Proceedings of the Royal Society A: Mathematical, Physical Sciences*, 355(1682):313–333, 1977.

[12] Lennart Bergstrm. Hamaker constants of inorganic materials. *Advances in Colloid and Interface Science*, 70:125–169, 1997.

[13] A Berlemont, P Desjonqueres, and G Gouesbet. Particle Lagrangian simulation in turbulent flows. *International Journal of Multiphase Flow*, 16(1):19–34, 1990.

[14] JGA Bitter. A Study of Erosion Phenomena. Part I. *Wear*, 6, 1963.

[15] S Blanes and PC Moan. Practical symplectic partitioned RungeKutta and RungeKuttaNyström methods. *Journal of Computational and Applied Mathematics*, 142:313–330, 2002.

[16] FA Bombardelli, AE González, and YI Niño. Computation of the particle Basset force with a fractional-derivative approach. *Journal of Hydraulic Engineering*, 134(October):1513–1520, 2008.

[17] R.S. Bradley. The cohesive force between solid surfaces and the surface energy of solids. *The London, Edinburgh, and Dublin Philosophical Magazine and Journal of Science*, 13(86):853–862, 1932.

[18] Nikolai V Brilliantov, Frank Spahn, Jan Martin Hertzsch, and P Thorsten. A model for collisions in granular gases. *Physics Rev. E*, 53(5), 1996.

[19] T M Burton and J K Eaton. Fully resolved simulations of particle-turbulence interaction. *Journal of Fluid Mechanics*, 545(1):67–111, 2005.

[20] Y A Buyevich. Statistical hydromechanics of disperse systems Part 1. Physical background and general equations. *Journal of Fluid Mechanics*, 49(03):489–507, 1971.

[21] Y A Buyevich. Statistical hydromechanics of disperse systems. Part 2. Solution of the kinetic equation for suspended particles. *Journal of Fluid Mechanics*, 52(02):345–355, 1972.

[22] GT Camacho and M Ortiz. Computational Modelling of Impact Damage in Brittle Materials. *International Journal of Solids and Structures*, 33(2):2899–2938, 1996.

[23] J L Chaboche. Continuum damage mechanics. *Journal of Applied Mechanics*, 55(1):59–64, 1988.

[24] A. Chatterjee and A. Ruina. A New Algebraic Rigid-Body Collision Law Based on Impulse Space Considerations. *Journal of Applied Mechanics*, 65(4):939, 1998.

[25] Anindya Chatterjee. On the realism of complementarity conditions in rigid body collisions. *Nonlinear Dynamics*, 20:159–168, 1999.

[26] GJ Cheng, AB Yu, and P Zulli. Evaluation of Effective Thermal Conductivity from the Structure of a Packed Bed. *Chemical Engineering Science*, 54:4199–4209, 1999.

[27] Ariel a. Chialvo and Pablo G. Debenedetti. On the use of the Verlet neighbor list in molecular dynamics. *Computer Physics Communications*, 60(2):215–224, September 1990.

[28] S Corrsin. Estimates of the relations between Eulerian and Lagrangian scales in large Reynolds number turbulence. *Journal of Atmospheric Sciences*, 20:115–119, 1963.

[29] C T Crowe, J D Schwarzkopf, M Sommerfeld, and Y Tsuji. *Multiphase flows with droplets and particles*. CRC press, 2011.

[30] P. a. Cundall and O. D. L. Strack. A discrete numerical model for granular assemblies. *Géotechnique*, 29(1):47–65, January 1979.

[31] Peter Alan Davidson. *Turbulence: An Introduction for Scientists and Engineers: An Introduction for Scientists and Engineers*. Oxford University Press, 2004.

[32] B V Derjaguin. Friction and adhesion. IV. The theory of adhesion of small particles. *Kolloid Zeits*, 69:155–164, 1934.

[33] B.V. Derjaguin, V.M. Muller, and Y.P. Toporov. Effect of contact deformations on the adhesion of particles. *Journal of Colloid and Interface Science*, 53(2):314–326, November 1975.

[34] O A Druzhinin and S Elghobashi. Direct numerical simulations of bubble-laden turbulent flows using the two-fluid formulation. *Physics of Fluids*, 10(3):685–697, 1998.

[35] J Duran. *Sands, powders, and grains: An introduction to the physics of granular materials*. Springer Verlag, 2000.

[36] S Elghobashi. On predicting particle-laden turbulent flows. *Applied Scientific Research*, 52(4):309–329, 1994.

[37] S Elghobashi and G C Truesdell. Direct simulation of particle dispersion in a decaying isotropic turbulence. *Journal of Fluid Mechanics*, 242(3):655–700, 1992.

[38] S Elghobashi and G C Truesdell. On the two-way interaction between homogeneous turbulence and dispersed solid particles. I: Turbulence modification. *Physics of Fluids A: Fluid Dynamics*, 5:1790, 1993.

[39] S E Elghobashi and T W Abou-Arab. A two-equation turbulence model for two-phase flows. *Physics of Fluids*, 26(4):931–938, 1983.

[40] C Farhat and M Lesoinne. Two effcient staggered algorithms for the serial and parallel solution of three-dimensional nonlinear transient aeroelastic problems. *Computer Methods in Applied Mechanics and Engineeringe*, 182:499–515, 2000.

[41] CA Felippa and KC Park. Staggered Transient Analysis Procedures for Coupled Mechanical Systems: Formulation. *Computer Methods in Applied Mechanics and Engineering*, 24(0), 1980.

[42] Carlos a. Felippa, K.C. Park, and Charbel Farhat. Partitioned analysis of coupled mechanical systems. *Computer Methods in Applied Mechanics and Engineering*, 190(24-25):3247–3270, March 2001.

[43] Y.T. Feng, K. Han, C.F. Li, and D.R.J. Owen. Discrete thermal element modelling of heat conduction in particle systems: Basic formulations. *Journal of Computational Physics*, 227(10):5072–5089, May 2008.

[44] Y.T. Feng, K. Han, and D.R.J. Owen. Discrete thermal element modelling of heat conduction in particle systems: Pipe-network model and transient analysis. *Powder Technology*, 193(3):248–256, August 2009.

[45] A Ferrante and S Elghobashi. On the physical mechanisms of two-way coupling in particle-laden isotropic turbulence. *Physics of fluids*, 15:315, 2003.

[46] J Ferry and S Balachandar. A fast Eulerian method for disperse two-phase flow. *International journal of multiphase flow*, 27(7):1199–1226, 2001.

[47] J Ferry, S L Rani, and S Balachandar. A locally implicit improvement of the equilibrium Eulerian method. *International journal of multiphase flow*, 29(6):869–891, 2003.

[48] F Feuillebois and A Lasek. On the rotational historic term in non-stationary Stokes flow. *The Quarterly Journal of Mechanics and Applied Mathematics*, XXXI(November 1977), 1978.

[49] P Fevrier, O Simonin, and K D Squires. Partitioning of particle velocities in gas-solid turbulent flows into a continuous field and a spatially uncorrelated random distribution: theoretical formalism and numerical study. *Journal of Fluid Mechanics*, 533:1–46, 2005.

[50] I Finnie. Erosion of surfaces by solid particles. *Wear*, 3:87–103, 1960.

[51] R O Fox, F Laurent, and M Massot. Numerical simulation of spray coalescence in an Eulerian framework: direct quadrature method of moments and multi-fluid method. *Journal of Computational Physics*, 227(6):3058–3088, 2008.

[52] Daan Frenkel and Berend Smit. *Understanding molecular simulation: from algorithms to applications*. Access Online via Elsevier, 2001.

[53] U Fritsching. *Spray simulation: modelling and numerical simulation of sprayforming metals*. Cambridge Univ Pr, 2004.

[54] F Génot and Bernard Brogliato. New Results on Painleve Paradoxes. *European Journal of Mechanics-A/Solids*, 18(4):653–677, 1999.

[55] Werner Goldsmith. IMPACT, The theory and physical behavior of colliding solids. 1964.

[56] MA Goodman and SC Cowin. A continuum theory for granular materials. *Archive for Rational Mechanics and Analysis*, 44, 1972.

[57] G Gouesbet and A Berlemont. Eulerian and Lagrangian approaches for predicting the behaviour of discrete particles in turbulent flows. *Progress in Energy and Combustion Science*, 25:133–159, 1998.

[58] JA Greenwood. Adhesion of elastic spheres. *Proceedings of the Royal Society of London. Series A: Mathematical, Physical and Engineering Sciences*, 453(1961):1277, 1997.

[59] Gary S. Grest, Burkhard Dünweg, and Kurt Kremer. Vectorized link cell Fortran code for molecular dynamics simulations for a large number of particles. *Computer Physics Communications*, 55(3):269–285, October 1989.

[60] D D Gu, W Meiners, K Wissenbach, and R Poprawe. Laser additive manufacturing of metallic components: materials, processes and mechanisms. *International Materials Reviews*, 57(3):133–164, May 2012.

[61] P.K. Haff and B.T. Werner. Computer simulation of the mechanical sorting of grains. *Powder Technology*, 48(3):239–245, November 1986.

[62] A. Haider and O. Levenspiel. Drag coefficient and terminal velocity of spherical and nonspherical particles. *Powder technology*, 58(1):63–70, 1989.

[63] HC Hamaker. The Londonvan der Waals attraction between spherical particles. *Physica*, 4(10):1058–1072, 1937.

[64] GM Hamilton. Explicit equations for the stresses beneath a sliding spherical contact. *ARCHIVE: Proceedings of the Institution of*, 197:53–59, 1983.

[65] Z Hashin and S Shtrikman. A Variational Approach to the Theory of the Effective Magnetic Permeability of Multiphase Materials. *Journal of applied Physics*, 33(10):3125–3131, 1962.

[66] Z. Hashin and S. Shtrikman. A variational approach to the theory of the elastic behaviour of multiphase materials. *Journal of the Mechanics and Physics of Solids*, 11(2):127–140, 1963.

[67] Heinrich Hertz. *Miscellaneous papers*. Macmillan, 1896.

[68] G Hetsroni. Particles-turbulence interaction. *International Journal of Multiphase Flow*, 15(5):735–746, 1989.

[69] M.L. Hunt. Discrete element simulations for granular material flows: effective thermal conductivity and self-diffusivity. *International Journal of Heat and Mass Transfer*, 40(13):3059–3068, September 1997.

[70] K Hutter and KR Rajagopal. On flows of granular materials. *Continuum Mechanics and Thermodynamics*, 6:81–139, 1994.

[71] CL Brooks III, BM Pettitt, and Martin Karplus. Structural and energetic effects of truncating long ranged interactions in ionic and polar fluids. *The Journal of chemical physics*, 02138(December):5897–5908, 1985.

[72] J N Israelachvili. Van der Waals forces in biological systems. *Quarterly reviews of biophysics*, 6(4):341–87, November 1973.

[73] J N Israelachvili. *Intermolecular and surface forces*. Academic press, 2011.

[74] Heinrich M Jaeger, Sidney R Nagel, and Robert P Behringer. The physics of granular materials. *Physics Today*, (April):32–38, 1996.

[75] HM Jaeger and SR Nagel. Physics of the Granular State. *Science*, 871(1975), 1992.

[76] HM Jaeger, SR Nagel, and RP Behringer. Granular solids, liquids, and gases. *Reviews of Modern Physics*, 68(4):1259–1273, 1996.

[77] K L Johnson. *Contact mechanics*. Cambridge Univ Pr, 1987.

[78] KL Johnson and JA Greenwood. An adhesion map for the contact of elastic spheres. *Journal of Colloid and Interface Science*, 192(2):326–333, 1997.

[79] KL Johnson, K. Kendall, and AD Roberts. Surface energy and the contact of elastic solids. *Proceedings of the Royal Society of London. A. Mathematical and Physical Sciences*, 324(1558):301–313, 1971.

[80] Ken Kamrin. Nonlinear elasto-plastic model for dense granular flow. *International Journal of Plasticity*, 26(2):167–188, February 2010.

[81] Anuraag R. Kansal, Salvatore Torquato, and Frank H. Stillinger. Computer generation of dense polydisperse sphere packings. *The Journal of Chemical Physics*, 117(18):8212, 2002.

[82] I Kim, S Elghobashi, and W A Sirignano. On the equation for spherical-particle motion: effect of Reynolds and acceleration numbers. *Journal of Fluid Mechanics*, 367(1):221–253, 1998.

[83] A Klarbring. Examples of Non-uniqueness and Non-existence of Solutions to Quasistatic Contact Problems with Friction. *Ingenieur-Archiv*, 60:529–541, 1990.

[84] JP Kruth, MC Leu, and T Nakagawa. Progress in additive manufacturing and rapid prototyping. *CIRP Annals-Manufacturing Technology*, 47(I):525–540, 1998.

[85] Benedict Leimkuhler and Sebastian Reich. *Simulating hamiltonian dynamics*, volume 14. Cambridge University Press, 2004.

[86] Jean Lemaitre and Rodrigue Desmorat. *Engineering damage mechanics: ductile, creep, fatigue and brittle failures*. Springer, 2005.

[87] EM Lifshitz. The theory of molecular attractive forces between solids. *Soviet Physics*, 2(1), 1956.

[88] BD Lubachevsky and F.H. Stillinger. Geometric properties of random disk packings. *Journal of Statistical Physics*, 60(5):561–583, 1990.

[89] J Luo and D.a. Dornfeld. Material removal mechanism in chemical mechanical polishing: theory and modeling. *IEEE Transactions on Semiconductor Manufacturing*, 14(2):112–133, May 2001.

[90] JM MacInnes and FV Bracco. Stochastic particle dispersion modeling and the tracer-particle limit. *Physics of Fluids A: Fluid Dynamics*, 4(12):2809–2824, 1992.

[91] F E Marble. Dynamics of a gas containing small solid particles. 1963.

[92] F E Marble. Dynamics of dusty gases. *Annual Review of Fluid Mechanics*, 2(1):397–446, 1970.

[93] P Martin. *Introduction to Surface Engineering and Functionally Engineered Materials*, volume 74. Wiley-Scrivener, 2011.

[94] P M Martin. *Handbook of deposition technologies for films and coatings: science, applications and technology*. William Andrew, 2009.

[95] D Maugis. Adhesion of spheres: the JKR-DMT transition using a Dugdale model. *Journal of Colloid and Interface Science*, 150(1), 1992.

[96] M R Maxey and J J Riley. Equation of motion for a small rigid sphere in a nonuniform flow. *Physics of Fluids*, 26:883, 1983.

[97] Martin R Maxey. The equation of motion for a small rigid sphere in a nonuniform or unsteady flow. *ASME-PUBLICATIONS-FED*, 166:57, 1993.

[98] M.R. Maxey and J.J. Riley. Equation of motion for a small rigid sphere in a nonuniform flow. *Physics of Fluids*, 26:883–889, 1983.

[99] J B McLaughlin. Aerosol particle deposition in numerically simulated channel flow. *Physics of Fluids A: Fluid Dynamics*, 1:1211, 1989.

[100] R Mei. Flow due to an oscillating sphere and an expression for unsteady drag on the sphere at finiteReynolds number. *Journal of Fluid Mechanics*, 270:133–174, 1994.

[101] R Mei and RJ Adrian. Flow past a sphere with an oscillation in the free-stream velocity and unsteady drag at finite Reynolds number. *Journal of Fluid Mechanics*, 237:323–341, 1992.

[102] R Mei, RJ Adrian, and TJ Hanratty. Particle dispersion in isotropic turbulence under Stokes drag and Basset force with gravitational settling. *Journal of Fluid Mechanics*, 225:481–495, 1991.

[103] EE Michaelides. A novel way of computing the Basset term in unsteady multiphase flow computations. *Physics of Fluids A: Fluid Dynamics*, 4(7):1579–1582, 1992.

[104] EE Michaelides and Z Feng. Heat transfer from a rigid sphere in a nonuniform flow and temperature field. *International journal of heat and mass transfer*, 37(14):2069–2076, 1994.

[105] R D Mindlin and H Deresiewicz. Elastic spheres in contact under varying oblique forces. *Journal of applied mechanics*, 20, 1953.

[106] RD Mindlin. Compliance of elastic bodies in contact. *Journal of Applied Mechanics*, 16:259–268, 1949.

[107] J J Monaghan. Implicit SPH drag and dusty gas dynamics. *Journal of Computational Physics*, 138(2):801–820, 1997.

[108] JEAN JACQUES Moreau. Application of convex analysis to some problems of dry friction. *Trends in Applications of Pure Mathematics to Mechanics*, 2:263–280, 1979.

[109] ME Muller. A note on a method for generating points uniformly on n-dimensional spheres. *Communications of the ACM*, pages 19–20, 1959.

[110] VM Muller, VS Yushchenko, and BV Derjaguin. On the influence of molecular forces on the deformation of an elastic sphere and its sticking to a rigid plane. *Journal of Colloid and Interface Science*, 77(1):91–101, 1980.

[111] VM Muller, VS Yushchenko, and B.V. Derjaguin. General theoretical consideration of the influence of surface forces on contact deformations and the reciprocal adhesion of elastic spherical particles. *Journal of Colloid and Interface Science*, 92(1):92–101, 1983.

[112] A Munjiza and John Wiley. The combined finite-discrete element method. 2004.

[113] Katta G Murty. *Linear complementarity, linear and nonlinear programming*. Heldermann Berlin, 1988.

[114] John R. Nicholls, Y. Jaslier, and D.S. Rickerby. Erosion and Foreign Object Damage of Thermal Barrier Coatings. *Materials Science Forum*, 251-254:935–948, 1997.

[115] E. Oñate and J. Rojek. Combination of discrete element and finite element methods for dynamic analysis of geomechanics problems. *Computer Methods in Applied Mechanics and Engineering*, 193(27-29):3087–3128, July 2004.

[116] J T Oden and E B Pires. Nonlocal and nonlinear friction laws and variational principles for contact problems in elasticity. *Journal of Applied Mechanics*, 50(March 1983), 1983.

[117] V a Parsegian and B W Ninham. Temperature-dependent van der Waals forces. *Biophysical journal*, 10(7):664–74, July 1970.

[118] MD Pashley. FURTHER CONSIDERATION OF THE DMT MODEL FOR ELASTIC CONTACT. *Colloids and Surfaces*, 12:69–77, 1984.

[119] Lech Pawlowski. *The science and engineering of thermal spray coatings*. John Wiley & Sons, 2008.

[120] A Picart, A Berlemont, and G Gouesbet. Modelling and predicting turbulence fields and the dispersion of discrete particles transported by turbulent flows. *International Journal of Multiphase Flow*, 12(2):237–261, 1986.

[121] Steve Plimpton. Fast parallel algorithms for short-range molecular dynamics. *Journal of Computational Physics*, 117(1):1–19, 1995.

[122] T Pöschel and T Schwager. *Computational granular dynamics: models and algorithms*. Springer, 2005.

[123] Jacek Pozorski and Sourabh V Apte. Filtered particle tracking in isotropic turbulence and stochastic modeling of subgrid-scale dispersion. *International Journal of Multiphase Flow*, 35(2):118–128, 2009.

[124] Jacek Pozorski and Jean-Pierre Minier. On the Lagrangian turbulent dispersion models based on the Langevin equation. *International Journal of Multiphase Flow*, 24(6):913–945, September 1998.

[125] JM Rallison. Note on the Faxen relations for a particle in Stokes flow. *Journal of Fluid Mechanics*, 88:529–533, 1978.

[126] Narayanan Ramanujam and Toshio Nakamura. Erosion mechanisms of thermally sprayed coatings with multiple phases. *Surface and Coatings Technology*, 204(1-2):42–53, September 2009.

[127] R Ramirez, T Pöschel, NV Brilliantov, and Thomas Schwager. Coefficient of Restitution of Colliding Viscoelastic Spheres. *Physical review E*, 60(4):24–26, 1999.

[128] WE Ranz and WR Marshall. Evaporation From Drops. *Chem. Eng. Prog*, 48(3):141–146, 1952.

[129] M. Raous, L. Cangémi, and M. Cocu. A consistent model coupling adhesion, friction, and unilateral contact. *Computer Methods in Applied Mechanics and Engineering*, 177(3-4):383–399, July 1999.

[130] M W Reeks. On a kinetic equation for the transport of particles in turbulent flows. *Physics of Fluids A: Fluid Dynamics*, 3(3):446–456, 1991.

[131] M W Reeks. On the continuum equations for dispersed particles in nonuniform flows. *Physics of Fluids A: Fluid Dynamics*, 4:1290, 1992.

[132] M W Reeks. On the constitutive relations for dispersed particles in nonuniform flows. I: Dispersion in a simple shear flow. *Physics of Fluids A: Fluid Dynamics*, 5:750, 1993.

[133] SI Rubinow. The transverse force on a spinning sphere moving in a viscous fluid. *Journal of Fluid Mechanics*, (1955), 1961.

[134] Chris H. Rycroft, Ken Kamrin, and Martin Z. Bazant. Assessing continuum postulates in simulations of granular flow. *Journal of the Mechanics and Physics of Solids*, 57(5):828–839, May 2009.

[135] EB Saff and ABJ Kuijlaars. Distributing Many Points on a Sphere. *The Mathematical Intelligencer*, 19(1):5–11, 1997.

[136] C Sagui and T a Darden. Molecular dynamics simulations of biomolecules: long-range electrostatic effects. *Annual review of biophysics and biomolecular structure*, 28:155–79, January 1999.

[137] BA Schrefler. A Partitioned solution procedure for geothermal reservoir analysis. *Communications in Applied Numerical Methods*, 1(September 1984):53–56, 1985.

[138] J Shäfer, S Dippel, and D E Wolf. Force schemes in simulations of granular materials. *Journal de physique I*, 6(1):5–20, 1996.

[139] M Sibuya. A Method for Generating Uniformly Distributed Points on N-dimensional Spheres. *Annals of the Institute of Statistical Mathematics*, (3), 1962.

[140] W.W.M. Siu and S.H.-K. Lee. Transient temperature computation of spheres in three-dimensional random packings. *International Journal of Heat and Mass Transfer*, 47(5):887–898, February 2004.

[141] WH Snyder and JL Lumley. Some measurements of particle velocity autocorrelation functions in a turbulent flow. *Journal of Fluid Mechanics*, 48:41–71, 1969.

[142] K D Squires and J K Eaton. Particle response and turbulence modification in isotropic turbulence. *Physics of Fluids*, 2:1191–1203, 1990.

[143] K D Squires and J K Eaton. Measurements of particle dispersion obtained from direct numerical simulations of isotropic turbulence. *Journal of Fluid Mechanics*, 226(1):1–35, 1991.

[144] K D Squires and J K Eaton. Preferential concentration of particles by turbulence. *Physics of Fluids A: Fluid Dynamics*, 3(5):1169–1178, 1991.

[145] D.E. Stewart. Rigid-Body Dynamics with Friction and Impact. *SIAM Review*, 42(1):3–39, 2000.

[146] Michael C Sukop and Daniel T Thorne Jr. *Lattice Boltzmann modeling: an introduction for geoscientists and engineers*. Springer Publishing Company, Incorporated, 2007.

[147] J. Sun and M.M. Chen. A theoretical analysis of heat transfer due to particle impact. *International Journal of Heat and Mass Transfer*, 31(5):969–975, May 1988.

[148] G. Sutmann and V. Stegailov. Optimization of neighbor list techniques in liquid matter simulations. *Journal of Molecular Liquids*, 125(2-3):197–203, April 2006.

[149] WC Swope and HC Andersen. Computer Simulation Method for the Calculation of Equilibrium Constants for the Formation of Physical Clusters of Molecules : Application to Small Water Clusters. *The Journal of Chemical Physics*, 76(1):637–649, 1982.

[150] D Tabor. Surface forces and surface interactions. *Journal of Colloid and Interface Science*, 58(1), 1977.

[151] Tomohiko Tanaka and John K Eaton. Classification of Turbulence Modification by Dispersed Spheres Using a Novel Dimensionless Number. *Phys. Rev. Lett.*, 101(11):114502, September 2008.

[152] Yoshihiro Tashiro. On methods for generating uniform random points on the surface of a sphere. *Annals of the Institute of Statistical Mathematics*, 29(1):295–300, December 1977.

[153] FB Tatom. The Basset Term as a Semiderivative. *Applied Scientific Research*, 45:283–285, 1988.

[154] G I Taylor. Diffusion by continuous movements. *Proceedings of the London Mathematical Society*, 20:196–211, 1921.

[155] S. Torquato, O. Uche, and F. Stillinger. Random sequential addition of hard spheres in high Euclidean dimensions. *Physical Review E*, 74(6):1–16, December 2006.

[156] Abdulnour Y. Toukmaji and John a. Board. Ewald summation techniques in perspective: a survey. *Computer Physics Communications*, 95(2-3):73–92, June 1996.

[157] W. F. Van Gunsteren and H. J. C. Berendsen. A Leap-frog Algorithm for Stochastic Dynamics. *Molecular Simulation*, 1(3):173–185, March 1988.

[158] M.a.T. van Hinsberg, J.H.M. ten Thije Boonkkamp, and H.J.H. Clercx. An efficient, second order method for the approximation of the Basset history force. *Journal of Computational Physics*, 230(4):1465–1478, February 2011.

[159] Loup Verlet. Computer "Experiments" on Classical Fluids. I. Thermodynamical Properties of Lennard-Jones Molecules. *Physical Review*, 159(1):98–103, 1967.

[160] J Visser. On Hamaker Constants: A Comparison Between Hamaker Constants and Lifshitz - Van Der Waals Constants. *Advances in Colloid and Interface Science*, 3:331–363, 1972.

[161] DJ Vojir and EE Michaelides. Effect of the history term on the motion of rigid spheres in a viscous fluid. *International Journal of Multiphase Flow*, 20(3):547–556, 1994.

[162] L. Vu-Quoc and Xiang Zhang. An accurate and effcient tangential force-displacement model for elastic frictional contact in particle flow simulations. *Mechanics of materials*, 31(4):235–269, 1999.

[163] OR Walton and RL Braun. Viscosity, granular temperature, and stress calculations for shearing assemblies of inelastic frictional disks. *Journal of Rheology*, 30(5):949–980, 1986.

[164] Christian Wellmann and Peter Wriggers. A two-scale model of granular materials. *Computer Methods in Applied Mechanics and Engineering*, 205-208:46–58, January 2012.

[165] B Widom. Random sequential addition of hard spheres to a volume. *The Journal of Chemical Physics*, 44(10):3888, 1966.

[166] M Wilsea, KL Johnson, and MF Ashby. Indentation of Foamed Plastics. *International Journal of Mechanical Sciences*, 17:457–460, 1975.

[167] Peter Wriggers and G Zavarise. *Computational contact mechanics*. Wiley Online Library, 2002.

[168] Y Yamamoto, M Potthoff, T Tanaka, T Kajishima, and Y Tsuji. Large-eddy simulation of turbulent gas-particle flow in a vertical channel: effect of considering inter-particle collisions. *Journal of Fluid Mechanics*, 442:303–334, 2001.

[169] D M York, a Wlodawer, L G Pedersen, and T a Darden. Atomic-level accuracy in simulations of large protein crystals. *Proceedings of the National Academy of Sciences of the United States of America*, 91(18):8715–8, August 1994.

[170] S Yuu, N Yasukouchi, Y Hirosawa, and T Jotaki. Particle turbulent diffusion in a dust laden round jet. *AIChE Journal*, 24(3):509–519, 2004.

[171] J.H. Zhou, a.B. Yu, and M. Horio. Finite element modeling of the transient heat conduction between colliding particles. *Chemical Engineering Journal*, 139(3):510–516, June 2008.

[172] Z.Y. Zhou, a.B. Yu, and P. Zulli. A new computational method for studying heat transfer in fluid bed reactors. *Powder Technology*, 197(1-2):102–110, January 2010.

[173] O.C Zienkiewicz, D.K Paul, and A.H.C Chan. Unconditionally Stable Staggered Solution Procedure for Soil-Pore Fluid Interaction Problems. *International Journal for Numerical Methods in Engineering*, 26(1987):1039–1055, 1988.

[174] T. I. Zohdi. An adaptive-recursive staggering strategy for simulating multifield coupled processes in microheterogeneous solids. *International Journal for Numerical Methods in Engineering*, 53(7):1511–1532, March 2002.

[175] T. I. Zohdi. A computational framework for agglomeration in thermochemically reacting granular flows. *Proceedings of the Royal Society A: Mathematical, Physical and Engineering Sciences*, 460(2052):3421–3445, December 2004.

[176] Tarek I Zohdi. *An introduction to modeling and simulation of particulate flows*, volume 4. Siam, 2007.

[177] TI Zohdi. On the tailoring of microstructures for prescribed effective properties. *International Journal of Fracture*, 118(4):89–94, 2002.

[178] T.I. Zohdi. Computation of strongly coupled multifield interaction in particlefluid systems. *Computer Methods in Applied Mechanics and Engineering*, 196(37-40):3927–3950, August 2007.

[179] TI Zohdi. On the dynamics of charged electromagnetic particulate jets. *Archives of Computational Methods in Engineering*, 17(2):109–135, 2010.